SEISMOLOGICAL ANALYSES OF VELA ARRAY DATA

Final Report
Period Covered: 1 February 1966 - 31 July 1970

30 August 1970

Work Sponsored By Advanced Research Projects Agency
ARPA Order No. 292 Amendment 72

Contract No.:	AF 49(638)-1687
Project Code No.:	8652
Date of Contract:	1 February 1966
Amount of Contract:	$104,522
Contract Termination Date:	31 July 1970
Project Scientist:	Robert L. Kovach (415) 321-2300 x 4827

Department of Geophysics
Stanford University
Stanford, California

SEISMOLOGICAL ANALYSES OF VELA ARRAY DATA

Final Report
Period Covered: 1 February 1966 - 31 July 1970

30 August 1970

Work Sponsored By Advanced Research Projects Agency
ARPA Order No. 292 Amendment 72

Contract No.:	AF 49(638)-1687
Project Code No.:	8652
Date of Contract:	1 February 1966
Amount of Contract:	$104,522
Contract Termination Date:	31 July 1970
Project Scientist:	Robert L. Kovach (415) 321-2300 x 4827

Table of Contents

Introduction and Summary

This is a final report summarizing research accomplished under contract no. AF49(638)-1687. This research utilized seismic data recorded by VELA arrays, such as LASA and those formed by individual LRSM stations to 1) investigate the velocity structure of the earth's mantle and core; 2) examine the attenuation characteristics of seismic waves; and 3) study the propagation of seismic waves across large seismic arrays. Abstracts of published scientific papers and papers presented at scientific meetings are given in the following section and significant research accomplishments are summarized below.

The velocity structure of the earth's core is an important baseline for routine determinations of the epicenter and focal depths of earthquakes. Once the velocity structure is accurately known observations of core phases, such as PKP, provide control on origin time and focal depth determinations because of the small gradient of the travel time curve with respect to distance. A novel approach used in this research contract towards deciphering the velocity structure of the core was to utilize velocity filtering of the seismic phase PKKP as recorded at LASA. Because of the large percentage of the total ray path spent in the core PKKP amplifies details of the core velocity structure. The velocity structure of the core was demonstrated to possess a complex tripartite structure but it is clear that more work yet needs to be done, particularly analyses of the

phase SKS to study the outer core.

One important development revealed in this study, pertinent to the propagation of seismic waves across large arrays, particularly LASA, was the need to correct for the dipping M-discontinuity. A clever empirical technique was discovered to correct for the apparent velocities of seismic waves moving across the array. Further details can be found in Zengeni (1970).

Determination of the shear velocity structure of the earth's mantle continues to be an important parameter in geophysics. Digital processing techniques were developed to study the propagation of shear waves across large arrays and the velocity structure determined for western North America is demonstrated to be as complex as that revealed from detailed P-wave studies. A further implication of these studies is that regional differences beneath shields, tectonic areas, and oceans extend to depths of at least 650 km in the mantle; it is clear that regional travel time tables are needed for precision epicenter locations.

Significant progress towards epicenter location in laterally inhomogeneous regions was made through development of a finite difference, time integration scheme (Wesson, 1970). Exploitation of this technique to the precision location of events is clear-cut and a possible approach to the problem of hypocenter location in island arcs, such as the Aleutian arc and the Kurile-Kamchatka arc is described in the section entitled

Epicenter Location in Laterally Inhomogeneous Regions.

The attenuation of seismic energy in the earth's mantle and core is an important parameter in discussions of source mechanisms, earthquake magnitude and the range of detectability of seismic signals. Studies initiated under the aegis of Project VELA and continued under this contract have demonstrated that the average Q for shear throughout the mantle is about 600 and is an order of magnitude less in the upper mantle than the rest of the mantle. The average Q for compressional waves appears to be at least 2.5 times that for shear waves (Kovach, 1967).

Abstracts of Published Papers and Papers Presented at Scientific Meetings

Anderson, D. L. and R. L. Kovach, Universal Dispersion Tables III. Free Oscillation Variational Parameters, Bull. Seism. Soc. Amer., 59, 1667 - 1693, 1969.

The effect of a small change in any parameter of a realistic Earth model on the periods of free oscillation is computed for both spheroidal and torsional modes. The normalized partial derivatives, or variational parameters, are given as a function of order number and depth in the Earth. For a given mode it can immediately be seen which regions of the Earth are controlling the period of free oscillation. Except for $_0S_0$ and its overtones the low-order free oscillations are relatively insensitive to properties of the core. The shear velocity of the mantle is the dominant parameter controlling the periods of free oscillation and density can be determined from free oscillation data only if the shear velocity is known very accurately. Once the velocity structure is well known free oscillation data can be used to modify the average density of the upper mantle. The mass and moment of inertia are then the main constraints on how the mass must be redistributed in the lower mantle and core.

Kovach, R. L., Relative Attenuation of Compressional Wave Energy in the Mantle, Geophysical Journ. 13, 371, 1967.

The attenuation of compressional energy relative to shear energy in the mantle is determined by spectral amplitude comparison of the seismic phases SKS and SKP with common paths in the mantle and core. Assuming that the average Q, for shear in the mantle is 500, the average Q for compressional waves is at least twice that for shear in the frequency range 0.2 - 0.6 cps.

Kovach, R. L., Attenuation of Seismic Body Waves in the Mantle, Geophysical Journal, 14, 165 - 170, 1967.

The attenuation of seismic body waves is a direct measure of the absorption due to nonelastic processes within the Earth. Accurate amplitude decrement data for seismic body waves require the measurement of the spatial decay rate along a given ray, but measurements are restricted to the surface of the Earth. Recent studies have shown that the average Q, for shear, throughout the mantle is about 600 and that the average Q for the upper 600 km of the mantle is an order of magnitude less than the rest of the mantle. Spectral amplitude comparison of the seismic phases SKS and SKP with common paths in the mantle and core allows the Q, for compression, in the mantle to be estimated. Preliminary results indicate that the Q for compression is at least 2·5 times that for shear.

Kovach, R. L., Travel Times and Attenuation of Seismic Waves in the Earth's Core, presented at the XIVth General Assembly,

International Union of Geodesy and Geophysics, Zurich, 1967.

A statistical treatment of about 500 observations of PKP in the range $115° \leq \Delta \leq 140°$ yields for the DE branch (PKIKP) the empirical relation

$$t = 909.25s + 1.876\Delta \text{ (s)}$$

later by 1.8 to 1.0 seconds from the corresponding Jeffreys-Bullen times. The mean residual of all PKIKP observations from nuclear explosions against the empirical times is nearly zero emphasizing that average PKIKP times for a reference earth are now satisfactorily known. Observations of precursors to PKIKP satisfy the relation

$$t = 853.4s + 2.2\Delta \text{ (s)}$$

with a large standard error; these observations probably correspond to one or more precursor branches.

Knowledge of the attenuation function for P-waves in the earth's core is pertinent to understanding mechanisms of energy dissipation in the earth. The attenuation of P-waves in the core has been measured by spectral amplitude comparison of the seismic phases ScS and SKS which have left the source at nearly identical azimuths and vertical takeoff angles. Assuming that the core can be treated as a viscous liquid a value for the viscosity of 2.6×10^{10} poise is obtained. Since the core behaves as a fluid Q is dependent on frequency. For a 20 second period wave a Q equalling 750 is compatible with the observed data.

Kovach, R. L., and P. Glover, Travel Times of PKP in the Range 115° $\leq \Delta \leq$ 140°, Geophysical Journal, 15, 367-376, 1968.

Approximately 500 observations of PKP in the range 115° $\leq \Delta \leq$ 140° have been statistically examined to yield a set of empirical travel times. Observations for the DE branch (PKIKP) fit the form t = 909.25 s + 1·876Δ later by 1·8 to 1·0 s than the corresponding times given by Jeffreys and Bullen. The mean residual of all observations of PKIKP from nuclear explosions, including recent data from Longshot, against the empirical times does not significantly differ from zero emphasizing that average PKIKP times for a reference Earth are now satisfactorily known. In the interval 125° $\leq \Delta \leq$ 140° observations preceding the DE branch satisfy the relation t = 1145·0 + 2·2(Δ-132·5°) with a large standard error; these observations probably correspond to one or more precursor branches to the DE branch.

Kovach, R. L. and D. L. Anderson, Study of the Energy of the Free Oscillations of the Earth, J. Geophys. Research, 71, 2155 - 2188, 1967.

The energies of the radial, torsional, and spheroidal free oscillations for a Gutenberg model earth were studied. Each mode of oscillation has a characteristic radial distribution of elastic and kinetic energy that fixes the

parts of the earth that contribute most heavily in determining a particular resonant frequency. An examination of the partitioning of energy among compressional, shear, and gravitational energy as a function of mode number and depth immediately explains the persistence of the purely radial mode compared with the other normal modes of the earth. Only the first few spheroidal modes are sensitive to the density of the inner core; they are particularly sensitive to the density of the outer part of the core. The low-order spheroidal modes also exhibit a rapid rise of potential energy near the base of the mantle; this rise will permit improved estimates of the velocity to be obtained in this region, which is difficult to examine with body waves. The tabulated results allow estimates to be made of the previously neglected energy contained in the free oscillations excited by large earthquakes. An estimate of the energy in the low-order spheroidal oscillations excited by the great Alaskan shock suggests a value of 10^{23} ergs over the period range from 450 to 830 sec, implying that the energy density increases towards high frequencies if the total energy in the earthquake was of the order of 10^{24} - 10^{25} ergs.

Kovach, R. L., and R. Robinson, Upper Mantle Structure in the Basin and Range Province, Western North America from the Apparent Velocities of S Waves, Bull. Seism. Soc. Amer., 59

1654 - 1665, 1969.

The variation of shear velocity with depth in the upper mantle for the Basin and Range province of western North America has been studied with direct measurements of $dT/d\Delta$ for S waves in the distance range $14° < \Delta < 40°$. Three orthogonal components of digital data were used and onset times were determined using the product of the horizontal radial and vertical components of motion and particle motion diagrams. A linear LRSM array in Arizona was used for the measurement of $dT/d\Delta$.

An S-wave velocity distribution is derived, compatible with P-wave velocity models for the same region. The derived model consists of a thin lid zone of shear velocity 4.5 km/sec overlying a low-velocity zone and a change in velocity gradient at a depth of 160 km. Two regions of high-velocity gradient are located at depths beginning at 360 km and 620 km.

Robinson, R., and R. L. Kovach, Shear Wave Velocity Structure in the Western United States, Geophysical Journal, 20, 1-9 , 1970.

Direct measurements of $dT/d\Delta$ for S-waves over the distance range $14° < \Delta < 93°$ are used to derive a shear wave velocity model for the mantle beneath western North America. A network of seismograph stations in Arizona operated as an

array was used for the measurement of $dT/d\Delta$. The use of later arrivals is necessary to define the $dT/d\Delta$-Δ curve for distances less than 55°. Distinctive features of the derived model ORC-3, are a low velocity zone centered at 100 km depth and zones of high velocity gradient beginning at 400, 650, 900 and 1180 km depth.

Wesson, R. L., Amplitudes of Body Phases in a Spherically Layered Earth, presented at 1969 Annual Meeting of the Seismological Society of America, St. Louis.

Velocity laws commonly used (such as $v=ar^b$) for the evaluation of familiar ray theory integrals have proven satisfactory for the calculation of travel-time versus distance but are unsatisfactory for computation of the distance derivative $d\Delta/dp$, required for the calculation of intensity and amplitude. Specifically, false caustics and regions of low intensity are introduced and real caustics are omitted. The spurious discontinuities in curves of $d\Delta/dp$ versus distance, calculated from the laws which contain two or fewer free parameters, stem from the inability of the laws to maintain continuity of dv/dr and higher derivatives across layer boundaries. However, satisfactory results may be obtained by integration using the variable η (defined as r/v) and expressing the radius, r as a function of η, using as many free parameters as required to fit the desired number of derivatives at the layer boundaries.

Functions which reduce to the form:

$$\frac{1}{r}\frac{dr}{d\eta} = a_0 + a_1\eta + a_2\eta^2 + \ldots$$

facilitate the evaluation of the integrals by a simple recursion. Examples are given that demonstrate the improvement obtained in amplitude-distance curves over those calculated using the law $v=ar^b$, particularly in the vicinity of true discontinuities and caustics.

Wesson, R. L., A Time Integration Method for Computation of the Intensities of Seismic Waves, Bull. Seism. Soc. Amer., 60, 307-316, 1970.

A finite-difference time integration method for the calculation of seismic ray intensity is developed. Discontinuities in the depth derivative of the velocity-depth function at layer boundaries cause anomalies in the intensity distance curves calculated using the standard integral formulation. The time integration method overcomes these difficulties. Calculations for a simple analytic case and a Gutenberg earth model demonstrate the difficulties with the standard integral method and the superior performance of the time integration scheme. The method may also be applied to laterally inhomogeneous earth models.

Wesson, R. L., Seismic Ray Computations in Laterally Inhomogeneous Crustal Models, Ph.D. thesis, Stanford University, 1970.

The realistic interpretation of seismic travel-time data from structurally complex areas, and the accurate location of earthquake hypocenters in such areas, require seismic ray computations for laterally inhomogeneous velocity models. Numerical simulation of the ray differential equations provides a practical means of performing the necessary calculations. In addition to the calculation of travel-time, the ray intensity and the partial derivatives of travel-time with respect to the parameters of the model may be calculated. Results from such numerical simulations are in excellent agreement with those analytically obtainable for a simple constant gradient velocity model. An algorithm for the direct solution of ray boundary value problems, based on the iterative solution of a tridiagonal set of simultaneous equations, allows for the input of geophysical intuition in finding the rays between a source and a station.

A model fitting procedure is described for laterally inhomogeneous models which is based on the description of a velocity model by combinations of simple continuous functions which are chosen to reflect the available geologic data. A least squares scheme is used to obtain models which fit the travel-time data and are consistent with geologic data. Laterally inhomogeneous velocity models are obtained for travel-time data from explosions for two areas in California: the Bear Valley area, 25 miles southeast of Hollister, and the Borrego Mountain area, 100 miles northeast

of San Diego. Both regions are characterized by a substantial lateral variation of seismic velocity and the derived models exhibit most of the significant structural features of the areas. The Bear Valley explosion is relocated in the velocity model as a test for the validity of the model and of a computational procedure for the location of hypocenters in structurally complex areas. [This report is attached as Appendix A].

Zengeni, T. G., PKKP and the Earth's Core, presented at 1969 Annual meeting of the Seismological Society of America, St. Louis.

Much of the information concerning the velocity structure of the earth's core is based on studies of the seismic waves PKP and SKS. Detailed observations of the core phase PKKP are a previously unexploited tool for studying the fine structure of the core. Because of the large percentage of the total ray path which is spent in the core PKKP amplifies details of the core velocity structure. Direct measurements of $dT/d\Delta$ for PKKP in the distance range from 85° to 150° have been made at the Montana LASA for a number of earthquakes and the data inverted to extract a velocity model for the core. The model is discussed in the light of other velocity models which have been proposed for the core.

Zengeni, T. G., A Note on Azimuthal Correction for dT/dΔ for a Single Dipping Plane Interface, Bull. Seism. Soc. Amer., 60, 299-306, 1970.

A relation is derived for correcting dT/dΔ for a single dipping interface under seismic array:

$$\frac{dT}{d\Delta} = \left(\frac{\delta T}{\delta \Delta}\right)' \frac{\sin(\Omega-\omega')}{\sin(\Omega-\omega)}$$

The formula depends on the azimuth angles: ω and ω' are the computed and observed azimuths, Ω is the azimuth of the normal to the tilted interface, and $(\delta T/\delta\Delta)'$ is the observed quantity. The relation is explicitly independent of the dip and the velocities of the media on either side of the interface.

Zengeni, T., PKKP and the Fine Structure of the Earth's Core, Ph.D. thesis, Stanford University, 1970.

The slowness factor dT/dΔ for the core phase PKKP was measured at the Large Aperture Seismic Array (LASA), Montana, in the epicentral distance range $75° < \Delta < 125°$. Due to the high phase velocities involved, or equivalently, low slowness factor, corrections for simple geologic structures under the array were imperative. A method was derived to correct for the dipping M-discontinuity under LASA.

A velocity model for the earth's core was computed from the dT/dΔ observations, together with PKP travel

times, using the Wiechert-Herglotz integration method. The PKKP core velocity model derived is essentially tripartite, but differs from other proposed models in important details.

The major part of the outer core exhibits no striking differences from the standard Jeffreys' model: fairly constant velocity gradients in the SKS and ABC (Bullen 'E') region. However, at a radius of 1654 km there is a discontinuity in the velocity gradient and the next 250 km in depth is a distinct region of slightly higher velocity. The transition zone into the inner core is only 200 km in thickness and is characterized by a gentle negative velocity gradient This zone has an average velocity of 10.45 km/sec. The inner core starts at radius 1217 km with an average velocity of about 11.20 km/sec and possesses a slight negative velocity gradient towards the center of the earth. A slight drop in compressional velocity in the mantle at the core-mantle boundary is also inferred.

It is conjectured that the transition zone (liquid or viscous) and the inner core (solid) are of the same chemical composition, but differ from that of the outer core. [This paper is attached in toto as Appendix B].

Structure of the Earth Using Seismic Body Waves

The ability to locate natural and artificial seismic sources depends on the precise knowledge of the travel times of seismic waves. Work towards the determination of earth structure from seismic body waves was pursued using arrays such as LASA and arrays formed from LRSM stations. Considerable effort was devoted towards deciphering the velocity structure of the earth's core. Accurate travel times for the earth's core are required because observations of core phases provide control on origin time and focal depth observations.

One of the most promising techniques for studying the velocity structure of the core was to measure $dT/d\Delta$ for various core phases directly using large seismic arrays, such as LASA. Analyses of the core phase PKKP in the distance range $75° < \Delta < 125°$ was particularly fruitful in delineating the somewhat surprising complexity indicated for the velocity structure of the core. The advantageous use of the core phase PKKP is illustrated by the amplification of various travel time branches. The clustering of the branches of the core phase PKP at the crucial distances around the caustic B make it difficult to discern such a structure. PKKP branches are spread out more conveniently such that branch terminal

points A, C, I, J and the caustic B are less obscure than in corresponding PKP points.

The core model derived is essentially tripartite, differing from existing tripartite models mainly in fine structure. The inner core fine structure is not resolvable, and the velocity distribution is thus fairly arbitrary. The structure derived is constrained solely to give the observed PKIKP (DF branch) travel times.

The greater part of the outer core exhibits no new or major features -- fairly constant velocity gradients in the SKS and ABC regions, slightly higher in the former, and lower in the latter. The gradient diminishes to near zero in the subregion CI. However, the next 250 km show a distinct region (IJ) characterized by a humped velocity distribution.

The transition zone is found to be rather narrower than existing tripartite models, only about 200 km thick, and has a slight negative velocity gradient (with depth). Further details concerning the velocity structure of the core can be found in Appendix B, Kovach and Glover (1968) and Zengeni (1970).

Even though the velocity structure of the earth's core has been demonstrated to be more complex than heretofore believed it is clear that more work yet needs to be done,

particularly studies of the outer core using the seismic phase SKS.

Determination of the shear wave velocity structure of the earth's mantle continues to be an important problem in geophysics. During this research effort work was directed towards analysis of the shear velocity structure through direct measurements of $dT/d\Delta$ for S waves in the distance range $14° < \Delta < 90°$. A linear LRSM array in Arizona was used for the measurement of $dT/d\Delta$.

S-wave data collected to date are summarized in Figure 1, Kovach and Robinson (1969) and Robinson and Kovach (1970a) The shear wave velocity structure has been demonstrated to be as complex as that revealed by array studies of P-waves. In the Basin and Range province of western North America the derived velocity model possesses a thin 'lid' of velocity 4.45 km/sec overlying a broad low velocity zone and pronounced regions of high velocity gradient centered at depths of 410 km and 650 km. A lesser zone of high velocity gradient has been detected at a depth of 1225 km.

The shear wave velocity structure in the upper mantle (above 650 km or so) has been shown from surface wave dispersion studies (particularly Love waves) to be strongly dependent on the particular province traversed -- mountain-tectonic, shield or oceanic (Toksöz and Anderson, 1966;

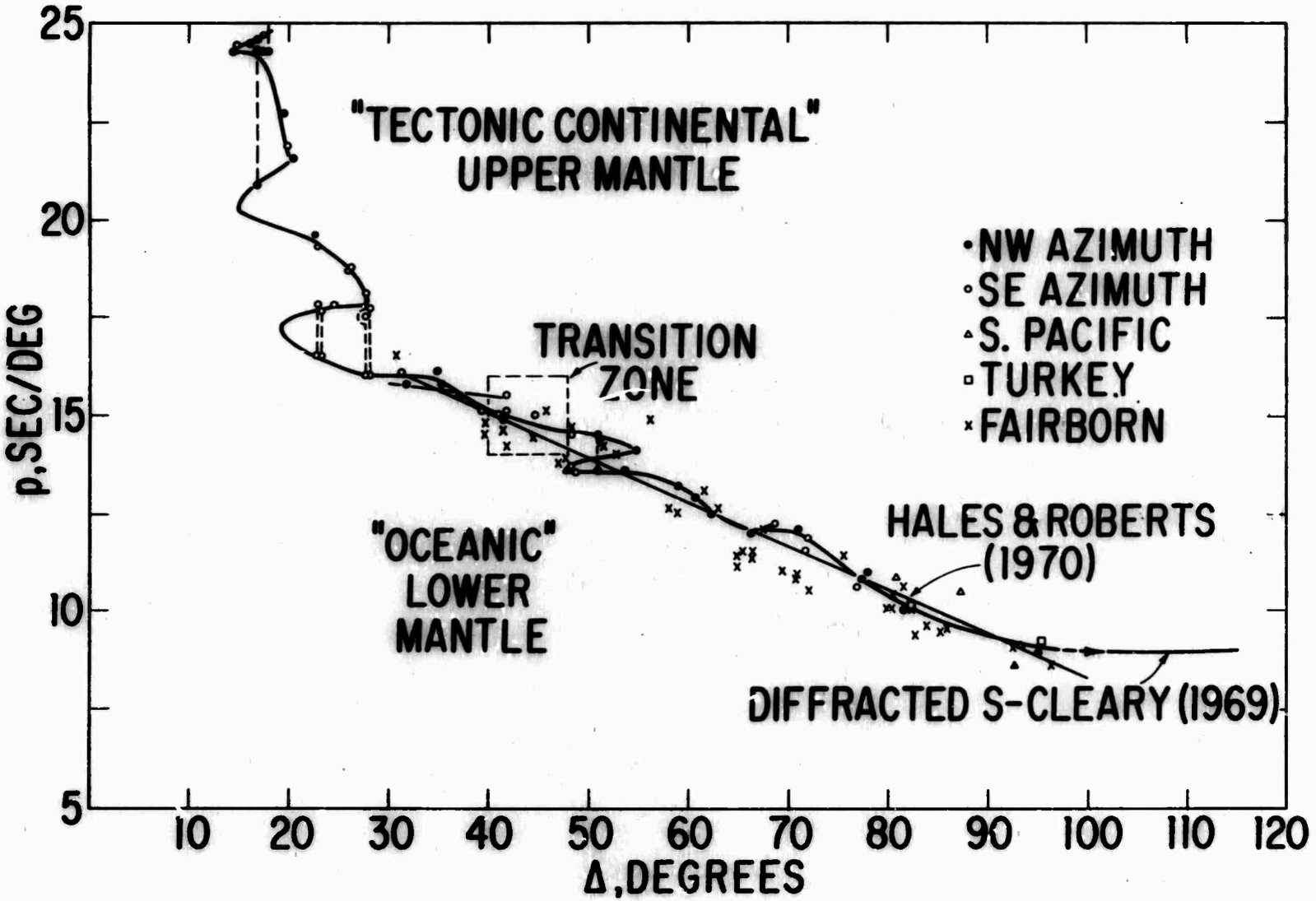
"TECTONIC CONTINENTAL"
UPPER MANTLE
TRANSITION
ZONE
"OCEANIC"
LOWER
MANTLE
•NW AZIMUTH
°SE AZIMUTH
▵S. PACIFIC
▫TURKEY
×FAIRBORN
HALES & ROBERTS
(1970)
DIFFRACTED S-CLEARY (1969)
p, SEC/DEG
Δ, DEGREES
25
20
15
10
5
10
20
30
40
50
60
70
80
90
100
110
120

Figure 1

Kanamori, 1970). This fact in turn dictates that considerable care must be exercised in extracting a shear wave velocity structure for the lower mantle, since inversion by the Wiechert-Herglotz technique is dependent on the velocity structure assumed in the upper mantle. Conversely, free oscillation inversions which purport to determine details of the upper mantle are strongly dependent on the shear velocity structure assumed for the lower mantle.

The upper mantle structure determined from the inversion of $dT/d\Delta$ for S-waves during this research effort is applicable for the Basin and Range province of western North America. In order to determine a velocity structure for the lower mantle compatible with travel time and free oscillation observations it was necessary to 'strip' the velocity structure to depths exceeding 650 km and fit the upper mantle with an 'average' structure before inverting the lower mantle $dt/d\Delta$ versus Δ data.

The implication that regional heterogeneities exist to such depths in the earth's mantle, particularly for S-waves, is important and argues that regional travel time tables are needed for precision epicenter locations. Further details of the S-wave inversion problem can be found in Robinson and Kovach (1970b).

Epicenter Location in Laterally Inhomogeneous Regions

Application to the San Andreas Fault

The precision location of epicenters is particularly difficult in regions of lateral inhomogeneities. A finite difference, time integration technique has been developed to determine three-dimensional velocity models for laterally inhomogeneous regions from seismic data. The essence of the method is as follows, and exploitation of this technique to the precision location of events is clear-cut.

Velocity models are specified as a function of the space coordinates $\vec{X}$ through a set of parameters p_j, $C(\vec{X}, p_j)$ where C is the velocity. Travel times between the source and the stations are calculated using a finite-difference, time integration procedure. The appropriate ray from the source which passes through the station is obtained using an iterative algorithm. Partial derivatives of the travel time with respect to the model parameters p_j are also calculated. Starting with an initial guess p_j, a least squares iteration is used to minimize the sum of the squares of the differences between the observed travel times and the travel times calculated using the new model. A detailed explanation of the technique and application

to the problem of epicenter location on the San Andreas fault is described in detail in Appendix A.

Application to Hypocenter Location in Island Arcs

Lateral inhomogeneities of seismic velocity in the earth's crust and upper mantle introduce bias into the location of earthquakes and explosions by seismic methods. This bias is most severe for events occuring in geographic areas characterized by substantial lateral velocity variations, such as island arcs. The magnitude of this bias was perhaps most clearly indicated by the detonation of the nuclear explosion LONGSHOT on Amchitka Island in the Aleutian Arc. Attempts to relocate this shot by standard means indicated an epicenter approximately 20 km north of the true location and a depth 60-80 km deeper than the actual event (Lambert et al., 1970). This discrepancy has been extensively studied by Douglas (1967), Douglas and Lilwall (1968), Lilwall and Douglas (1969, 1970), Herrin and Taggart (1968), Chiburis and Ahner (1969), and Lambert et al. (1970).

Evidence for both network bias (resulting from global velocity variations and the position of the event within the station network) and source bias (resulting from the velocity structure in the immediate vicinity of the event) has also been found for an event in Hawaii (Herrin and

Taggart, 1968), although this is argued by Douglas and Lilwall (1968). Evidence for network bias is extensive. In addition to the papers cited above for LONGSHOT, bias for regional events in North America has been found by Herrin and Taggart (1962, 1966). The method of joint epicenter determination of Douglas (1967) (see also Bolt and Freedman, 1968) has yielded promising results in the elimination of network bias. On the other hand, it has only been possible to eliminate source bias for events of known origin time and position (e.g. LONGSHOT).

The calculation of travel-times for laterally inhomogeneous velocity models may be simply accomplished by numerical simulation of the ray differential equation. Briefly, the initial value problem of finding the ray emanating from a given point in a given direction may be solved by a simple Runge-Kutta or similar integration scheme. The more difficult boundary value problem, which must be solved in the hypocenter location problem for the rays from the trial source position to the stations, may be solved, either by a succession of initial value problems, or by a direct iterative algorithm developed for this purpose based on the solution of a tridiagonal set of equations.

Several possible inputs exist to the process of finding three-dimensional velocity models of island arc

structures. The first is the seismicity data summarized by Isacks et al. (1968), and others which indicates the geometric shape of the structures and suggests that the dominant feature is a downgoing slab of lithosphere. This geometric picture, assumption as to the general rock types present, and temperature distribution calculations such as those of Minear and Toksöz (1970) may be combined and used to calculate velocity models. Seismic refraction data (e.g. Murdock (1967)) can also be used for the uppermost mantle. Minear and Toksöz, for example, give two-dimensional plots of the temperature distribution in a downgoing slab of lithosphere under a broad range of assumptions. Using available laboratory data on the partial derivatives of seismic velocity with temperature (e.g. Birch, 1966), it is a simple matter to calculate two-dimensional velocity models. In fact, Minear and Toksöz obtain the velocities in selected regions of the slab in just this way in order to calculate the travel-time anomalies for the simple cases of rays arriving parallel and perpendicular to the faces of the slab.

For ray calculations of the sort discussed above, the velocity models may be specified in either of two ways. For the maximum flexibility in describing the velocity distribution, a two- or three-dimensional grid may be used. This would necessitate a table lookup

interpolation scheme to define the velocity at intermediate points. The other approach is to find a simple analytic function or combination of functions which describe in a general way the desired distribution.

Travel-time data from earthquakes may also be useful in a general way. Of course the best single restraint on velocity models in addition to the overall geometric shape is travel-time data from events with known location and origin time.

In order to very accurately locate events in island arc structures two avenues of attack are possible. The first is to model a sufficient portion of the globe, and to use the finite difference integration approach exclusively. A more practical approach is to model the structure in the vicinity of the source and perform the integration by the finite difference technique in this region, and use a standard one-dimensional earth model, specified by travel-time tables and supplemented with station corrections.

In summary, the following seems to be a promising approach for precision epicentral locations in island arc regions:

1) obtain through a synthesis of techniques three-dimensional velocity models of a few island arc areas (the Aleutian arc and the Kurile-Kamchatka arc);

2) develop computer programs coupling our finite difference technique with standard table lookup and station correction procedures to calculate the travel-times from events located on these structures to world wide stations;

3) use these programs to locate events in these structures and compare the results with those obtained from other techniques; in particular, the method of joint epicenter determination;

4) finally, determine <u>if it is possible to eliminate source bias in event location</u> without <u>a priori</u> knowledge of the location of the events.

References

Bolt, B. A., and H. Freedman, Group analysis of variance for earthquake location and magnitude, Nature, 217, 47-48, 1968.

Birch, F., Compressibility: elastic constants, in Handbook of Physical Constants, Geol. Soc. Amer. Mem. 97, 97-173, 1966.

Chiburis, E. F., and R. O. Ahner, A location and travel-time study of Aleutian island explosions and earthquakes, Seismic Data Lab. Report #239, Teledyne, 1969.

Cleary, J., The S velocity at the core-mantle boundary, from observations of diffracted S, Bull. Seism Soc. Amer., 59, 1399-1405, 1969.

Douglas, A., Joint epicenter determination, Nature, 215, 47-48, 1967.

Hales, A., and J. L. Roberts, Shear velocities in the lower mantle and the radius of the core, Bull. Seism. Soc. Amer., in press, 1970.

Douglas, A., and R. C. Lilwall, Does epicenter source bias exist? Nature, 220, 469-470, 1968.

Herrin, E., and J. Taggart, Regional variations in P_n velocity and their effect on the location of epicenters, Bull. Seism. Soc. Amer., 52, 1037-1046, 1962.

Herrin, E., and J. Taggart, Epicenter determination for the Salmon event, J. Geophys. Res., 71, 3503-3506, 1966.

Herrin, E., and J. Taggart, Source bias in epicenter determinations, Bull. Seism. Soc. Amer., 58, 1791-1796, 1968.

Isacks, B., J. Oliver and L. Sykes, Seismology and the new global tectonics, J. Geophys. Res., 73, 5855-5899, 1968.

Jacob, K. H., P-residuals and global tectonic structures investigated by three-dimensional seismic ray tracing with emphasis on Longshot data, EOS, Trans. Amer. Geophys. Union., 51, 359, 1970.

Kanamori, H., Velocites and Q of mantle waves, J. Geophys. Res., in press, 1970.

Kovach, R. L., and P. Glover, Travel times of PKP in the range 115°<Δ<140°, Geophys. J., 15, 367-376, 1968.

Kovach, R. L., and R. Robinson, Upper mantle structure in the Basin and Range province, western North America from the apparent velocities of S waves, Bull. Seism. Soc. Amer., 59, 1654-1665, 1969.

Lambert, D. G., D. H. Von Seggern, S. S. Alexander and G. A. Galat, The Longshot experiment, vol. 2, Comprehensive analysis, Seismic Data Lab. Report #234, 1970.

Lilwall, R. C., and A. Douglas, Estimation of P-wave travel times using the joint epicenter method, Geophys.J., 19, 165-181, 1970.

Lilwall, R. C., and A. Douglas, Quest for a P travel time standard, Nature, 222, 975-977, 1969.

Minear, J. W., and M. N. Toksoz, Thermal regime of a downgoing slab and new global tectonics, J. Geophys. Res., 75, 1397-1420, 1970.

Murdock, J. N., Configuration of the crust-mantle system in the central Aleutians, a hypothesis, ESSA Technical Memorandum IERTM-EML3, 1967.

Robinson, R., and R. L. Kovach, Shear wave velocity structure in the western United States, Geophys. J., 20, 1970a.

Robinson R., and R. L. Kovach, S waves revisited, in preparation, 1970b.

Toksoz, N., and D. L. Anderson, Phase velocities of long-period surface waves and structure of the upper mantle, 1, Great circle Love and Rayleigh wave data, J. Geophys. Res., 71, 1649-1658, 1966.

Zengeni, T., A note on azimuthal correction for dT/dΔ for a single dipping plane interface, Bull. Seism. Soc. Amer., 60, 299-306, 1970.

APPENDIX A

SEISMIC RAY COMPUTATIONS IN LATERALLY INHOMOGENEOUS CRUSTAL MODELS

A DISSERTATION
SUBMITTED TO THE DEPARTMENT OF GEOPHYSICS
AND THE COMMITTEE ON GRADUATE STUDIES
OF STANFORD UNIVERSITY
IN PARTIAL FULFILLMENT OF THE REQUIREMENTS
FOR THE DEGREE OF
DOCTOR OF PHILOSOPHY

By
Robert Laughlin Wesson

June 1970

ABSTRACT

The realistic interpretation of seismic travel-time data from structurally complex areas, and the accurate location of earthquake hypocenters in such areas, require seismic ray computations for laterally inhomogeneous velocity models. Numerical simulation of the ray differential equations provides a practical means of performing the necessary calculations. In addition to the calculation of travel-time, the ray intensity and the partial derivatives of travel-time with respect to the parameters of the model may be calculated. Results from such numerical simulations are in excellent agreement with those analytically obtainable for a simple constant gradient velocity model. An algorithm for the direct solution of ray boundary value problems, based on the iterative solution of a tridiagonal set of simultaneous equations, allows for the input of geophysical intuition in finding the rays between a source and a station.

A model fitting procedure is described for laterally inhomogeneous models which is based on the description of a velocity model by combinations of simple continuous functions which are chosen to reflect the available geologic data. A least squares scheme is used to obtain models which fit the travel-time data and are consistent with geologic data. Laterally inhomogeneous velocity models are obtained for

travel-time data from explosions for two areas in California: the Bear Valley area, 25 miles southeast of Hollister, and the Borrego Mountain area, 100 miles northeast of San Diego. Both regions are characterized by a substantial lateral variation of seismic velocity and the derived models exhibit most of the significant structural features of the areas. The Bear Valley explosion is relocated in the velocity model as a test for the validity of the model and of a computational procedure for the location of hypocenters in structurally complex areas.

ACKNOWLEDGMENTS

The author is indebted to Professor Robert L. Kovach for his encouragement, patience and guidance throughout this study. Professor Kovach initially stimulated my interest in ray tracing and encouraged me to work with real data. Discussions with Professor Jon F. Claerbout resulted in many useful ideas including the investigation of time integration and the description of velocity models with simple functions. Professor Claerbout also offered needed encouragement regarding the tridiagonal matrix formulation. Discussions with Dr. Jerry P. Eaton of the National Center for Earthquake Research, U.S.G.S., about crustal refraction work and locating earthquakes in Central California provided motivation for the crustal application of numerical ray tracing. Dr. Eaton also generously provided the data from the Bear Valley area. Dr. Robert M. Hamilton, also of the U.S.G.S., provided the data from the Borrego Mountain area in advance of publication.

The theoretical competence of my colleague Dr. Teddy G. Zengeni gave me the courage to explore the foundation of ray theory. Russell Robinson listened patiently to some of my wilder ideas and offered constructive criticism. Bruce D. Smith was a valuable resource on the geology and structure of the Hollister trough. Joan Gast typed the majority of the manuscript.

I am delighted to acknowledge the support which made my graduate studies possible: McCurdy Fellowship (1966-67), National Science Foundation Traineeship (1967-68) and Pan American Petroleum Foundation Fellowship (1968-69). This research was supported by the Advanced Research Projects Agency and was monitored by the Air Force Office of Scientific Research under contract AF 49(638)-1687. Support was also provided by NASA grant NGL 05-020-232.

My wife, Corki, alternated between enthusiasm, patience and delightful skepticism. To her I am most deeply indebted.

TABLE OF CONTENTS

LIST OF ILLUSTRATIONS

LIST OF TABLES

I. INTRODUCTION

Seismologists have in the past relied almost exclusively on layered models of earth structure, either flat or spherical, for the interpretation of seismic data for several reasons: 1) to first order the earth is a layered sphere; 2) adequate data to detail the deviations from the layered case were not available and 3) useful theoretical and computational tools did not exist for the interpretation of such data. Recently, however, the existence of important lateral variations has become increasingly obvious and digital computers have made it possible to escape from the narrow confines of analytically obtainable solutions and utilize numerical solutions.

Various numerical approaches present themselves for the solution of the wave propagation problems of seismology. Alterman and Karal (1968) and Boore (1970) have used direct numerical integration of the wave equation to obtain solutions to surface wave problems, Boore for laterally inhomogeneous situations. Claerbout (1970) has described techniques whereby trial solutions are inserted into the wave equation to obtain difference equations which may be integrated to obtain amplitude and phase maps for laterally inhomogeneous structures. This thesis is directed to numerical techniques based on ray theory and their applications in seismology. Ray theory for inhomogeneous media has been studied extensively for electromagnetic waves (Kline and

Kay, 1965). Karal and Keller (1959) and Vlaar (1969) have studied ray theory for elastic solids. Ugincius (1969) has made both theoretical and numerical computational studies of ray theory in laterally inhomogeneous media in regard to underwater sound propagation. Russian investigators (Burmakov & Oblogina, 1968; Belonosova, et al. 1967) have made limited attempts at the numerical integration of ray equations for application to seismology.

The history of the application of ray theory to seismology is intimately tied to the history of seismology itself. The fundamental inferences about the structure of the earth are based on ray theory through the Wiechert-Herglotz inversion procedure. Classical seismological ray theory based on the assumption of radial symmetry, i.e., velocity a function of one coordinate only, converts the differential equations for rays to integrals usually involving radius or depth as a variable of integration. Such methods have been detailed by Bullen (1963), Jeffreys (1962), Slichter (1932) and others and have proven immensely useful in understanding the structure of the earth, but such methods are not easily modified to account for lateral inhomogeneities. A notable exception is the method of time-term analysis originally due to Scheidigger & Willmore (1957) and expanded by Berry and West (1966 a & b). This method has proven quite successful in the treatment of the case of a constant velocity medium, or flat lying layers resting on an undulating basement of relatively fast velocity, provided the dips involved are small.

The laterally inhomogeneous nature of the earth's crust is obvious to anyone possessing a rudimentary knowledge of geology. This observation is born out, in terms of seismology, by the multitude of crustal refraction profiles to date. Sedimentary basins, large scale faults, intrusions and mountain ranges all are examples of laterally inhomogeneous structures of interest to seismologists. Documentation for the laterally inhomogeneous nature of the earth's mantle is less abundant, but still difficult to refute. Seismological observations include those by Bolt and Nuttli (1966), Otsuka (1966 a & b), Hales, et al.(1968), Oliver and Isacks (1967) and others. The definition of velocity inhomogeneities in the upper mantle is extremely difficult for at least three reasons. First, we see the mantle only through the crust, which because of its complex structure tends to blur and confuse our observations. Secondly, the amount of data available is insufficient to resolve detail in the mantle. Thirdly, our knowledge of the inter-relationship between crust and mantle is not yet at a point where we can use surficial geology as an unambiguous guide to mantle structure. In other words, in attempting to define velocity variations in the crust, we can use surficial geology as a constraint. At the present time this can only be done in the most general way for the mantle.

This thesis briefly reviews the bases for ray theory in an appendix. The body of the thesis describes briefly

how these results may be used to calculate travel-times, apparent velocities, ray intensities (or amplitudes) and their partial derivatives with respect to model parameters. The application of these calculations to the seismological problems of finding velocity models and hypocenter location are explored.

These techniques are then applied to seimic data obtained in two regions in California: Bear Valley, 25 miles southeast of Hollister along the trace of the San Andreas fault and the Borrego Mountain area 100 miles northeast of San Diego in the San Jacinto fault zone. Both of these areas are characterized by complex geologic structure and possess large lateral variations in seismic velocity. Each of these areas was also the scene of a large aftershock sequence. Three-dimensional velocity models are constructed for each of these areas based on seismic refraction data and the use of these models to locate earthquakes is demonstrated.

II. THEORY

The calculation of seismic rays for laterally inhomogeneous media rests on the numerical solution of the equation

$$\frac{d}{ds}\left(\frac{1}{c}\cdot\frac{d\vec{r}}{ds}\right) = \nabla(1/c)$$

where s is arc length along the ray, $\vec{r}(s)$ is the space curve defining the ray and $c = c(\vec{x})$ is the seismic velocity (compressional or shear) as a function of position. The solution of this differential equation for $\vec{r}$ yields the geometry of the ray and sufficient information to calculate the travel time and apparent velocity. The derivation of this equation can be found in Appendix A. This chapter discusses two questions of fundamental geophysical interest: 1) How to determine a velocity model from a set of travel-time data for a laterally inhomogeneous region and 2) How to use a velocity model derived for such a region to locate explosions or earthquakes.

Derivation of a velocity model

For an assumed one-dimensional velocity function, the Wiechert-Herglotz inversion procedure provides a unique construction of a velocity model given a curve of apparent velocity versus distance (Bullen, 1963). This construction requires that no discontinuities exist in the velocity function

and that it is a monotonically increasing function, except for small reversals less than a critical amount. When discontinuities or low velocity zones are present the method becomes formally non-unique although in practice it is possible to use geophysical intuition and auxiliary data to reduce the ambiguity. At the present time there is no analogous method for obtaining a two-or three-dimensional velocity distribution. It is unlikely that such a method will be found because the Wiechert-Herglotz method relies on an integral formulation of ray theory which does not lend itself to generalization to more than one dimension.

Lacking such a constructive method, we are faced with the prospect of "model fitting," i.e. an iterative process, based either on trial-and-error or a systematic perturbation of the trial model until the calculated quantities agree with the observations. Once agreement is obtained the question of whether the model is unique remains. This problem is a special case of the so-called "geophysical inverse problem" which has been discussed by many authors, notably by Backus and Gilbert (1967, 1968, 1969) and Backus (1970). These authors have attacked the general problem of the inversion of geophysical data in a very general and elegant manner. Although formally most of their results apply only to a spherical, one-dimensional earth, their ideas may be applied in an intuitive way to the three-dimensional velocity

distribution problem. Because the set of possible models is continuous, the number of possible models is infinite. Because we can only hope for a finite number of observations, the resolving power of these observations is also limited and gives rise to non-uniqueness. This problem is not usually severe because normally the limited resolving power gives to a set of relatively similar models. More problematical, Backus and Gilbert (1967) demonstrate that for each model which fits the data exactly, there exists a family of models which satisfy the data. The most severe difficulty, however, is that substantially different families of models may exist.

The object of the present work is to determine velocity models which in some sense satisfy travel time data in addition to constraints imposed by other data, in particular surface geology. Four methods have been used for obtaining models which fit travel time data: 1) trial-and-error; 2) Monte Carlo; 3) iteration with an underdetermined system used as a constraint to fit the data exactly and least squares used to minimize something like the difference between the old and new models (cf. Backus and Gilbert, 1969); and 4) iteration with least squares used on an overdetermined system. The first three methods have been widely applied to analyses of mantle travel time data. The fourth method has the disadvantage that it requires more observations than unknown parameters. This is unrealistic in that the real earth is

sufficiently complicated to require an infinite, continuous distribution of parameters for an accurate description. On the other hand, certain general features of the velocity distribution in the earth may be inferred from other geologic and geophysical data to suggest the form of a relatively simple function or combination of simple functions. Such a function or functions would not form a "complete" set in the sense of orthogonal functions, but they can provide a relatively accurate description of the average structure with a vastly reduced number of parameters.

For example, suppose we wish to describe a velocity model in a cube of side L. Suppose that the dimension of the smallest structural detail which we wish to appear in the model is ℓ. Then the number of points required on an evenly spaced grid, or the number of coefficients of orthogonal functions, required for an adequate description is of the order of $(L/\ell)^3$. On the other hand, if we use simple functions to describe the individual geologic features of interest there is no such relationship. The number of parameters required depends more or less linearly on the number of features described. The philosophical question which arises is whether the description of the model should include many more unknowns than observations or should geological evidence be used to limit the number of unknowns.

Partial derivatives of travel time with respect to model parameters

For purposes of deriving a velocity model from a set of observational data it is useful to calculate the change in travel-time between the observation points with respect to perturbations in the velocity model. It is thus useful to consider velocity as a function of the space coordinates through a set of N parameters p_i. A particular model may, therefore, be represented as a point in parameter space, and a set of similar models may be represented by a cluster of points in parameter space. Define a velocity c

$$c = c(\vec{x};\bar{p})$$

where $\vec{x}$ is a three-dimensional position vector and $\bar{p}$ is an N-dimensional vector of parameters. The desired result is a set of partial derivatives of the travel-time between each source-station pair with respect to the parameters p_i. The time required to move along a ray is

$$T = \int_{\text{along the ray}} \frac{ds}{c} \qquad 2.1$$

A slight perturbation in the velocity c will change the integral in 2.1 in two ways. First, the path of the ray will be changed slightly. Secondly, the time required to

traverse each segment of the ray will be perturbed. To first order, Backus and Gilbert (1969) have argued that the change in the path may be neglected and the integration of the velocity perturbation may be carried out along the unperturbed path. Formally, this amounts to differentiating with respect to the parameter through which the model is perturbed

$$\frac{\partial T}{\partial p_i} = \int_{\text{along the ray}} -\frac{1}{c^2}\frac{\partial c}{\partial p_i}\, ds \qquad 2.2$$

This integration may be carried out numerically once the path of the ray is known.

Many investigators have obtained expressions for partial derivatives of travel time with respect to model parameters for application to one-dimensional velocity functions including Jeffreys (1966), Julian and Anderson (1968), Archambeau et al. (1969) and Backus and Gilbert (1969).

Least Squares Model Fitting

Consider a vector of M observations of travel-time $\bar{T}_{obs}$ and calculate a vector of travel-times $\bar{T}_{calc}$ for corresponding points for a trial velocity model together with a matrix of partial derivatives of the travel-time between the i^{th} source station pair with respect to the j^{th} parameter of the velocity

model. Also define a vector of residuals

$$\bar{T}_{obs} = \begin{bmatrix} T_{obs_1} \\ \cdot \\ \cdot \\ \cdot \\ \cdot \\ T_{obs_m} \end{bmatrix}, \quad \bar{T}_{calc} = \begin{bmatrix} T_{calc_1} \\ \cdot \\ \cdot \\ \cdot \\ T_{calc_m} \end{bmatrix}, \quad \bar{R} = \begin{bmatrix} T_{obs_1} - T_{calc_1} \\ \cdot \\ \cdot \\ \cdot \\ T_{obs_m} - T_{calc_m} \end{bmatrix}$$

$$\tilde{P} = \begin{bmatrix} \frac{\partial T_{calc_1}}{\partial p_1} & \cdots & \frac{\partial T_{calc_1}}{\partial p_n} \\ \cdot & & \cdot \\ \cdot & & \cdot \\ \cdot & & \cdot \\ \frac{T_{calc_m}}{\partial p_1} & \cdots & \frac{\partial T_{calc_m}}{\partial p_n} \end{bmatrix} \qquad 2.3$$

We seek to perturb the initial velocity model (with parameters $\bar{p}_0$) by a small vector $\delta\bar{p}$ so as to reduce the sum of squares of the residuals. Write the time calculated with the perturbed model $\bar{T}_{calc\text{-}new}$ as a first order Taylor series in parameter space about $\bar{p}_0$,

$$\bar{T}_{\substack{calc \\ new}} = \bar{T}_{\substack{calc \\ old}} + \tilde{P}\ \delta p \qquad 2.4$$

We hope to minimize the sum of squares of the new residual vector

$$\bar{R}_{new} = \bar{T}_{obs} - \bar{T}_{calc_{new}} \qquad 2.5$$

Making use of equations 2.3 - 2.5 we obtain for the sum of the squared error

$$S.S.E. = \bar{R}^{T}_{new}\,\bar{R}_{new} = \left(\bar{R}_{old} - \hat{P}\delta p\right)^{T}\left(R_{old} - \hat{P}\delta\bar{p}\right) \qquad 2.6$$

Differentiating with respect to $\delta\bar{p}^{T}$, setting the partial derivative of the error equal to zero and solving for $\delta\bar{p}$ we obtain the standard least squares result

$$\delta\bar{p} = \left(\tilde{P}^{T}\tilde{P}\right)^{-1}\tilde{P}^{T}\,\bar{R}_{old} \qquad 2.7$$

Because the problem is non-linear, the convergence procedure is iterative.

This procedure seeks a minimum of error. In fact, there may be more than one minimum. If there exist multiple minima, there is no way except comparison of the associated error values to distinguish the global minimum. If two or more minima corresponding to different models yield similar

values of the sum squared error, the selection between them must be based on other data. It thus may be desirable to include a weighting scheme to reduce biases due to data quality and distribution.

Hypocenter location

The Taylor series expansion of the travel-time about the source location is

$$T_{\substack{calc \\ new}} = T_{\substack{calc \\ old}} + \frac{\partial T}{\partial x}\delta x + \frac{\partial T}{\partial y}\delta y + \frac{\partial T}{\partial z}\delta z \qquad 2.8$$

where x, y, z are the coordinates of the trial focus and $x + \delta x$, $y + \delta y$, $z + \delta z$ will be the coordinates of the new trial focus. Once we obtain the partial derivatives $\partial T/\partial x$ etc., the solution to the location problem proceeds in a fashion analogous to the travel time problem.

We seek to obtain the partial derivatives of the travel-time along the path between the source and the station with respect to the coordinate of the source. The rate of change travel-time with respect to arc length along the ray is

$$\frac{dT}{ds} = \frac{1}{c} \qquad 2.9$$

The quantity dT/ds is the directional derivative along the ray

$$\frac{dT}{ds}\hat{t} = \frac{1}{c}\hat{t} \qquad 2.10$$

where $\hat{t}$ is the unit tangent vector along the ray. The right hand side of 2.10 is just the slowness vector $\vec{L}$. The components of the left hand side represent the projections of dT/ds onto the coordinate axes, dT/dx, dT/dy and dT/dz. The result is that the vector of partial derivatives is

$$\begin{bmatrix} \partial T/\partial x \\ \partial T/\partial y \\ \partial T/\partial z \end{bmatrix} = \vec{L} \qquad 2.11$$

From Figure A.2 it may be seen that if the ray is traced from the source to the station the vector $-\vec{L}_0$ will yield the desired partial derivatives.

III. COMPUTATIONAL METHOD

Rays

Two methods of integrating the ray equations have been explored, each useful in different circumstances. The more straightforward method, simple Runge-Kutta integration, treats a ray as an initial value problem; that is a ray is traced from a given starting point in a given direction. Frequently, however, the particular ray between an event and a station is required. This constitutes a two-point boundary value problem. If close approximations to the starting values for the corresponding initial value problem are known, it is often possible to iterate such initial value problems to find the solution to the desired boundary value problem. Unfortunately it is not generally possible to make sufficiently accurate guesses at the starting values for the initial value problem *a priori* for this method to be of universal application. A direct method for the solution of the boundary value problem by means of tridiagonal matrices is more appropriate.

Initial value problem

A second-order Runge-Kutta scheme was selected for the initial value problem. This scheme provides an improvement in speed and accuracy over simple point slope methods, but requires more evaluations of the velocity function and its spatial derivatives. The basic equations used which relate

the values of position vector $\vec{r}_n$, slowness vector $\vec{L}_n$ and time t_n to their respective values at $t_{n+1} = t_n + \delta t$ are (simulating Equations A.15 and A.17)

$$\vec{r}_{n+1} = \vec{r}_n + \frac{1}{2} (\vec{k}_1 + \vec{k}_3)$$

$$\vec{L}_{n+1} = \vec{L}_n + \frac{1}{2} (\vec{k}_2 + \vec{k}_4) \qquad 3.1$$

where

$$\vec{k}_1 = c^2(\vec{r}_n)\ \vec{L}_n\ \delta t$$

$$\vec{k}_2 = - \frac{1}{c(\vec{r}_n)} \nabla c(\vec{r}_n)\ \delta t$$

$$\vec{k}_3 = c^2(\vec{r}_n + \vec{k}_1)\{\vec{L}_n + \vec{k}_2\}\ \delta t$$

$$\vec{k}_4 = - \frac{1}{c(\vec{r}_n + \vec{k}_1)} \nabla c(\vec{r}_n + \vec{k}_1)\ \delta t$$

The truncation error for this simulation is of order $(\delta t)^3$ (Hildebrand, 1968).

Given the initial values of position vector $\vec{r}_0$ and slowness vector $\vec{L}_0$, the ray "shoots" out integrating in

time. Curves of travel time, partial derivatives of travel time with respect to model parameters and intensity versus distance for a simple velocity model, $c = 5.0 + .1z$, are shown in Figures 3.1 and 3.2. All these quantities were calculated using the second-order Runge-Kutta scheme. Calculations for this simple model permit comparison with the analytic results found in Officer (1957). The agreement of the values obtained numerically with analytical values is exact within the accuracy of the plots, except very near $x = 0$ where the total travel time is the order of a few time steps. Agreement here could be obtained by reducing the time step. In practice, where no analytic solutions are available for comparison, the most practical test for convergence to the true value is simply to repeat the calculation with a reduced time step. If the resulting value is the same as the calculated with the full time step, convergence may be assumed. In most realistic examples attempted, a time step of between 0.25 seconds and 0.05 seconds was found to give good convergence. The smaller values were only required for models containing very steep velocity gradients.

Boundary Value Problem

Runge-Kutta integration may be used to solve the problem of finding the ray between two points by iteration using the partial derivatives of position with respect to the initial take-off angles and estimating the required perturbations

in these angles. These derivatives may be calculated directly by integrating equations A.26 or estimated by tracing several rays.

The alternate approach is to solve the boundary value problem directly. So-called "two-point" boundary value problems for second order differential equations have been studied from the point of view of numerical solution; such methods are described in Fox (1957), Hildebrand (1968), and Henrici (1962). Such methods require equations of the form

$$\frac{d^2y}{dx^2} + G(x, y) = 0 \qquad 3.2$$

where the solution y(x) is sought on an interval (a, b) and the values of y are specified at the end points

$$y(a) = A$$
$$y(b) = B \qquad 3.3$$

In terms of rays, this approach changes the method of attach from "tracing" a ray to"finding" a ray. Instead of shooting rays out, hoping that one will intersect the desired point, we construct a curve between the event and the station and then distort the trial curve until it satisfies the differential equation and, therefore, becomes a ray. The requirement that the solution be sought on a known interval with

specified values at the end points, forces us to abandon the parametric description of a ray by means of time or arc length. We must eliminate the parameter so that the interval over which the solution is sought will be predetermined. In other words, in a parametric description of the ray, x(t), y(t), z(t), the value of the parameter t is known at the initial end but not at the final end until the ray is found. On the other hand, if one of the space coordinates may be used as the independent variable, say y(x), z(x), then the values of x are known at both ends of the ray and the boundary value problem is well posed.

Consider a transformation of coordinates with a new origin so placed that the source lies on the z axis and the station also lies in the x-z plane (Fig. 3.3). Then the known y and z coordinates of the source and station will be the values of the solution at the two end points of the known interval in x. We seek to transform the differential equation for the ray (equation A.19)

$$\frac{d}{ds}\left(\frac{1}{c}\frac{d\vec{r}}{ds}\right) = \nabla(1/c)$$

into an equation with x as the independent variable considering only the geometric properties of the ray. Consider the angle, θ, between the ray at each point and the

x-axis. This angle is defined by the direction cosine between the ray and the axis

$$\cos \theta = \frac{dx}{ds} \qquad 3.4$$

where dx is an increment along the x-axis corresponding to an increment of arc length ds. The differential equation for the unknown coordinates of the ray in the independent variable x then becomes

$$\cos \theta \quad \frac{d}{dx}\left(\frac{\cos\theta}{c} \quad \frac{d\vec{u}}{dx} \right) = \nabla(1/c) \qquad 3.5$$

where $\vec{u}$ is the vector of y and z components $\vec{u} = (y, z)$. Imagine the line segment along the x-axis corresponding to the ray divided into equal segments of length h. Then we may simulate equation 3.5 with a difference equation. Taking a central difference for the interior derivative, associating a $\cos\theta$ with each term and then taking another central difference for the derivative outside the parenthesis we obtain

$$\frac{\cos \theta_i}{h^2}\left[\frac{\cos \theta_{i-1/2}}{c_{i-1/2}} \vec{u}_{i-1} - \left(\frac{\cos\theta_{i-1/2}}{c_{i-1/2}} + \frac{\cos\theta_{i+1/2}}{c_{i+1/2}} \right) \vec{u}_i \right.$$

$$\left. + \frac{\cos \theta_{i+1/2}}{c_{i+1/2}} \vec{u}_{i+1} \right] = \nabla(1/c_i) \qquad 3.6$$

To obtain an expression for cos θ_i we use a finite approximation to 3.4

$$\cos \theta_i = \frac{h}{\delta s_i}$$

where h is the interval between successive values of x and

$$\delta s_i = (h^2 + (y_{i+1/2}-y_{i-1/2})^2 + (z_{i+1/2}-z_{i-1/2})^2)^{1/2}$$

Since equation 3.6 is non-linear it must be solved iteratively; therefore the apparently cumbersome form of δs_i is no disadvantage. For the initial guess at the solution it will be necessary to compute the square roots, but in successive iterations the changes to δs_i will normally be small and it is possible to use the first few terms of a binomial series expansion for their calculation.

Writing an equation of the form 3.6 for each point on the ray, we obtain

$$\tilde{A}\vec{v} = \vec{g} \qquad 3.7$$

where

$$b_i = (\delta s_{i+1/2}\ c_{i+1/2})^{-1}, \quad a_i = -b_{i-1}-b_i$$

$$\hat{A} = \begin{bmatrix} a_1 & o & b_1 & o & & & & \\ o & a_1 & o & b_1 & & & & \\ b_1 & o & a_2 & o & b_2 & o & & \\ o & b_1 & o & a_2 & o & b_2 & & \\ & & b_2 & o & \ddots & & \ddots & \\ & & o & b_2 & & \ddots & & \ddots \\ & & & & & & b_{n-2} & o & a_{n-1} & o \\ & & & & & & o & b_{n-2} & o & a_{n-1} \end{bmatrix}$$

$$\vec{v} = \begin{bmatrix} y_1 \\ z_1 \\ y_2 \\ z_2 \\ \vdots \\ y_{n-2} \\ z_{n-2} \\ y_{n-1} \\ z_{n-1} \end{bmatrix} \qquad \vec{g} = \begin{bmatrix} \vec{\gamma}_1 - b_0 \begin{bmatrix} y_0 \\ z_0 \end{bmatrix} \\ \vec{\gamma}_2 \\ \vdots \\ \vec{\gamma}_{n-2} \\ \vec{\gamma}_{n-1} - b_n \begin{bmatrix} y_n \\ z_n \end{bmatrix} \end{bmatrix}, \quad \vec{\gamma}_i = -\delta s_i \begin{bmatrix} \frac{\partial}{\partial y}\left(\frac{1}{c_i}\right) \\ \frac{\partial}{\partial z}\left(\frac{1}{c_i}\right) \end{bmatrix}$$

The boundary conditions

$$\vec{v}(a) = \begin{bmatrix} y_0 \\ z_0 \end{bmatrix}, \quad \vec{v}(b) = \begin{bmatrix} y_n \\ z_n \end{bmatrix}$$

have been included in the definition of $\vec{g}$. Note that the two equations for y and z decouple at this stage, but the iterative algorithm used to solve this non-linear system will introduce coupling.

Denoting the trial solution at some stage with a superscript, $\vec{v}^{(j)}$, the error at this stage will be

$$\vec{e}^{(j)} = \underset{\sim}{A}^{(j)}\vec{v}^{(j)} - \vec{g}^{(j)} \qquad 3.8$$

We use an adaptation of Newton's method for finding roots described by Henrici (1962) to find a new trial solution

$$\vec{v}^{(j+1)} = \vec{v}^{(j)} + \delta\vec{v}^{(j)} \qquad 3.9$$

chosen so as to attempt to make the new error $\vec{e}^{(j+1)}$ equal to zero, i.e.

$$0 = \underset{\sim}{A}^{(j+1)}\, v^{(j+1)} - \vec{g}^{(j+1)} \qquad 3.10$$

Using 3.9 to expand $\vec{g}^{(j+1)}$ in Taylor series about $\vec{v}^{(j)}$ and assuming $\underset{\sim}{A}^{(y+1)} \approx \underset{\sim}{A}^{(j)}$ we have

$$0 = \hat{A}^{(j)}\,\vec{v}^{(j)} + \hat{A}^{(j)}\,\delta\vec{v}^{(j)} - \vec{g}^{(j)} - \hat{P}^{(j)}\,\delta\vec{v} \qquad 3.11$$

where

$$\hat{P} = \begin{bmatrix} \dfrac{\partial g_{y_1}}{\partial y} & \dfrac{\partial g_{y_1}}{\partial z} & & & \\ \dfrac{\partial g_{z_1}}{\partial y} & \dfrac{\partial g_{z_1}}{\partial z} & & & \\ & & \ddots & & \\ & & & \dfrac{\partial g_{y_{n-1}}}{\partial y} & \dfrac{\partial g_{y_{n-1}}}{\partial z} \\ & & & \dfrac{\partial g_{z_{n-1}}}{\partial y} & \dfrac{\partial g_{z_{n-1}}}{\partial z} \end{bmatrix}$$

Making use of 3.8 and the fact that $\hat{A}$ and $\hat{P}$ are conformable we have

$$-\vec{e}^{(j)} = \hat{A}'^{(j)}\,\delta\vec{v}^{(j)} \qquad 3.12$$

where

$$\hat{A}'^{(j)} = \hat{A}^{(j)} + \hat{P}^{(j)}$$

Equation 3.12 may be easily solved for $\delta\vec{v}^{(j)}$ because $\hat{A}^{(j)}$ is a block tridiagonal matrix, composed of 2x2 blocks. Such systems may be solved very rapidly using a variation of Gaussian elimination described by Richtmeyer and Morton (1967). The iterative procedure is repeated until either the r.m.s. error is less than some value

$$\sqrt{\frac{\vec{e}^{T}\vec{e}}{N}} < \varepsilon \qquad 3.13$$

or until the change in the integral of time along the ray is very small.

Once the geometry of the ray is described by the set of coordinates, it is straightforward to calculate the travel time and other desired ray quantities by summing the appropriate quantities along the ray. For example, for travel time, this amounts to Fermat's principle

$$T = \int_{\text{along the ray}} \frac{ds}{c} \approx \sum_{i=1} \frac{ds_i}{ci} \qquad 3.14$$

Choice of Method

Whether the Runge-Kutta integration or the tridiagonal

matrix technique is used for a particular ray problem depends on 1) whether the problem at hand is an initial value problem or a boundary value problem and 2) the complexity of the velocity model and the manner in which it is specified.

The advantages of the Runge-Kutta technique are 1) only the first derivatives of the velocity model are required and 2) the traced curve is certain to be a ray (provided a small enough time increment is used). The disadvantages of the method occur in the solution of boundary value problems. Only crude estimates of the initial values (take-off angles) required to solve a given boundary value problem are possible and the ray is quite sensitive to these parameters. The primary advantages of the tridiagonal matrix technique are, on the other hand, the ease with which reasonable trial rays for boundary-value problems are selected and the relative insensitivity of the solution to a trial guess slightly in error. These advantages arise from the fact that the first trial guess is actually a space curve connecting the source and station which is chosen to be a good guess at the final ray shape based on geophysical experience. For example, consider a simple continuous velocity model consisting of a relatively low velocity region near the surface, increasing rapidly at some depth to a higher velocity. Experience suggests that for some distance range there will be a triplication of the travel

time curve, corresponding to three rays: 1) a direct ray through the low velocity region 2) a ray refracted from the zone of rapid increase and 3) a ray refracted from slightly deeper in the zone of increase. Given the added complexity of any lateral variation the selection of take-off angles corresponding to the different arrivals is very difficult. On the other hand the selection of trial ray curves which go through the regions known to be required for a particular arrival is relatively straightforward. The two disadvantages of the tridiagonal matrix method are 1) second derivatives of the velocity model are required and 2) frequently convergence of the solution is slow. The second disadvantage is not severe, however, because once the ray is approximately found (after a few iterations) the travel-time is relatively insensitive to further refinement.

The conclusions are 1) for initial value problems use the Runge-Kutta method, 2) for boundary value problems in velocity models for which the second derivatives are difficult or impossible to obtain use the Runge-Kutta method with iteration of initial values, 3) for boundary value problems in models for which the second derivatives are obtainable use the tridiagonal matrix method.

Description of Velocity Model

Theory places comparatively few restrictions on the way in which the velocity model is specified. The restrictions

imposed by practicality are more severe. For all purposes except the calculation of partial derivatives with respect to model parameters, a tabular or three-dimensional grid specification would be adequate, provided that the interpolation scheme maintained continuity of the first derivatives, and preferably the second, except at specified discontinuities. The importance of continuity of derivatives is discussed by Wesson (1970) but a feeling for this sensitivity may be obtained from observation of the ray differential equation A.19. The explicit dependence of this equation on $\nabla(1/c)$ demonstrates that artificially induced discontinuities in this quantity will produce spurious results. An interpolation scheme which guarantees continuity of the first derivative is not unduly difficult, however, and may be executed using the technique of Snyder (1961). The central difficulty of using the velocity specified on a three-dimensional grid is the awkwardly large amount of storage required. Satisfactory solution of this problem requires clever use of computer storage.

Combinations of simple analytic functions were chosen for the description of models in this work. The essential criterion for these functions is that they be well behaved away from the region of immediate interest. For this reason, rational functions are particularly appealing. A function found useful for abrupt one-dimensional velocity changes is:

to divergence of the successive iterations. A more prudent approach is to adopt the algorithm proposed by Marquardt (1963). In essence this algorithm proposes the solution of the alternate system:

$$(\hat{P}^T\hat{P} + \lambda\hat{I})\ \delta\bar{p} = \hat{P}^T R$$

where $\hat{I}$ is the identity matrix and λ is a scalar to be determined. Note that as $\lambda \to 0$ the new system returns to ordinary least squares. This will be appropriate near the minimum where, hopefully, the problem is nearly linear. As $\lambda \to \infty$ the direction of $\delta\bar{p}$ will approach that of the right hand side of equation 3.17, $\hat{P}^T\bar{R}$. This vector is, to a scale factor, the negative gradient of the sum squared error. This may be shown simply by calculating the gradient. The definition of sum squared error is

$$\underset{\text{old}}{\text{S.S.E.}} = \sum_i (T_{obs_i} - T_{calc_i})^2.$$

Diferentiating with respect to p_j and making use of the definition of $\bar{R}$ (Equation 2.3) yields

$$\frac{\partial \text{S.S.E.}}{\partial pj} = -2 \sum_i R_i \frac{\partial T_{calc_i}}{\partial pj}$$

Again using the definitions of equation 2.3, we have

$$\text{grad (S.S.E.)} = -2P^{WT}R. \qquad \text{Q.E.D.}$$

As $\lambda \to \infty$ however $|\delta\bar{p}| \to 0$, so we have shorter and shorter steps closer to the negative gradient. The strategy of this technique is as follows: If for some value of λ, the correction $\delta\bar{p}$ reduces the error, decrease λ. If it increases the error, increase λ. Unless a minimum is currently occupied, a small enough step in the direction of the gradient must always reduce the error.

A simple test of the solution of the model improvement equations is illustrated in Figure 3.4. Travel-times were calculated to an arbitrary array of 13 stations distributed in an area of about 50 km. diameter about a point approximately in the center. The travel-times were calculated for a simple constant gradient velocity model $c = 5.0 + .1z$. Using these calculated times as data the least squares algorithm started from an initial model of $c = 4.0 + .02z$. After eight iterations the r.m.s. residual at the 13 stations was .0002 seconds and the model was $5.000 + .1008z$. As a further test of stability, a random error selected from a population with zero mean and standard deviation, $\sigma = .05$, was added to each of the calculated times. The convergence for this data with simulated reading error is shown in Figure 3.5. The r.m.s. residual after seven iterations was .058 seconds and the resulting model $c = 4.961 + .1355z$. The difference between the noise-free and noisy models gives

some idea of the resolving power of travel-time data.

IV. GEOLOGIC APPLICATION

Bear Valley Area

The Bear Valley Area lies 25 miles southeast of Hollister in the Coast Ranges of California, astride the trace of the San Andreas Fault (Figure 4.1). The fault zone forms the contact between two very different types of basement rock. Figure 4.2 is a generalized geologic map of the area. Southwest of the northwest-southeast trending fault, granite of Mesozoic age forming a "granitic-metamorphic core complex" is topographically expressed as the Gabilan Range. Within the Gabilan Range, separated from the granite by north-south trending faults are rhyolites and pyroclastic deposits of Miocene age. Topographically, these deposits form the familiar Pinnacles. The Salinas Valley forms the western margin of the Gabilan Range. Toward the southern end of the range the granite is covered with an increasingly thick mantle of sedimentary rocks. Northeast of the fault zone the "Franciscan eugeosynclinal core complex" of Jurassic-Cretaceous age forms the basement. Greywackes predominate, but the complex includes shales, greenstones, and ultramafic rocks. The internal structure of the Franciscan is complicated and discontinuous. Some of the rocks have been subjected to high pressure-low temperature metamorism. These rocks rise in a broad anticline to form the core of the Diablo Range.

The fault zone ocupies a broad structural trough, trending subparallel to the fault zone, bounded on the southwest

by the San Andreas and Bear Valley faults and to the northeast by the anticlinal structure of the Diable Range. Located in this truncated synclinal structure, which overlies the Franciscan formation, are Upper Cretaceous marine sediments and Tertiary sediments. The fault zone itself is approximately five km wide in which slivers of the various rock groups are juxtaposed, although they are predominately Tertiary in age. Interspersed in the fault zone are pods of ultrabasics, usually serpentine. Some distinct fault strands have been mapped: the San Andreas, Bear Valley, Paicines and San Benito faults.

A recent and detailed review of the geology of the Coast Ranges has been given by Page (1966). More specific descriptions of the geology of the Bear Valley area have been given by Andrews (1936) and Wilson (1943). A synthesis of the geology and geophysics of the region may be found in Smith (1970).

Motivated by a desire to test for bias in the routine location of earthquakes in this region, the National Center for Earthquake Research set up a temporary seismometer array in this area during the summer of 1967. To derive a velocity model and station corrections for hypocenter location two shots were detonated in the general area. For this work the shot in Bickmore Canyon, about three kilometers southeast of Bear Valley was used. The other shot was located about 50 km to the northeast, somewhat north of the termination of the Gabilan Range.

The station locations and travel-time data for this shot are given in Table 4.1. A plot of the travel-time data reduced

to 6.0 km/sec is shown in Figure 4.3. The lower group of stations and the shot were located southwest of the fault on granite or on sediments presumably underlain by granite. The upper group of stations (except HP8) lie northeast of the fault on sedimentary rocks underlain by the Franciscan formation or on the Franciscan formation directly. HP8 was located directly in the fault zone and is apparently underlain by a large thickness of sediments. It was excluded from the subsequent analysis for computational convenience. The wide separation of the two groups of stations readily indicates that a one-dimensional velocity model cannot explain the data with an rms error of less than about 0.4 seconds.

To facilitate the model fitting a cartesian coordinate system was laid out based on Richter's method of calculation of short distances (1958). The coordinates were then translated and rotated so that one of the axes was coincident with the average strike of the San Andreas fault zone. The resulting coordinate system is centered 16.30 km due north of 36°30' north latitude 121°15' west longitude with the y axis striking N48.4° W (Figure 4.2).

The first attempt to fit the data was made with a simple vertical fault model with a constant velocity gradient in the z-direction

$$c = c_0 + c_1 z + \frac{A(x-x_0)}{\varepsilon^2 + |x-x_0|} \qquad 4.1$$

In this model x_0 is the position of the fault, x is the distance away from the fault, $c_0 + A$ and $c_0 - A$ are the maximum and minimum velocities on opposite sides of the fault in the plane z=0, $2\epsilon^2$ is the bandwidth of the change in velocity across the fault and c_0 is the velocity gradient with depth z.

The best fitting model of this analytic form, Model I, yields an r.m.s. residual of slightly less than 0.1 sec. A SW-NE cross section, A-A', representative of this model is shown in the top half of Figure 4.4. As might be expected the model is characterized by faster velocities to the southwest and slower velocities to the northeast. The residuals between the observed travel-times and those predicted on the basis of the model are given in Table 4.1; the values of the parameters in Table 4.2. A systematic pattern may be observed. The predicted travel-times to the stations relatively close to the fault on the northeast side are fast relative to the observed times. This can be explained by the presence of the synclinal basin in this vicinity.

In an attempt to explain this additional complexity a model which includes a low velocity basin along the fault was formulated:

36

$$c = c_0 + c_1 z + \frac{A(x-x_0)}{\epsilon^2 + |x-x_0|} + \frac{c_p}{1 + a(x-x_0)^2 + b(y-y_0)^2 + d(z-z_0)^2} \qquad 4.2$$

where c_p (in this case negative) is the maximum amplitude of the low-velocity material and a, b, d control the decay along the x, y, z directions away from the point x_0, y_0, z_0, respectively.

The parameters of the best fitting model of this form (Model II) are given in Table 4.2 and the residuals in Table 4.1. A vertical section through Model II at the location of Bear Valley is plotted in the lower half of Figure 4.4. This model is an improvement in that its general features, high velocities southwest of the fault, lower velocities northeast of the fault and a low velocity trough slightly northeast of the fault zone are in agreement with the known geology. It also yields an r.m.s. residual of 0.084 sec compared to the estimated reading error of 0.05 sec. The high velocities reached at the bottom of the model may be somewhat unrealistic, but this depth is not sampled by the data used. The model for the Gabilans (southwest of the fault zone) is in general agreement with the results presented by Stewart (1968) which indicate velocities increasing with depth from about 4.8 km/sec to 6.1 or perhaps as high as 6.35 km/sec in the upper few kilometers of crust.

As a test both of Model II and of the technique discussed in Chapter 2 to locate earthquakes, the shot was relocated as if it were an earthquake, using the data of Table 4.1. The initial guess at the location was more than 8 km from the true location. The calculated epicenter after five iterations

Table 4.1

Data and Residuals for Bear Valley Area

Station	Latitude	Longitude	Elevation (m)	Distance (km)	Travel Time (sec)	Residual (sec) Model I	Residual (sec) Model II
SHOT-BVSP	36°33.91'	121°12.71'	500				
HP2	36°38.41'	121°16.17'	345	9.80	2.03	-0.09	-0.13
HP3	36°41.64'	121°19.51'	310	17.54	3.52	0.03	-0.05
HP4	36°44.31'	121°15.20'	295	19.59	4.74	0.15	0.16
HP5	36°39.73'	121°8.10'	495	12.78	3.38	-0.14	-0.09
HP6	36°35.89'	121°24.21'	295	17.56	3.42	0.02	0.04
HP7	36°31.35'	121°20.80'	375	12.98	2.67	0.01	0.08
HP9	36°26.14'	121°13.62'	425	14.43	2.82	-0.09	-0.04
HP10	36°44.58'	121°5.54'	640	22.45	5.21	-0.10	-0.08
HP12	36°34.45'	121°3.30'	1020	14.09	3.94	0.01	-0.01
J1BV	36°32.27'	121°18.00'	716	8.46	1.80	-0.05	0.01
L1BV	36°34.18'	121°5.13'	823	11.33	3.21	0.19	0.07
T1BV	36°39.29'	121°2.88'	594	17.73	4.52	0.02	0.02
A1BV	36°33.83'	121°11.92'	533	1.19	0.41	0.14	0.14

38

Table 4.2

Parameters for Bear Valley Models

	c_0	c_1	A	x_0	ε	c_p	a	x_0	b	y_0	d	z_0
MODEL I	3.7526	.5506	1.02268	0.*	.75*							
MODEL II	4.2474	.4514	.9320	0.*	.75*	-1.1393	.05*	0.*	.00050*	-38.00*	.1*	-1.*

* held fixed and/or established by trial and error

converged to within 0.2 km of the true location. The error in depth is somewhat larger, .49 km. This depth error may be the result of the relatively large model residual at the closest station A1BV (Table 4.1). The convergence of the location is illustrated in Table 4.3. This location was done disregarding the model residuals completely. Accuracy would probably improve if they were used as station corrections.

Borrego Mountain Area

The Borrego Mountain area lies about 100 miles northeast of San Diego, along the San Jacinto fault zone (Figure 4.1). The surface geology of this area is shown in Figure 4.5. Basement in this area is composed of highly faulted pre-Cenozoic granitic and metamorphic rocks. The fault zone strikes through a trough filled with predominantly Tertiary sediments and alluvium and this trough deepens to the southeast to join the Imperial Valley. Coyote Mountain, Borrego Mountain, and Superstition Mountain are slivers of basement rock uplifted along faults. The principal mapped faults in the area are the San Jacinto, the Coyote Creek, the Superstition Hills and the Superstition Mountain Faults.

A more detailed geologic description of this area may be found in Dibblee (1954). Geophysical interpretation of the regional structure may be found in Kovach et al. (1962) and Biehler et al. (1964).

Table 4.3

Relocation of Bear Valley Shot

Iteration	Latitude	Longitude	Origin Time	Cartesian Coordinates (km) x	y	z	R.M.S. Error (sec)
True	36.33.91	121.12.71	.79	4.51	- 8.58	- .5	
Start	36.30.00	121.10.00	0.0	7.24	-16.40	0.*	.757
1	36.30.57	121.10.60	.21	7.04	-15.02	0.*	.639
2	36.32.50	121.12.11	.68	5.87	-10.97	0.*	.275
3	36.33.73	121.12.76	.87	4.82	- 8.75	0.*	.091
4	36.34.01	121.12.78	.87	4.45	- 8.38	0.*	.0771
5	36.34.01	121.12.76	.86	4.43	- 8.40	- .01	.0770
6	36.34.01	121.12.76	.86	4.43	- 8.41	- .04	.0770

origin time error (obs-calc) = - .07 sec.
horizontal distance error = .197 km.
depth error = - .49 km.
total distance error = .528 km.
* held fixed.

The travel-time data for the central shot (shot 2) located approximately 3 km southeast of Borrego Mountain (Figure 4.5), were used to derive a velocity model consistent with the geologic structure. These data are tabulated in Table 4.3. Figure 4.5 is a reduced plot of the travel-time data. The wide scatter indicates the complexity of the area. A coordinate system was established with the origin 2.62 km due east of 33° 9' north latitude, 116°8' west longitude with the y-axis striking N49°W (See Figure 4.5). The first model attempted consists of a constant velocity with depth with two superimposed low velocity basins, one oriented along the trough containing the fault zone and the other to the southeast representing the margin of the Imperial Valley:

$$c = c_0 + \sum_i \frac{c_p}{1. + a(x-x_0)^2 + b(y-y_0)^2 + d(z-z_0)^2} \qquad 4.3$$

The parameters of this model, Model I, are specified in Table 4.5; the resulting residuals are given in Table 4.4. The residuals reveal that this model does not contain sufficient detail to explain the early arrivals observed at Coyote Mountain, and the Fish Creek Mountains. Therefore, in an attempt to more accurately represent the velocity structure near Coyote Mountain and the Fish Creek Mountains, two more functions of the same type were added to the description given by equation 4.3. Since only one station, BM15, was situated on Superstition

Table 4.4

Data and Residuals for Borrego Mountain Area

Station	Latitude	Longitude	Elevation (m)	Distance (km)	Travel Time (sec)	Residual (sec) Model I	Residual (sec) Model II
SHOT-SP2B	33°9.36'	116°7.82'	9				
1	33°0.90	116°12.76	591	17.42	3.68	.09	0.10
2	33°7.30'	116°18.92	401	17.68	3.9	.25	0.24
3	33°13.07'	116°24.28'	291	26.50	5.22	-.06	-0.07
4	33°5.03'	115°54.64'	-29	22.00	5.28	.10	-0.17
5	33°17.94'	116°17.75'	244	22.14	4.65	-.18	-0.34
6	33°15.98'	116°13.91'	341	15.47	4.00	.28	-0.02
7	33°10.15'	115°58.39'	43	14.74	3.61	-.07	-0.19
8	33°10.19'	116°9.22'	61	2.66	0.98	.14	0.08
9	33°7.17'	116°5.70'	49	5.22	1.81	.093	0.10
10	32°59.87'	115°58.25'	12	23.00	4.73	-.38	-0.36
11	33°17.50'	116°6.37'	265	15.21	3.58	.01	-0.02
12	33°22.04'	116°19.18'	221	29.35	5.72	-.31	-0.06
14	32°48.43'	115°59.24'	229	40.92	7.72	-.10	0.13

15	32°57.57'	115°48.98'	125	36.51	7.27	-.51	
16	33°31.10'	116°12.82"	213	40.93	7.58	-.33	-0.27
17	33°4.23'	116°1.67'	0	13.47	3.71	.18	0.26
18	33°11.95'	116°1182'	105	7.85	2.02	.17	-0.22
19	33°14.00'	116°1.05'	24	13.58	3.44	.11	0.05
20	33°4.46'	115°47.55'	-27	32.80	7.38	.20	-0.00
22	33°1.83'	116°3.50	92	15.46	3.34	-.21	-0.16
H1	33°12.40'	116°9.42'	103	6.15	1.89	-.09	-0.23
H6	33°11.24'	116°9.03'	70	3.95	1.37	-.04	-0.22
I1	32°53.64	115°47.17'	10	43.31	8.86	.12	0.06
I5	32°53.14'	115°46.07	12	45.20	9.17	.11	0.04
J1	32°56.58'	115°52.55	23	33.49	7.13	.09	0.04
J6	32°55.90'	115°51.18'	23	35.90	7.49	.02	-0.04
K1	32°58.95'	115°56.73'	18	25.84	5.44	-.20	-0.20
K6	32°57.77'	115°55.97'	26	28.26	5.86	-.17	-0.17
L1	33°18.19'	116°14.32'	222	19.20	4.68	.36	0.27
L6	33°17.21'	116°13.30'	264	16.83	4.31	.39	0.26
P2	33°6.29'	116°2.53'	0.0	9.99	3.15	.00	0.23
P6	33°5.86'	116°1.41'	-8	11.88	3.64	.00	0.28

R1	33°4.10'	115°57.21'	-23	19.15	5.03	.15	0.09
R6	33°2.88'	115°57.48'	-17	20.05	5.25	.17	0.26
S1	33°11.16'	116°5.08'	46	5.41	1.70	-.15	-0.19
S6	33°10.11'	116°4.40'	33	5.50	1.78	-.17	-0.18
T1	33°20.23'	116°17.77'	169	25.36	5.29	-.08	-0.00
T6	33°19.63'	116°16.56'	169	23.35	5.19	.17	0.15
SP1	33°19.99'	116°17.32'	169	24.58	5.30	.07	0.10
SP3	32°53.29'	115°46.43'	9	44.59	9.08	.12	0.06

Table 4.5

Parameters for Bear Valley Models

	c_0	c_{p_i}	a_i	x_{0_i}	b_i	y_{0_i}	d	z_{0_i}
MODEL I	6.2290	-4.1650	.07065	-.83	.001964	-9.94	.8171	.12
		-3.5817	.00547	-22.25	.002984	-22.84	.1374	-.17
MODEL II	6.1922	3.5000*	.2000*	-3.00*	.1*	30.00*	.20*	0.*
		-3.7256	.0628	-1.3522	.0004	17.68	.5863	-.13
		-4.0889	.0038	-13.58	.0036	-22.05	.1338	-.51
		1.2877	.0098	15.12	.0176	-9.59	.1625	3.36

* held fixed and/or established by trial and error

Mountain, insufficient data existed to define this velocity anomaly and this observation was not used.

The parameters of the derived model are given in Table 4.5; travel-time residuals are given in Table 4.4. Velocity contours for northeast-southwest vertical sections (see Figure 4.5 for locations) through the model are plotted in Figure 4.7. The model gives a satisfactory picture of the average geologic structure of the region. Section N1 is located to the north of the sedimentary trough and generally high velocities prevail throughout. Moving southeastward the sections show a thickening of low velocity sediments within the trough. This is interrupted at profile N3 by the high velocities associated with Coyote Mountain. Farther to the southeast surficial velocities in the eastern half diminish reflecting the thickening sedimentary cover at the southern end of the Santa Rosa Mountains. In sections S1-S4 the protrusion of high velocity material to the east from the western margin reflects the position of the Fish Creek Mountains. Still farther to the southeast low velocity material dominates as the sections move into the Imperial Valley.

The average structure of the model is in general agreement with the layered model given by Hamilton (Figure 4.7). The travel-time residuals are compared with Hamilton's time terms in Figure 4. The smaller scatter of the residuals indicates that the laterally inhomogeneous model is a significantly more accurate description of the structure than the

layered model, even though it may lack the empirical precision of the time terms.

V. CONCLUSIONS

This thesis discusses ray theory computations for the solution of seismological problems in laterally inhomogeneous regions. These methods are in excellent agreement with analytical solutions for tractable cases. Laterally inhomogeneous crustal velocity models are obtained from real travel-time data. Inherent in the models are most of the significant geologic structures of the regions. A procedure is demonstrated whereby events may be located in such models.

Insight into the actual mechanisms of earthquakes requires knowledge of where earthquakes occur in relation to geologic structure. The techniques discussed in this thesis apply both to the deciphering of the velocity structure of geologically complex regions and to the location of earthquakes in such regions once the structure is known. The problem of bias in the location of local earthquakes is ripe for attack by these methods and will be the subject of future work.

APPENDIX A

RAY THEORY

Foundations

Ray theory, despite certain fundamental limitations, presents a foundation for computational techniques of great usefulness in the study of the structure of the earth, particularly the study of laterally inhomogeneous regions. Karal and Keller (1959) showed that elastic ray theory could be thought of as resulting from the first terms of an asymptotic expansion solution of the wave equation in powers of reciprocal frequency.

Consider the linearized, elastic wave equation for an infinite inhomogeneous medium:

$$\rho \frac{\partial^2 \vec{u}}{\partial t^2} = (\lambda+\mu)\nabla(\nabla\cdot\vec{u}) + \mu\nabla^2\vec{u} + \nabla\lambda(\nabla\cdot\vec{u}) + \nabla\mu \times(\nabla \times \vec{u}) + 2(\nabla\mu\cdot\nabla)\vec{u} \qquad \text{A.1}$$

where $\vec{u}$ is particle displacement, ρ is density, and λ and μ are the Lamé constants. ρ, λ and μ are assumed to be continuous, differentiable functions of the space coordinates. Attempt a solution of this equation in the form

$$\vec{u} = \vec{A}\, e^{i\omega(S-t)} \qquad \text{A.2}$$

where S and $\vec{A}$ are space functions to be determined and ω

is angular frequency. Assume that S is independent of frequency, but that $\vec{A}$ depends on frequency in the form

$$\vec{A} = \sum_{n=0}^{\infty} (i\omega)^{-n} \vec{A}_n \qquad \text{A.3}$$

Under certain conditions of the spatial variation of ρ, λ and μ, the first few terms of A.3 (hopefully just $\vec{A}_0$) will provide an adequate representation of the solution for most frequencies of interest. Inserting A.2 and A.3 into A.1 Karal and Keller obtain a recursive relation for the $\vec{A}_n$'s. For $\vec{A}_0$ their results are identical with those that would be obtained from the homogeneous wave equation, namely

Case I

$$\vec{A}_0 \cdot \nabla S = 0$$
$$(\nabla S)^2 = \rho/\mu \qquad \text{A.4}$$

Case II

$$\vec{A}_0 \times \nabla S = 0$$
$$(\nabla S)^2 = \rho/(\lambda + 2\mu) \qquad \text{A.5}$$

but in contrast to the homogeneous case ρ, λ and μ are functions of the space coordinates. In Case I the particle motion given by $\vec{A}_0$ is perpendicular to the ray and the right hand side of A.4 is the reciprocal of the square of the velocity of shear waves. In Case II the particle motion is

parallel to the ray and the right hand side of A.5 is the reciprocal of the square of the compressional wave velocity. The important result is that under the appropriate conditions namely continuous gradients of relatively small magnitude i.e. no step discontinuities, $\vec{A}_0$ is an adequate representation of the solution and the compressional and shear waves uncouple and both A.4 and A.5 may be written in the form

$$(\nabla S)^2 = 1/c^2 \qquad \text{A.6}$$

where c is the wave velocity.

Under what conditions will only one term in the expansion A.3 be sufficient? Since all terms are fractions of previous terms one term should be adequate when the ratio of the magnitude of the second term to the first is

$$|\vec{A}_1|/|\vec{A}_0| \ll 1 \qquad \text{A.7}$$

Using the results of Karal and Keller, Archambeau et al. (1969) obtained an approximate expression for compressional waves for this ratio

$$\frac{|\vec{A}_1|}{\omega|\vec{A}_0|} = \mathcal{O}\left(\frac{1}{k_p}\left[\frac{\nabla\cdot\vec{A}_0}{|\vec{A}_0|} + \frac{\nabla v_p}{v_p} + \frac{\nabla\lambda}{\lambda+2\mu}\right]\right) \qquad \text{A.8}$$

where k_p is the wave number ω/v_p, and $v_p = ((\lambda+2\mu)/\rho)^{1/2}$.

This ratio will, of course, be large near a focus of rays where $\nabla\vec{A}_0$ is very large and also in regions where the gradients of the elastic parameters are large. Archambeau et al. argue that this ratio is small enough to be tolerable even for rays which approximate head waves (such as P_n).

Derivation of Ray Tracing Equations

Assuming that the use of just one term in the asymptotic expansion is justified, the problem of finding seismic rays is simply a matter of interpreting

$$(\nabla S)^2 = 1/c^2 \qquad \text{A.9}$$

This is the so called "eikonal equation" of geometrical optics. We desire a description of the surfaces of constant phase, S = constant, the wavefronts; this can be done by finding the set of curves orthogonal to the level surfaces of S, i.e., the set of curves defined by ∇S: the rays (see Figure A.1). The directional derivative along these curves is

$$\frac{dS}{ds} = |\nabla S| = 1/c \qquad \text{A.10}$$

where s is the arc length along the path. Applying the operator ∇ to both sides of A.10 and interchanging the order of integration on the left hand side, we obtain

$$\frac{d\,\nabla S}{ds} = -\frac{1}{c^2}\nabla c \qquad \text{A.11}$$

The element of arc length along the ray may be rewritten

$$ds = cdt \qquad \text{A.12}$$

which gives the result

$$\frac{d\,\nabla S}{dt} = -\frac{1}{c}\nabla c \qquad \text{A.13}$$

Define the slowness vector $\vec{L}$

$$\vec{L} \equiv \nabla S. \qquad \text{A.14}$$

Note that by this definition $\vec{L}$ is parallel to the ray at each point and has the magnitude 1/c. This gives the first ray tracing equation

$$\frac{d\vec{L}}{dt} = -\frac{1}{c}\nabla c \qquad \text{A.15}$$

The rate of change of the position vector $\vec{r}$ along the ray may be simply obtained from the definition of the velocity vector

$$\frac{d\vec{r}}{dt} \equiv \vec{v} \qquad \text{A.16}$$

$\vec{v}$ is along the ray and therefore parallel to $\vec{L}$, but has the magnitude c. Substitution yields

$$\frac{d\vec{r}}{dt} = c^2\vec{L} \qquad \text{A.17}$$

Equations A.15 and A.17 may be integrated from some starting values $\vec{L}_0$ and $\vec{r}_0$ to yield $\vec{L}(t)$ and $\vec{r}(t)$ providing a complete description of the ray. These relationships are depicted in Figure A.2.

For some purposes, such as the solution of boundary value problems, it is more convenient to combine A.15 and A.17 into one second order differential equation

$$\frac{d}{dt}\left(\frac{1}{c^2}\frac{d\vec{r}}{dt}\right) = -\frac{1}{c}\nabla c \qquad \text{A.18}$$

or more familiarly, using ds = cdt

$$\frac{d}{ds}\left(\frac{1}{c}\frac{d\vec{r}}{ds}\right) = \nabla(1/c) \qquad \text{A.19}$$

Commonly the index of refraction, $n \equiv c_0/c$, replaces $1/c$ in this equation. Equation A.19 may be derived from Fermat's principle of least time by the calculus of variations (Officer, 1958).

The results which have been derived to this point are applicable to a medium in which the velocity is a continuous function. This is not a fundamental restriction for they apply equally well in a piecewise continuous medium, using Snell's Law at the discontinuity. This law may be simply stated (Zengeni, 1970)

$$\vec{L}' = \vec{L} + \frac{\beta}{c}\hat{n} \qquad \text{A.20}$$

where $\vec{L}$ is the slowness vector incident on the discontinuity, $\vec{L}'$ is the refracted slowness vector, $\hat{n}$ is a unit normal to the discontinuity, c is the velocity at the point where the incident slowness vector impinges on the discontinuity. The scalar β may be found from

$$\beta = -\cos\alpha \pm [\cos^2\alpha + (c/c')^2 - 1]^{1/2} \qquad \text{A.21}$$

where α is the angle between the incident slowness vector

and the normal and c' is the velocity at the point where the refracted ray leaves the discontinuity. The plus sign is chosen if α is obtuse, the minus sign if α is acute.

Calculation of Intensity and Amplitude

To calculate the amplitude $\vec{A}_0$ we shall first calculate the intensity along the ray. To obtain the intensity consider a family of rays defined by $\vec{r}(\alpha,\beta,t)$ and $\vec{L}(\alpha,\beta,t)$ where α and β are the take-off angles of the initial slowness vector $\vec{L}_0$ (Figure A.2). For α and β fixed, with t varying, the functions $\vec{r}$ and $\vec{L}$ will describe one ray, but for t fixed as α and β vary, $\vec{r}$ and $\vec{L}$ describe a wavefront. In other words, α and β are the parameterization of a surface (the wavefront) defined by the function $\vec{r}$. An element of area on the wavefront is then

$$dA = \left| \frac{\partial \vec{r}}{\partial \alpha} \times \frac{\partial \vec{r}}{\partial \beta} \right| d\alpha \, d\beta \qquad \text{A.22}$$

Neglecting scattering and attenuation, we may assume that the intensity of the disturbance associated with the wavefront is inversely proportional to the area of the wavefront

$$I/I_0 = \frac{d\Omega}{dA} \qquad \text{A.23}$$

where I_0 is the initial intensity associated with the unit solid angle $d\Omega$ and I is the intensity associated with the element of area dA. Therefore, if we can calculate $\partial\vec{r}/\partial\alpha$ and $\partial\vec{r}/\partial\beta$, we can calculate dA and hence the intensity (and amplitude).

Expressions for $\frac{d}{dt}\frac{\partial\vec{r}}{\partial\alpha}$ and $\frac{d}{dt}\frac{\partial\vec{r}}{\partial\beta}$ may be simply obtained by considering two rays, one, described by $\vec{r}$ and $\vec{L}$ started with some initial slowness vector $\vec{L}_0$ and another ray described by $\vec{r}'$ and $\vec{L}'$ which began with some slightly different initial slowness vector $\vec{L}_0'$. We may then write the ray tracing equation for two rays

$$\frac{d\vec{r}}{dt} = c^2\vec{L} \qquad \frac{d\vec{r}'}{dt} = c'^2\vec{L}'$$

$$\frac{d\vec{L}}{dt} = -\frac{1}{c}\nabla c \qquad \frac{d\vec{L}'}{dt} = -\frac{1}{c'}\nabla c'$$

where c' is the slightly different velocity encountered by the primed ray. If we define

$$\delta\vec{r} = \vec{r}' - \vec{r}\,|_{t = \text{const}}$$

and

$$\delta\vec{L} = \vec{L}' - \vec{L}\,|_{t = \text{const}}$$

then we may expand $c'(\vec{r} + \delta\vec{r})$ in a Taylor series about the

point $\vec{r}$,

$$c'(\vec{r} + \delta\vec{r}) = c(\vec{r}) + \delta\vec{r}\cdot\nabla c + 0(|\delta\vec{r}|^2)$$

Using this expansion expressions correct to first order in $|\delta\vec{r}|$ may be obtained for c'^2, $1/c'$ and $\nabla c'$. The resulting ray tracing equations are

$$\frac{d\vec{r}'}{dt} = c^2\vec{L} + 2c\,(\nabla c\cdot\delta\vec{r})\vec{L} + c^2\delta\vec{L} \qquad \text{A.24}$$

$$\frac{d\vec{L}'}{dt} = -\frac{1}{c}\nabla c + 1/c^2\tilde{C}\,\delta\vec{r}$$

where $\tilde{C}$ is a symmetric matrix of partial derivatives

$$\tilde{C} = \begin{bmatrix} c_x^2 - cc_{xx} & c_xc_y - cc_{xy} & c_xc_z - cc_{xz} \\ \vdots & c_y^2 - cc_{yy} & c_yc_z - cc_{yz} \\ & \cdots & c_z^2 - cc_{zz} \end{bmatrix} \qquad \text{A.25}$$

where $c_x = \frac{\partial c}{\partial x}$, $c_{xx} = \frac{\partial^2 c}{\partial x^2}$ etc.

Substracting the unprimed equations in A.15 & A.17 from the primed set in A.24 we obtain expressions for the time

derivatives of $\delta\vec{r}$ and $\delta\vec{L}$. Dividing these expressions through by $\delta\alpha$ and $\delta\beta \to 0$ we obtain

$$\frac{d}{dt}\frac{\partial\vec{r}}{\partial\alpha} = 2c(\nabla c\cdot\frac{\partial\vec{r}}{\partial\alpha})\vec{L} + c^2\frac{\partial\vec{L}}{\partial\alpha}$$

$$\frac{d}{dt}\frac{\partial\vec{r}}{\partial\beta} = 2c(\nabla c\cdot\frac{\partial\vec{r}}{\partial\beta})\vec{L} + c^2\frac{\partial\vec{L}}{\partial\beta} \qquad \text{A.26}$$

$$\frac{d}{dt}\frac{\partial\vec{L}}{\partial\alpha} = \frac{1}{c^2}\tilde{C}\frac{\partial\vec{r}}{\partial\alpha}$$

$$\frac{d}{dt}\frac{\partial\vec{L}}{\partial\beta} = \frac{1}{c^2}\tilde{C}\frac{\partial\vec{r}}{\partial\beta}$$

These may be integrated from the starting values

$$\left.\frac{\partial\vec{r}}{\partial\alpha}\right|_{t=0} = 0 \qquad \left.\frac{\partial\vec{r}}{\partial\beta}\right|_{t=0} = 0$$

$$\left.\frac{\partial\vec{L}}{\partial\alpha}\right|_{t=0} = \frac{\partial\vec{L}_0}{\partial\alpha}, \qquad \left.\frac{\partial\vec{L}}{\partial\beta}\right|_{t=0} = \frac{\partial\vec{L}_0}{\partial\beta}$$

In the geometry of Figure A.2

$$\vec{L}_0 = \frac{1}{c(\vec{r}_0)}\ (\cos\alpha\sin\beta\,\hat{i} + \sin\alpha\sin\beta\,\hat{j} + \cos\beta\,\hat{k})$$

so the differentiation is straightforward.

Knowing $\frac{\partial \vec{r}}{\partial \alpha}$ and $\frac{\partial \vec{r}}{\partial \beta}$ at any time we can then calculate the intensity at that time by A.23 (using a vector identity to expand A.22 and $d\Omega = \sin\beta \, d\alpha d\beta$)

$$\frac{I}{I_0} = \frac{\sin \beta}{\sqrt{\left(\frac{\partial \vec{r}}{\partial \alpha} \cdot \frac{\partial \vec{r}}{\partial \alpha}\right)\left(\frac{\partial \vec{r}}{\partial \beta} \cdot \frac{\partial \vec{r}}{\partial \beta}\right) - \left(\frac{\partial \vec{r}}{\partial \alpha} \cdot \frac{\partial \vec{r}}{\partial \beta}\right)^2}} \qquad \text{A.27}$$

Formulas given by Karal and Keller may be used to calculate the magnitude of the first term in the asymptotic expansion, $\vec{A}_0$, in terms of its initial value at $\vec{r}_0$ and the relative intensity, for compressional waves:

$$|\vec{A}_0(t)| = |\vec{A}_0(t_0)| \left(\frac{v_p(\vec{r}_0)\ \rho(\vec{r}_0)\ \ I}{v_p(\vec{r})\ \rho(\vec{r})\ \ I_0} \right)^{1/2},$$

for shear waves

$$|\vec{A}_0(t)| = |\vec{A}_0(t_0)| \left(\frac{v_s(\vec{r})\ \mu(\vec{r}_0)\ \ I}{v_s(\vec{r}_0)\ \mu(\vec{r})\ \ I_0} \right)^{1/2}$$

At discontinuities, including the free surface, reflected waves must also be considered (Ewing, et al, 1957).

APPENDIX B

DESCRIPTION OF COMPUTER PROGRAM

Listings and decks of the FORTRAN programs used in this study are on file at the Department of Geophysics, Stanford University. The intent of this appendix is to describe briefly the model fitting program and the procedures for its use. The basic program takes a set of travel-time data, calculates the corresponding travel-times for a given velocity model and perturbs the parameters of the model so as to obtain a least squares best fit with the observations. Only minor modifications are required to use the program to locate event hypocenters in a given model.

The MAIN program functions as follows:

1) sets up a cartesian coordinate system centered at some point in the area of interest;
2) reads the station locations and obtains their coordinates in the new system, using subroutines TRANS and TRAROT;
3) reads the velocity model and parameters pertaining to its refinement;
4) optionally, plots the velocity model as maps at different depths (MDLPLT) or as vertical sections (MDPLT2);
5) reads the event location and origin time and obtains the coordinates in the cartesian sys-

tem, using TRANS and TRAROT;

6) reads a list of stations and arrival times, calculates the travel-times, and assigns them to the proper sets of station coordinates;

7) repeats 5 and 6 for all the events to be considered;

8) finds the rays and calculates the travel-times and partial derivatives of travel-time with respect to model parameters, using TIMCAL;

9) solves for a new set of model parameters using MAINE and MULT;

10) repeats steps 8 and 9 as desired.

The functions of the subroutines are as follows:

TIMCAL

1) initializes the model improvement equations;

2) finds the rays (using RAY) and calculates the travel-time residuals;

3) prints ray information;

4) builds least squares normal equations.

RAY

Subroutine RAY finds the ray between a source and a station using the tridiagonal matrix algorithm discussed in detail in Chapter 3. Specifically RAY

1) determines the rotation necessary to get the source and station in the x-z plane;

2) obtains an initial guess at the shape of the ray either from the stored shape of the ray from a previous iteration or by fitting arcs of

circles through the endpoints and the maximum estimated excursions in the y and z directions;

3) sets up the equations 3.7 (using subroutines VELO and QUKVEL to calculate the velocity and derivatives at each point);
4) calculates the error for the current ray estimate using TRIMLT;
5) if the error is less than or equal to the tolerable level, calculates the travel-time, partial derivatives, etc. and returns control;
6) if the error has increased from the previous iteration, the corrections to the coordinates from the previous iteration are reduced by a scale factor and control is returned to step 3;
7) if the error has decreased, but is still greater than tolerable, the matrix system of equation 3.7 is solved for the corrections using BLKTRI;
8) the coordinate corrections are added to the current coordinates to obtain the new ray;
9) calculates the travel-time for the new ray;
10) if the difference between the new travel-time and the previous iteration is less than some tolerance, the additional quantities are calculated and control is returned as in step 5;
11) steps 3-10 are repeated until one or the other

of the convergence criteria are satisfied or until the number of iterations exceeds the limit.

QUKVEL calculates the velocity, first and second spatial derivatives, partial derivatives with respect to model parameters, and the elements of the matrix $\hat{P}$ in equation 3.12 for a point using subroutines BLOB and JUMP. Subroutine VELO is an entry which provides for a return after the calculation of velocity only. It will be necessary to alter this subroutine if the combination of functions used is not an adequate description of the velocity structure of the area of interest.

TRIMLT multiplies a tridiagonal matrix times a vector to give a vector.

BLKTRI solves the 2x2 block tridiagonal system of equation 3.12, making use of special properties of this system.

JUMP evaluates the function of equation 3.15 and performs the spatial derivatives and derivatives with respect to model parameters.

BLOB evaluates the function of equation 3.16 and performs the spatial derivatives and derivatives with respect to model parameters.

TRANS converts latitude and longitude to cartesian system using Richter's method of short distances

(Richter, 1958).

TRAROT translates and rotates cartesian system.

MDLPLT uses VELO to calculate velocity at points on horizontal rectangular grid and plots result.

MDPLT2 uses VELO to calculate velocity at points on vertical rectangular grid and plots result.

MAINE inverts n x n matrix (written by J.F. Claerbout).

MULT multiplies n x n matrix times vector to give vector.

Input Parameters

CARD 1 Center of coordinate system and conversion factors

LTDO, LTMO, LGDO, LGMO, AA, BB (6F10.4)

Latitude (degrees), latitude (minutes), longitude (degrees), longitude (minutes), latitude conversion factor, longitude conversion factor.

CARD 2 Coordinate translation and rotation to line up with structural "grain."

XF, YF, PHI (3F10.4)

X-coordinate, y-coordinate, rotation angle (in radians, positive counter-clockwise from the x-axis).

CARD 3 Parameters for ray calculation

NTRYS, H, TOLER, TOLT, FACST, FACFAC (I2, 5F10.4)

Maximum number of iterations to obtain ray convergence (10), nominal grid spacing (1km), r.m.s. error tolerance (E-4), travel-time tolerance (E-3), initial ray convergence factor (2.), adjustment to ray convergence factor (2.) (See description of RAY for discussion).

CARDS 4-N1 Station list and coordinates

STA (I), LAD (I), LAM (I), LOD (I), LOM (I), ELEV (I)
(2X, A4, F2.0, F5.2, 1X, F3.0, F5.2, 1X, F4.0)

Station designation, latitude (degrees), latitude (minutes), longitude (degrees), longitude (minutes), elevation (m).

CARD N1+1 BLANK (Indicates end of station list.)

CARD N1+2 Model improvement parameters

NIMPRV, DELTAX, LAMDA, NU (I2, 3F10.4)

Number of times to repeat model improvement process, cutoff distance (observations from stations at distances greater than cutoff will be discarded), initial value of model improvement factor (10.), adjustment to model improvement factor (5.) (See section on model improvement in Chapter 3 or Marquardt [1963].).

CARD N1+3 Number of parameters in velocity model

NVEL (I2)

CARD N1+4-N2 Parameters of velocity model

VEL(1), VEL(2),...VEL(NVEL) (7F10.4)

Order will be changed depending on functions chosen to represent structure. Must conform with designation in subroutine QUKVEL.

CARD N2+1 Number of parameters to be perturbed in model improvement

NVARI (I2)

CARD N2+2 Array position in VEL of parameters to be varied

IVAR (1), IVAR (2),...IVAR (NVARI) (36I2)

CARD N2+3 Plot parameters

NZWIT, NSEC, DELZ, YGRID, YMAX, DELY (2I2, 4F10.4)

Number of horizontal grids to be plotted (if 0, vertical sections along y=constant will be plotted; if negative, no plots), number of vertical sections, vertical increment for horizontal grids, maximum y-dimension of horizontal grid, maximum value of y for vertical section, increment of y between vertical sections.

CARD N2+4 Event description

EV, ELAD, ELAM, ELOD, ELOM, ELEL, OT (2X, A4, F2.0, F5.2, 1X, F3.0, F4.0, F10.4)

Event designation, latitude (degrees), latitude (minutes), longitude (degrees), longitude (minutes), elevation (m), origin time (seconds past most recent minute).

CARDS N2+5-N3 Travel-time observations

ST, Q, ARTIM, ZEST, YEST (2X, A4, A3, 10X, F5.2, 2F10.4)

Station designation (must be identical, including positioning of blanks, with designation on station list), quality description (not used), arrival time (seconds past most recent minute; arrival time minus origin time is assumed to be less than one minute), maximum estimated vertical departure from line segment connecting source and station, maximum estimated horizontal departure from line segment (standing at source, looking toward station, right is positive, left is negative).

CARD N3+1 BLANK (indicates end of travel-time observation list)

CARD N3+2 If additional events, same as N2+4. CARDS N2+4-N3+1 repeated for each event.
If no additional events, BLANK

The inputs to the hypocenter location version of the program are the same, except that some parameters have different meanings:

CARD N1+2

NIMPRV, number of iterations for hypocenter
LAMDA, NU, hypocenter improvement conversion factors (2.,2.)

CARD N2+1

NVARI, =3, depth fixed; =4, depth free.

CARD N2+2 read, but not used

CARD N2+4 trial hypocenter location and origin time

If the program is to be used for any runs longer than 1-2 minutes, it is advisable to compile the program once under the "OPT=2" compiler option and create a load module. For instructions on how to do this see the User's Manual, Stanford University Computation Center.

BIBLIOGRAPHY

Alterman, Z.S., and F.C. Karal, Jr., Propagation of elastic waves in layered media by finite-difference methods, Bull. Seismol. Soc. Amer., 58, 367-398, 1968.

Andrews, Philip, Geology of the Pinnacles National Monument, Calif. Univ., Dept. Geol. Sci. Bull., 24, p. 1-38, 1936.

Archambeau, C. B., E. A. Flinn, and D. G. Lambert, Fine structure of the upper mantle, J. Geophys. Res., 74, 5825-5865, 1969.

Backus, G., Inference from inadequate and inaccurate data, I, Proc. Nat'l. Acad. of Sciences, 65, 1-7, 1970.

Backus, G. E., and J. F. Gilbert, Numerical applications of a formalism for geophysical inverse problems, Geophys. J. Roy. Astron. Soc., 13, 247-276, 1967.

Backus, G. E., and J. F. Gilbert, The resolving power of gross earth data, Geophys. J. Roy. Astron. Soc., 16, 169-205, 1968.

Backus, G. E., and J. F. Gilbert, Constructing p-velocity models to fit restricted sets of travel-time data, Bull. Seismol. Soc. Amer., 59, 1407-1414, 1969.

Backus, G. E., and F. Gilbert, Uniqueness in the inversion of inaccurate gross earth data, Phil. Trans. Roy. Soc. Lond., Series A, 266, 123-192, 1970.

Belonosova, A. V., S. S. Tadzhimukhamedova, and A. S. Alekseyer, Some methods and algorithms for the interpretation of geophysical data, Nauka, 1967.

Berry, M. J., and G. F. West, An interpretation of the first arrival data of the Lake Superior experiment by the time-term method, Bull. Seismol. Soc. Amer., 56, 141-171, 1966a.

Berry, M. J., and G. F. West, A time-term interpretation of the first-arrival data of the 1963 Lake Superior experiment, Am. Geophys. Union, Geophys. Monograph 10, 166-180, 1966b.

Biehler, S., R. L. Kovach and C. R. Allen, Geophysical framework of northern end of Gulf of California structural province, in Marine Geology of the Gulf of California - symposium, edited by T. H. Van Andel and G. G. Shor, Jr., Memior 3, Am. Assoc. Petr. Geol., 126-143,1964.

Bolt, B. A., and O. W. Nuttli, P wave residuals as a function of azimuth, 1, observations, J. Geophys. Res., 71, 5977-5986, 1966.

Boore, David M., Love Waves in nonuniform wave guides: finite difference calculations, J. Geophys. Res., 75, (8), 1970.

Bullen, K. E., An Introduction to the Theory of Seismology, 3rd ed., 381 pp., University Press, Cambridge, 1963.

Burmakov, Y. A., and T. I. Oblogina, Numerical determination of rays and travel-time curves of refracted waves, Izv. Physics of the Solid Earth, 12, 767-771, 1968.

Claerbout, J. F., Course grid calculations of waves in inhomogeneous media with application to delineation of complicated seismic structure, Geophysics, 35, no. 3, 1970.

Dibblee, T. W., Jr., Geology of the Imperial Valley region, in Geology of Southern California, edited by R. H. Jahns, Calif. Div. Mines Geol. Bull., 170, 23-34, 1954.

Ewing, W. M., W. S. Jardetsky, and F. Press, Elastic Waves in Layered Media, 380 pp., McGraw-Hill, New York, 1957.

Fox, L., The Numerical Solution of Two-Point Boundary Problems in Ordinary Differential Equations, 371 pp., University Press, Oxford, 1957.

Hamilton, R. M., Time-term analysis of explosion data from the vicinity of the Borrego Mountain, California, earthquake of 9 April 1968, Bull. Seismol. Soc. Amer., 60, 367-381, 1970.

Hales, A. L., J. R. Cleary, H. A. Doyle, R. Green, and J. Roberts, P-wave station anomalies and the structure of the upper mantle, J. Geophys. Res., 73, 3885-3896, 1968.

Henrici, P., Discrete variable methods in ordinary differential equations, 407 p., Wiley and Sons, New York, 1962.

Hildebrand, F. B. Finite-Difference Equations and Simulations, 338 pp., Prentice-Hall, Englewood Cliffs, N. J., 1968.

Jeffreys, Sir Harold, The earth: its origin, history, and physical constitution, 4th ed., 438 pp., University Press, Cambridge, 1962.

Jeffreys, Sir Harold, Revision of travel times, Geophys. J. Roy. Astron. Soc., 11, 5-12, 1966.

Julian, B. R., and D. L. Anderson, Travel-times, apparent velocities and amplitudes of body waves, Bull. Seismol. Soc. Amer., 58, 339-366, 1968.

Karal, F. C., Jr., and J. B. Keller, Elastic wave propagation in homogeneous and inhomogeneous media, J. Acoust. Soc. Amer., 31, 694-705, 1959.

Kline, M., and I. W. Kay, Electromagnetic theory and geometrical optics, 527 pp., Interscience, New York, 1965.

Kovach, R. L., C. R. Allen and F. Press, Geophysical investigations in the Colorado delta region, J. Geophys. Res., 67, 2845-2871, 1962.

Marquardt, D. W., An algorithm for least-squares estimation of nonlinear parameters, J. Soc. Indust. Appl. Math., 11, 431-441, 1963.

Officer, C. B., Introduction to the theory of sound transmission, 284 pp., McGraw-Hill, New York, 1958.

Oliver, J., and B. Isacks, Deep earthquake zones, anomalous structures in the upper mantle, and the lithosphere, J. Geophys. Res., 72, 4259-4275, 1967.

Otsuka, M., Azimuth and slowness anomalies of seismic waves measured on the Central California seismic array, Part I: Observation, Bull. Seismol. Soc. Amer., 56, 223-239, 1966a.

Otsuka, M., Azimuth and slowness anomalies of seismic waves measured on the Central California Seismic array, Part II: Interpretation, Bull. Seismol. Soc. Amer., 56, 655, 1966b.

Page, B. M., Geology of the coast ranges of California, in Geology of Northern California, edited by E. H. Bailey, Calif. Div. Mines Geol. Bull., 190, 255-276, 1966.

Richter, C. F., Elementary Seismology, 768 pp., W. H. Freeman & Co., San Francisco, 1958.

Richtmeyer, R. D., and K. W. Morton, Difference methods for initial-value problems, 405 pp., Interscience, New York, 1967.

Scheidigger, A. E., and P. L. Willmore, The use of a least squares method for the interpretation of data from seismic surveys, Geophysics, 22, 9-22, 1957.

Slichter, L. B., The theory of the interpretation of seismic travel-time curves in horizontal structures, Physics, 3, 273-295, 1932.

Smith, B. D., Geologic and geophysical interpretation of the Hollister trough, unpublished M.S. paper, Dept. of Geophysics, Stanford U., 1970.

Snyder, W. M., Continuous parabolic interpolation, Proc. ASCE, 87 (HY4), 1961.

Stewart, S. W., Preliminary comparison of seismic travel-times and inferred crustal structure adjacent to the San Andreas Fault in the Diablo and Gabrilan Ranges of Central California, in Proceedings of Conference on Geologic Problems of San Andreas Fault System, pp. 218-230, edited by Dickinson and Grantz, Stanford University Publications in Geological Sciences, XI, 1968.

Ugincius, P., Intensity equations in ray acoustics, I, J. Acoust. Soc. Amer., 45, 193-205, 1969a.

Ugincius, P., Intensity equations in ray acoustics, II, J. Acoust. Soc. Amer., 45, 206-209, 1969b.

Vlaar, N. J., Ray theory for an anisotropic inhomogeneous elastic medium, Bull. Seismol. Soc. Amer., 58, 2053-2072, 1968.

Wesson, R. L., A time integration method for computation of the intensities of seismic rays, Bull. Seismol. Soc. Amer., 60, 307-316, 1970.

Wiggins, R. A., Monte Carlo inversion of body-wave observations, J. Geophys. Res., 74, 3171-3181, 1969.

Wilson, I. F., Geology of the San Benito quadrangle, Calif. J. Mines and Geology, 39, 183-270, 1943.

FIGURE CAPTIONS

Fig. 3.1 Travel-time and $\partial T/\partial c_0$ calculated for constant gradient velocity model, $c = c_0 + c_1 z$, using second-order Runge-Kutta integration agree with analytic values within thickness of curve.

Fig. 3.2 Relative intensity and $\partial T/\partial c_1$ calculated for constant gradient velocity model, $c = c_0 + c_1 z$, using second-order Runge-Kutta integration agree with analytic values within thickness of curve.

Fig. 3.3 Geometry of tridiagonal matrix formulation of ray boundary value problem. The primed axes are translated so as to include the source and station in the x' - z' plane. The line segment on the x'-axis corresponding to the ray is subdivided into equal segments, h. The y' and z' coordinates at these discrete points are the unknown variables.

Fig. 3.4 Function used to represent one-dimensional velocity change, $f(x) = A(x - x_0)/(\varepsilon^2 + |x - x_0|)$. As $x \to x_0 \pm \infty$, $f(x) \to \pm A$; at $x = x_0 \pm \varepsilon^2$, $f(x) = \pm A/2$.

Fig. 3.5 Test of model improvement scheme. See text for discussion.

Fig. 4.1 Index map showing location of Bear Valley and Borrego Mountain areas and major faults of California.

Fig. 4.2 Generalized geologic map of Bear Valley area showing shot and station locations, origin of cartesian coordinate system and section line A-A'.

Fig. 4.3 Reduced travel-time plot of data from Bear Valley shot.

Fig. 4.4 Contour plots of velocity for Bear Valley models along vertical section A-A'. Model I above, Model II, below.

Fig. 4.5 Generalized geologic map of Borrego Mountain area showing shot and station locations. The ends of the SW-NE section lines, N1-N8 and S1-S8 are indicated. The triangles and numbers designate portable stations. The line segments and letters indicate refraction spreads. The readings at

each end of the refraction spreads were used as independent observations. The origin of the cartesian coordinate system is also shown. The basement outcrop between stations 5 and 12 is Coyote Mountain; that beneath station 15 is Superstition Mountain.

Fig. 4.6 Reduced travel-time plot of data from Shot 2 southeast of Borrego Mountain.

Fig. 4.7 Contour plots of velocity for Borrego Mountain area, Model II, along vertical sections N1-N8 and S1-S8 indicated in Figure 4.5. See text for discussion.

Fig. 4.8 Above: time-terms calculated by Hamilton (1970). Below: residuals between observed travel-times and those calculated for Model II. The residuals have less scatter than the time-terms, indicating that significant lateral variations have been included in the model.

Fig. A.1 Wavefronts are surfaces of constant phase, S= constant. Rays are orthogonal curves, parallel to ∇S.

Fig. A.2 Geometry of ray. The two take-off angles α and β, and the value of the velocity, c, at the point $\underset{\sim}{r}_0$, determine the initial slowness vector, $\underset{\sim}{L}_0$.

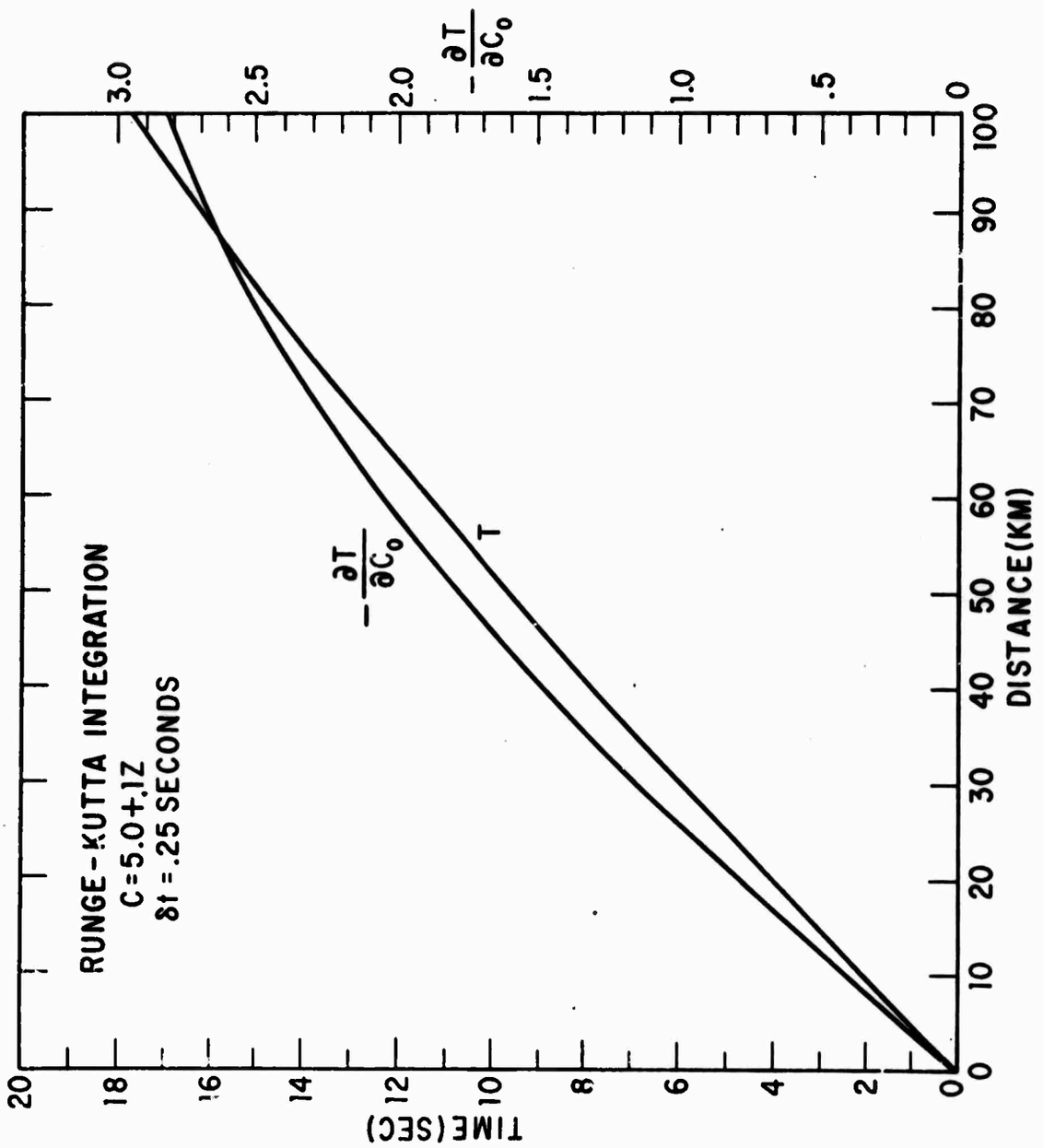
RUNGE-KUTTA INTEGRATION
C=5.0+.1Z
δt=.25 SECONDS
T
$-\frac{\partial T}{\partial C_0}$
TIME(SEC)
DISTANCE(KM)
$-\frac{\partial T}{\partial C_0}$

Fig. 3.1

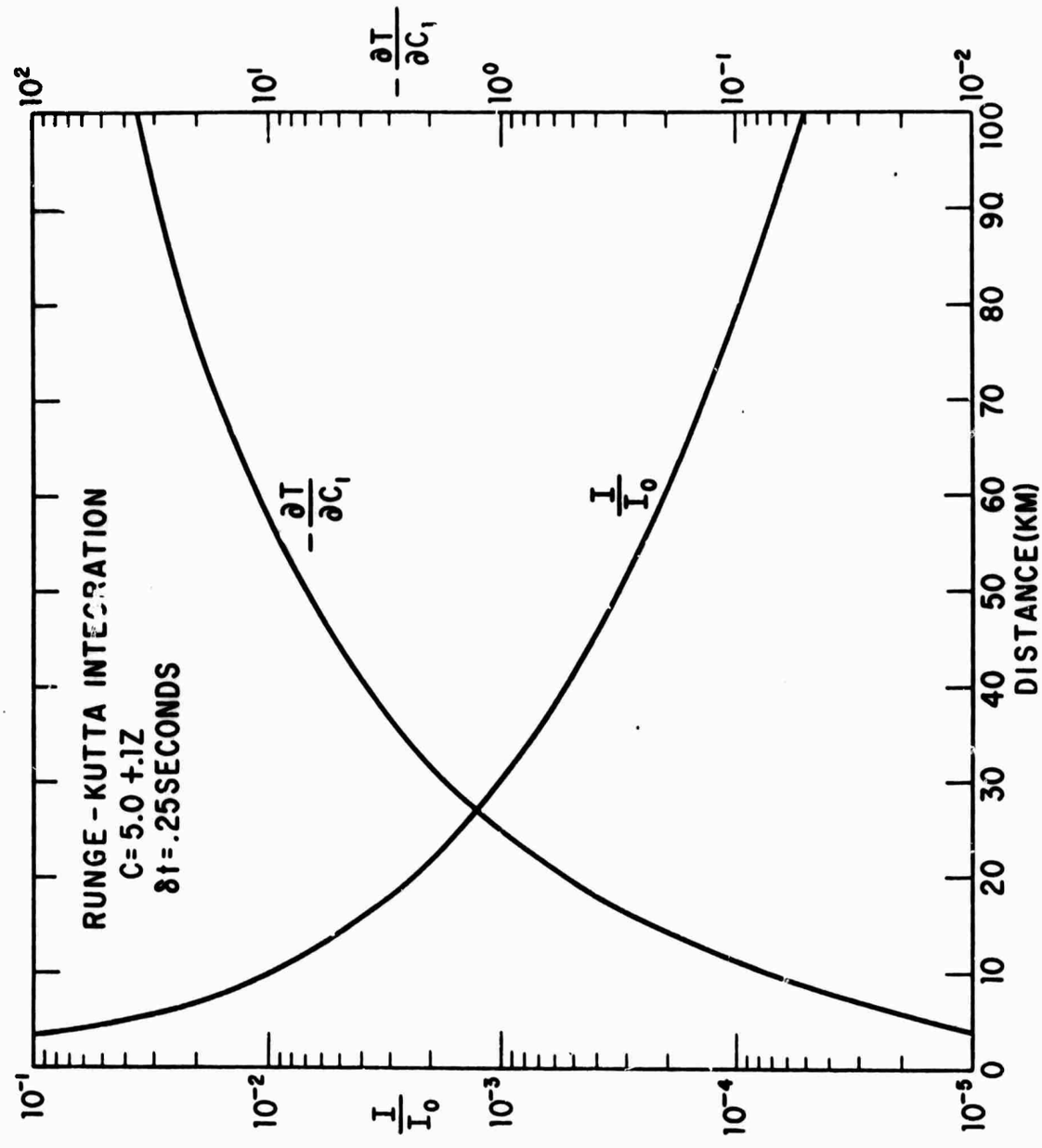
RUNGE-KUTTA INTEGRATION
C= 5.0 +.1Z
δt=.25SECONDS
$-\frac{\partial T}{\partial C_1}$
$\frac{I}{I_o}$
DISTANCE(KM)
10^{2}
10^{1}
10^{0}
10^{-1}
10^{-2}
10^{-3}
10^{-4}
10^{-5}
0
10
20
30
40
50
60
70
80
90
100

Fig. 3.2

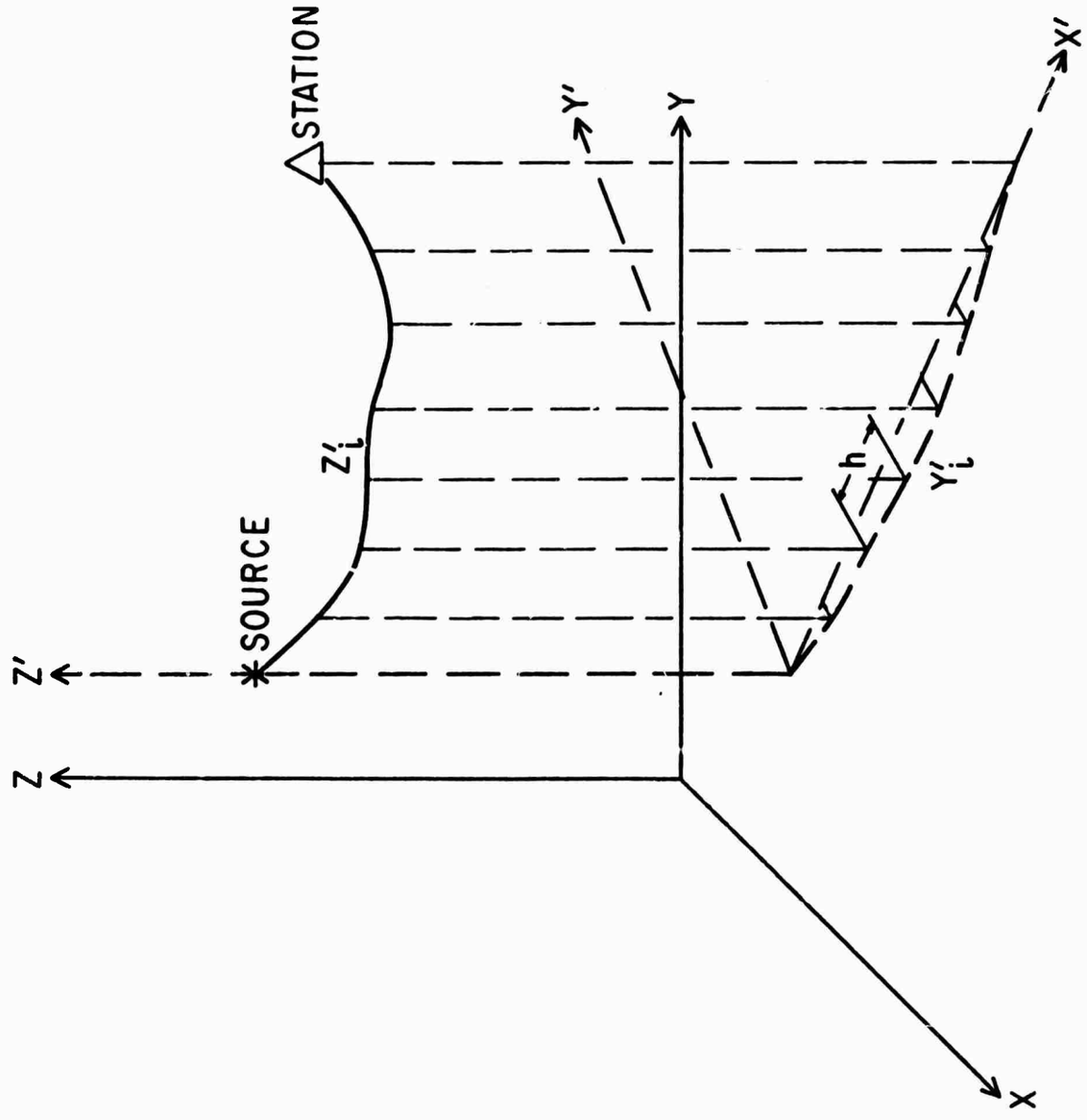

Fig. 3.3

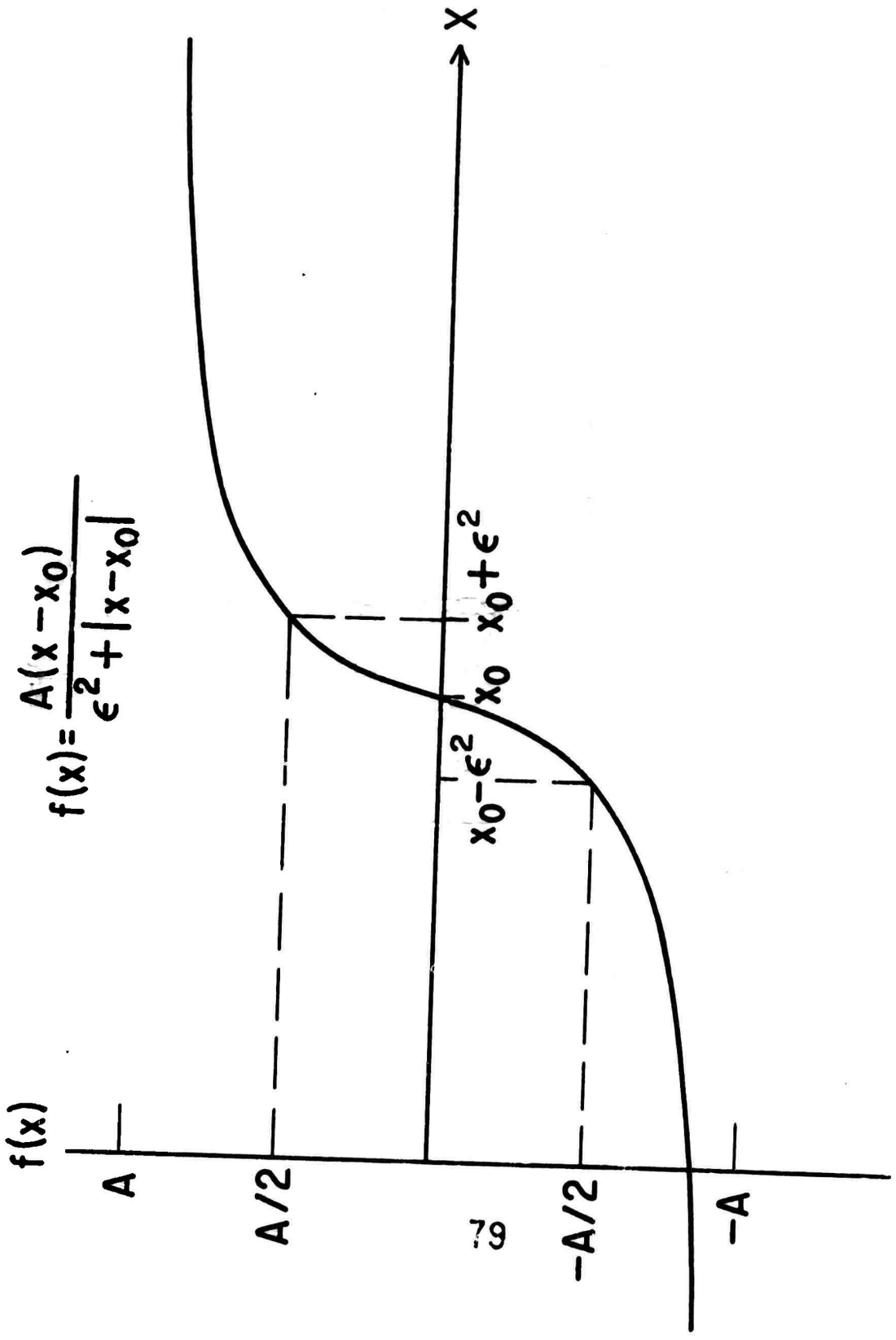
X
$f(x)=\frac{A(x-x_0)}{\epsilon^2+|x-x_0|}$
$x_0+\epsilon^2$
x_0
$x_0-\epsilon^2$
f(x)
A
A/2
-A/2
-A
79

Fig. 3.4

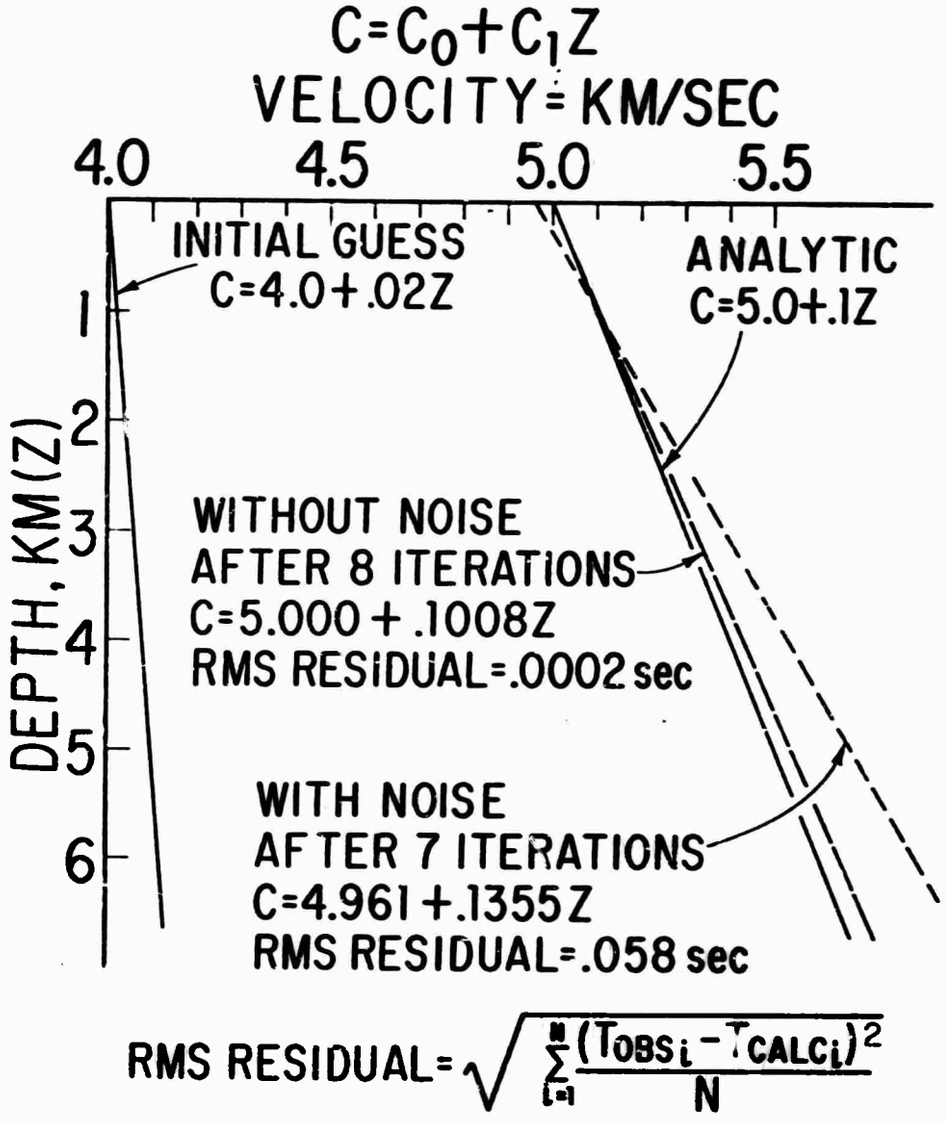
C=C0+C1Z
VELOCITY=KM/SEC
4.0
4.5
5.0
5.5
INITIAL GUESS
C=4.0+.02Z
ANALYTIC
C=5.0+.1Z
DEPTH, KM(Z)
1
2
3
4
5
6
WITHOUT NOISE
AFTER 8 ITERATIONS
C=5.000+.1008Z
RMS RESIDUAL=.0002 sec
WITH NOISE
AFTER 7 ITERATIONS
C=4.961+.1355Z
RMS RESIDUAL=.058 sec
RMS RESIDUAL=√(Σ(TOBSi−TCALCi)²/N)

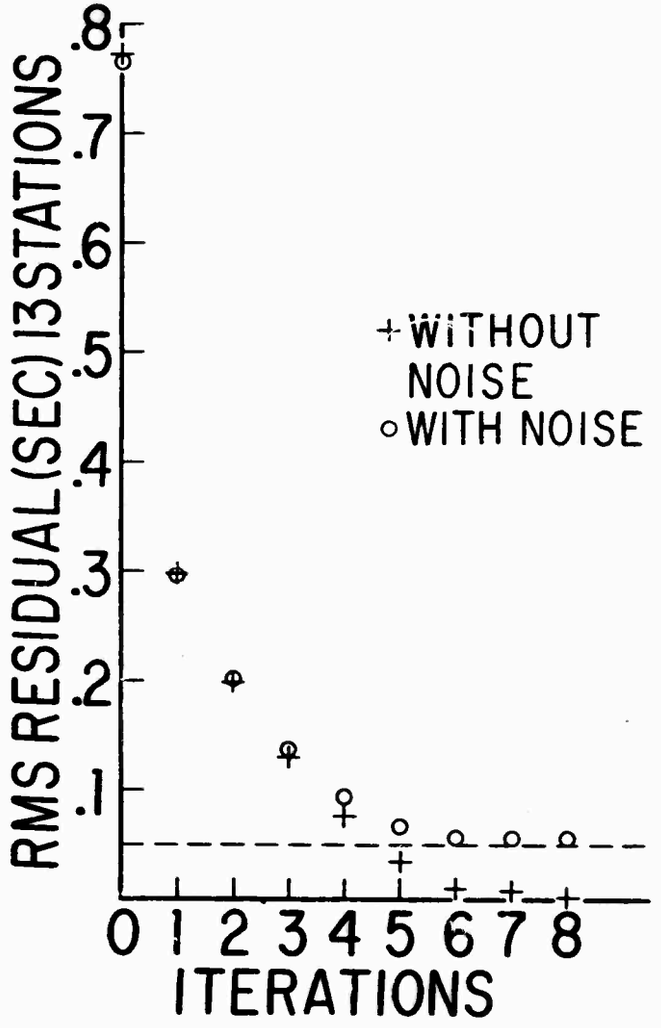
RMS RESIDUAL(SEC) 13STATIONS
.8
.7
.6
.5
.4
.3
.2
.1
+WITHOUT NOISE
oWITH NOISE
0 1 2 3 4 5 6 7 8
ITERATIONS

Fig. 3.5

80

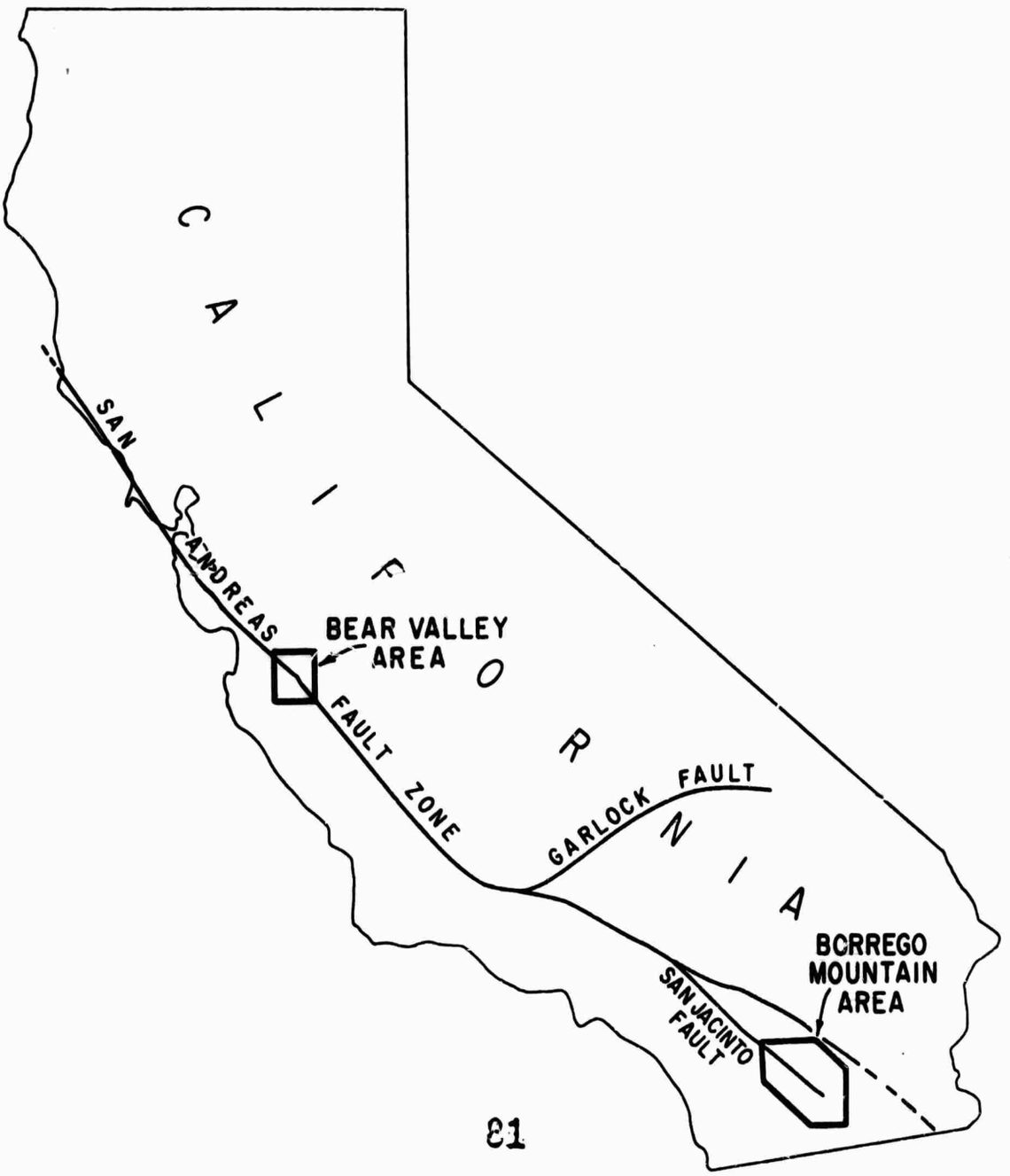
CALIFORNIA
SAN ANDREAS FAULT ZONE
BEAR VALLEY AREA
GARLOCK FAULT
SAN JACINTO FAULT
BORREGO MOUNTAIN AREA
81

Fig. 4.1

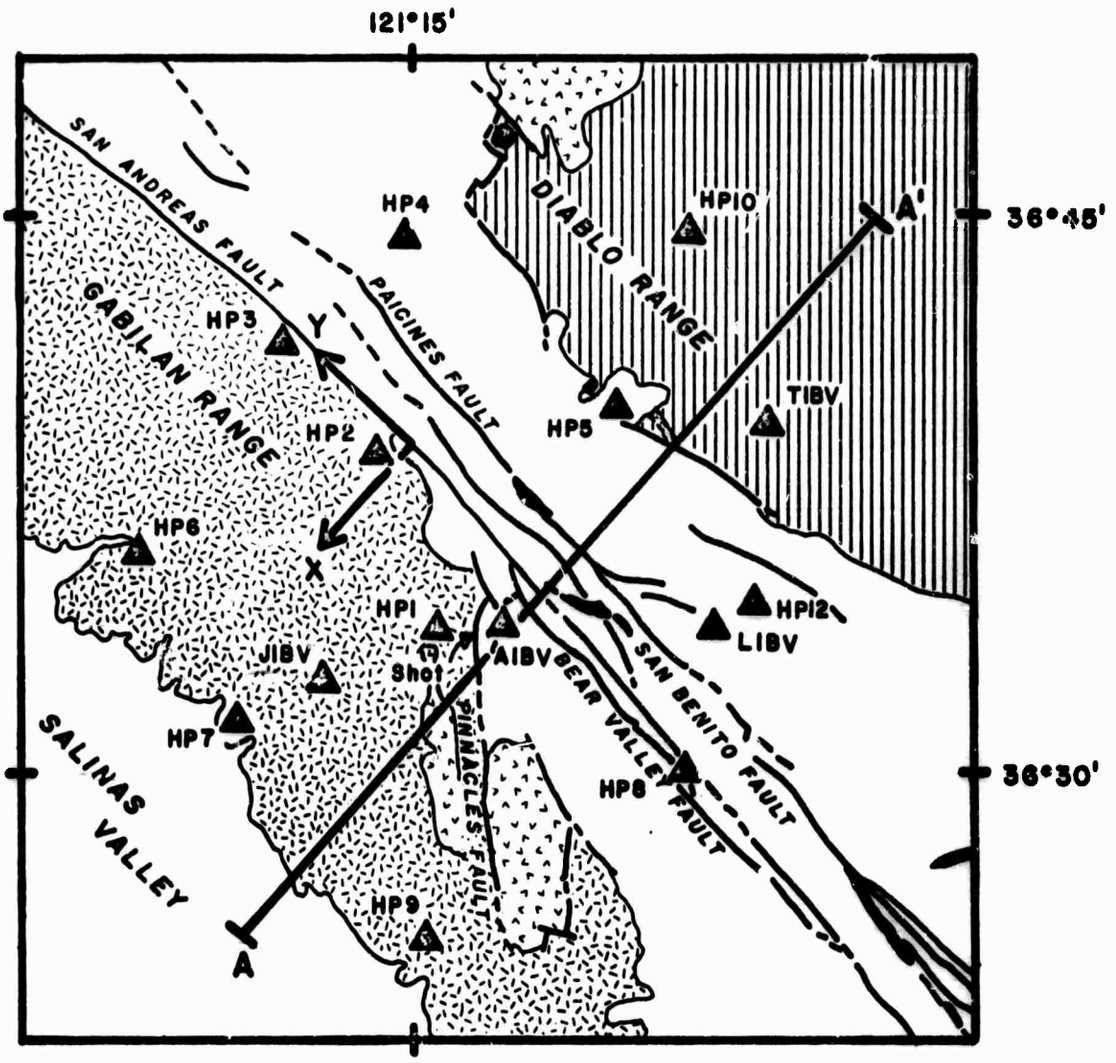

EXPLANATION

- Post-Franciscan
- Miocene volcanics
- Franciscan
- Mesozoic granite
- Ultrabasic rocks

0 5 10 km

82

Fig. 4.2

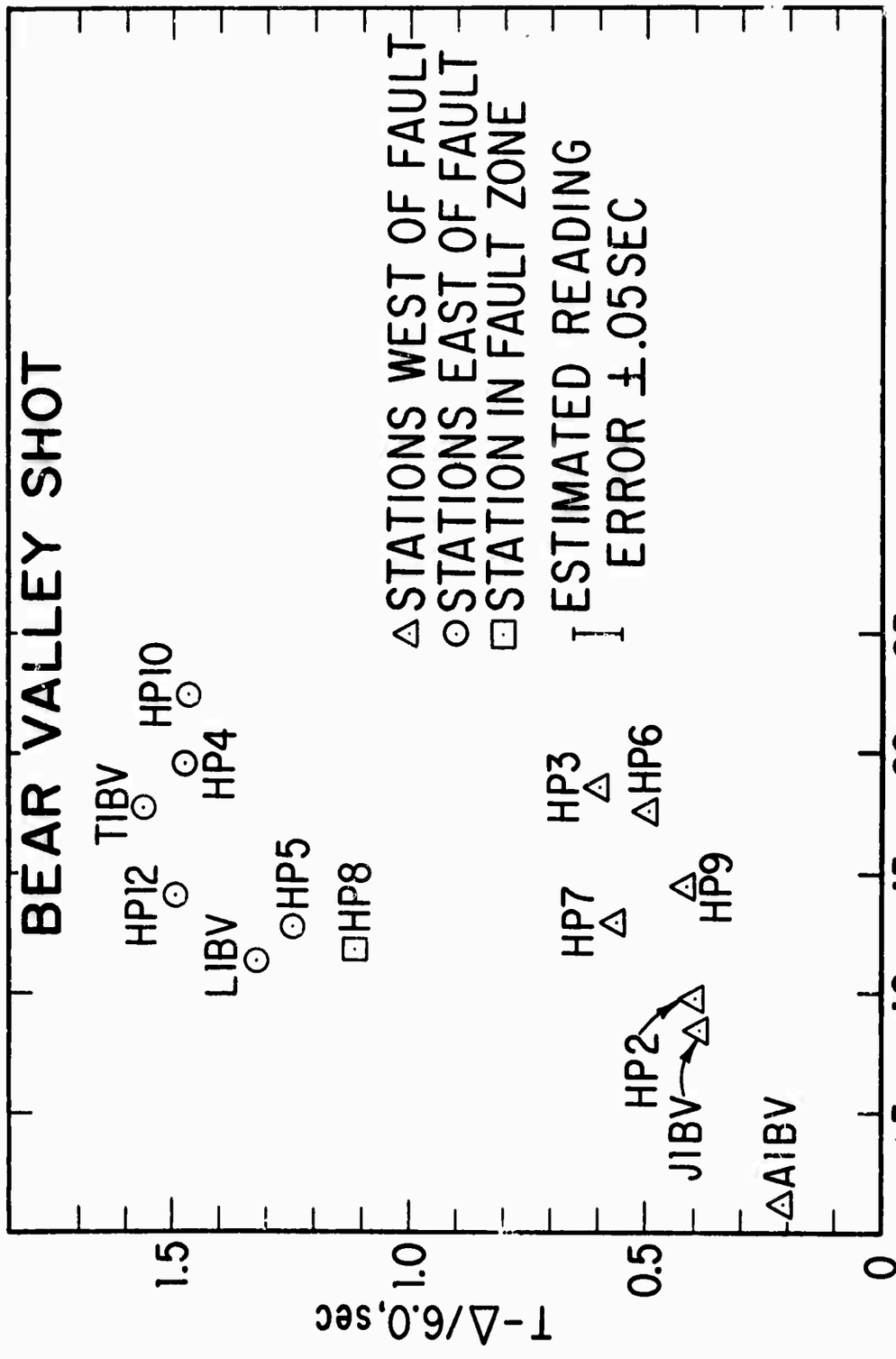
BEAR VALLEY SHOT
△STATIONS WEST OF FAULT
○STATIONS EAST OF FAULT
□STATION IN FAULT ZONE
I ESTIMATED READING ERROR ±.05SEC
T1BV
HP10
HP4
HP12
HP5
LIBV
HP8
HP3
HP6
HP7
HP9
HP2
J1BV
A1BV
T-Δ/6.0, sec
Δ, km
0
5
10
15
20
25
0.5
1.0
1.5

Fig. 4.3

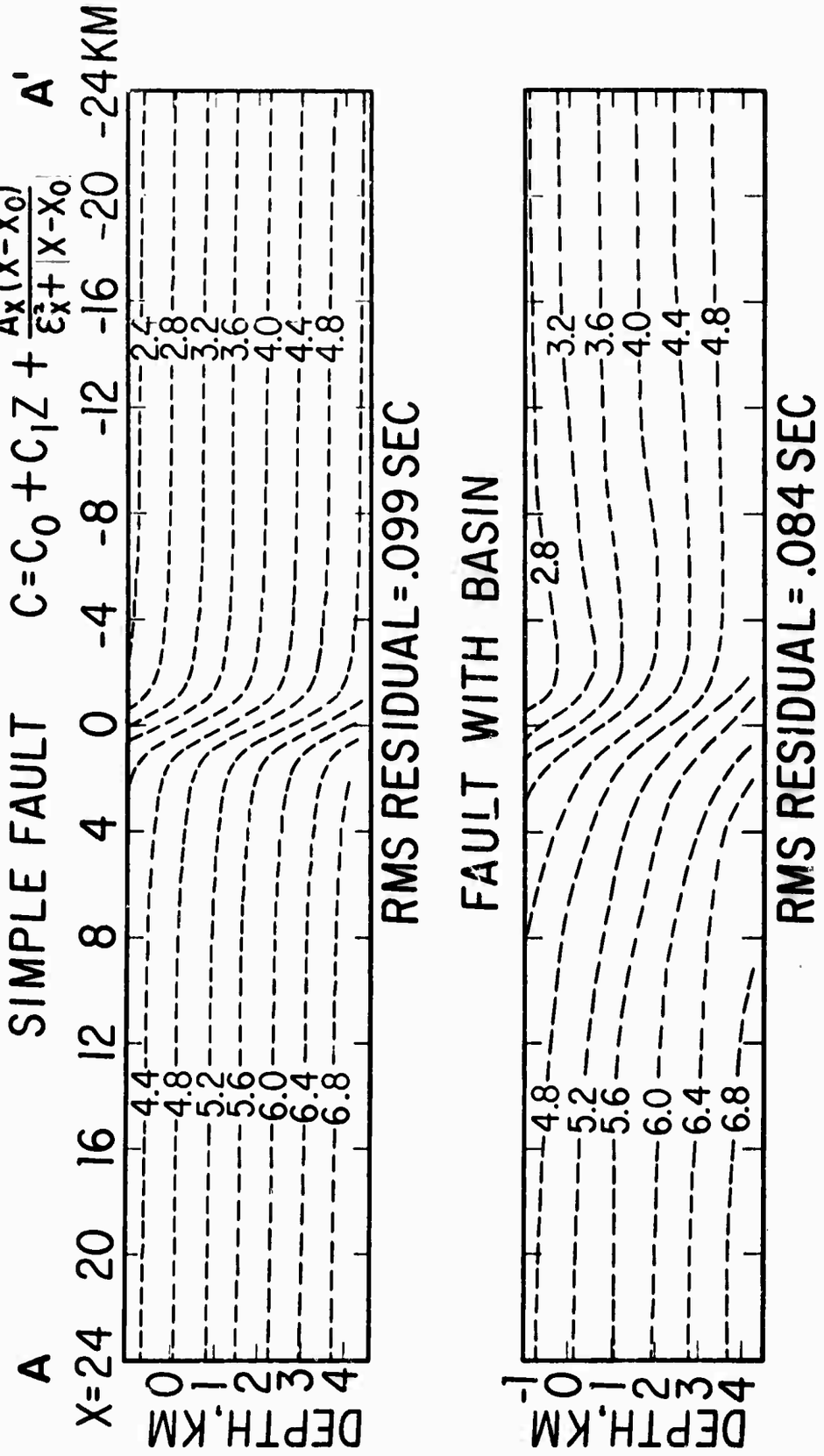
A
X=24 20 16 12 8 4 0 -4 -8 -12 -16 -20 -24KM
A'
SIMPLE FAULT
$C=C_0+C_1Z+\frac{A_x(X-X_0)}{\varepsilon_x^3+|X-X_0|}$
DEPTH, KM
RMS RESIDUAL=.099 SEC
FAULT WITH BASIN
RMS RESIDUAL=.084 SEC

Fig. 4.4

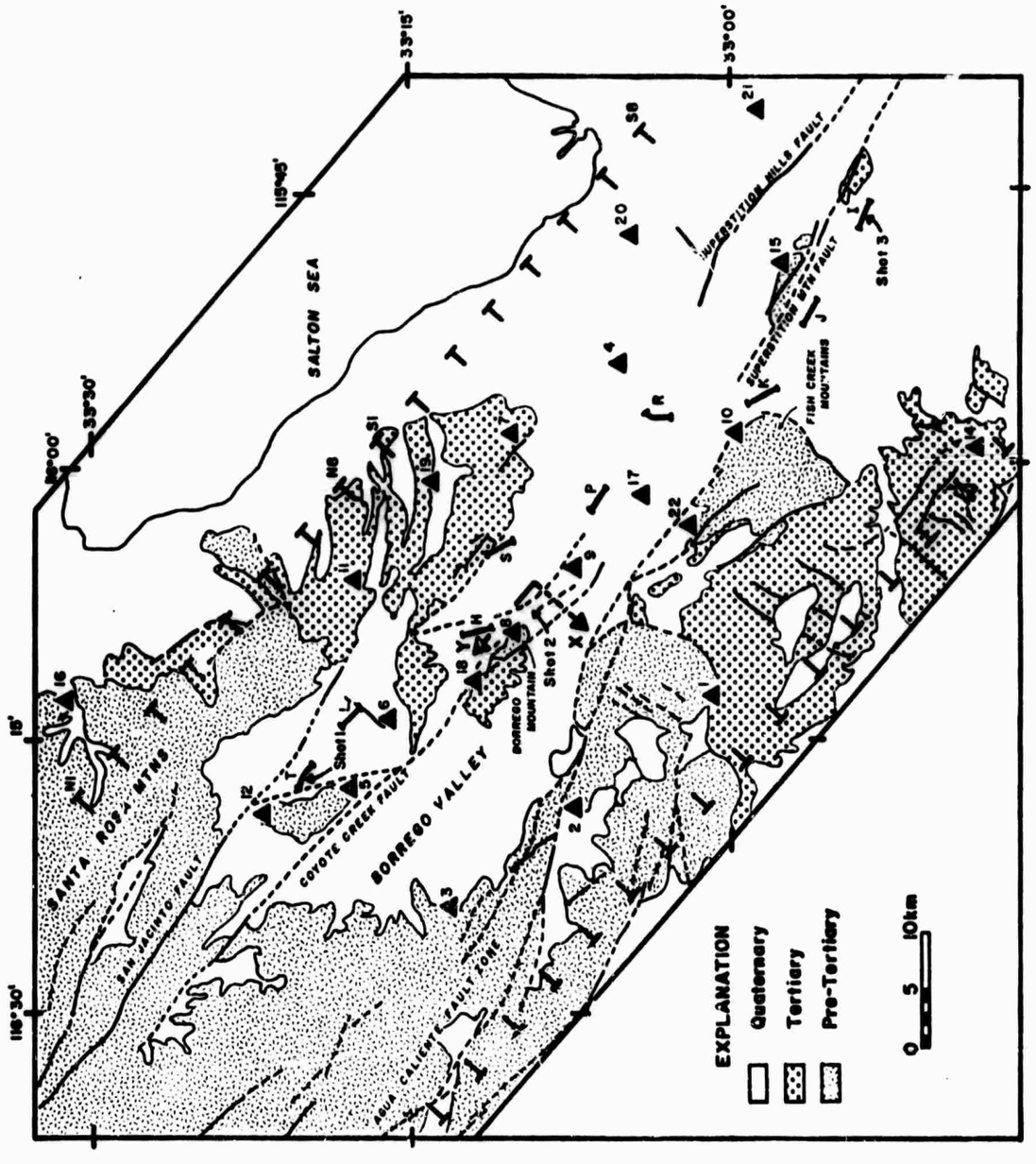
SALTON SEA
SANTA ROSA MTNS
SAN JACINTO FAULT
COYOTE CREEK FAULT
BORREGO VALLEY
BORREGO MOUNTAIN
SUPERSTITION HILLS FAULT
SUPERSTITION SITE FAULT
FISH CREEK MOUNTAINS
AQUA CALIENTE FAULT ZONE
Shot 1
Shot 2
Shot 3
EXPLANATION
Quaternary
Tertiary
Pre-Tertiary
0 5 10km

Fig. 4.5

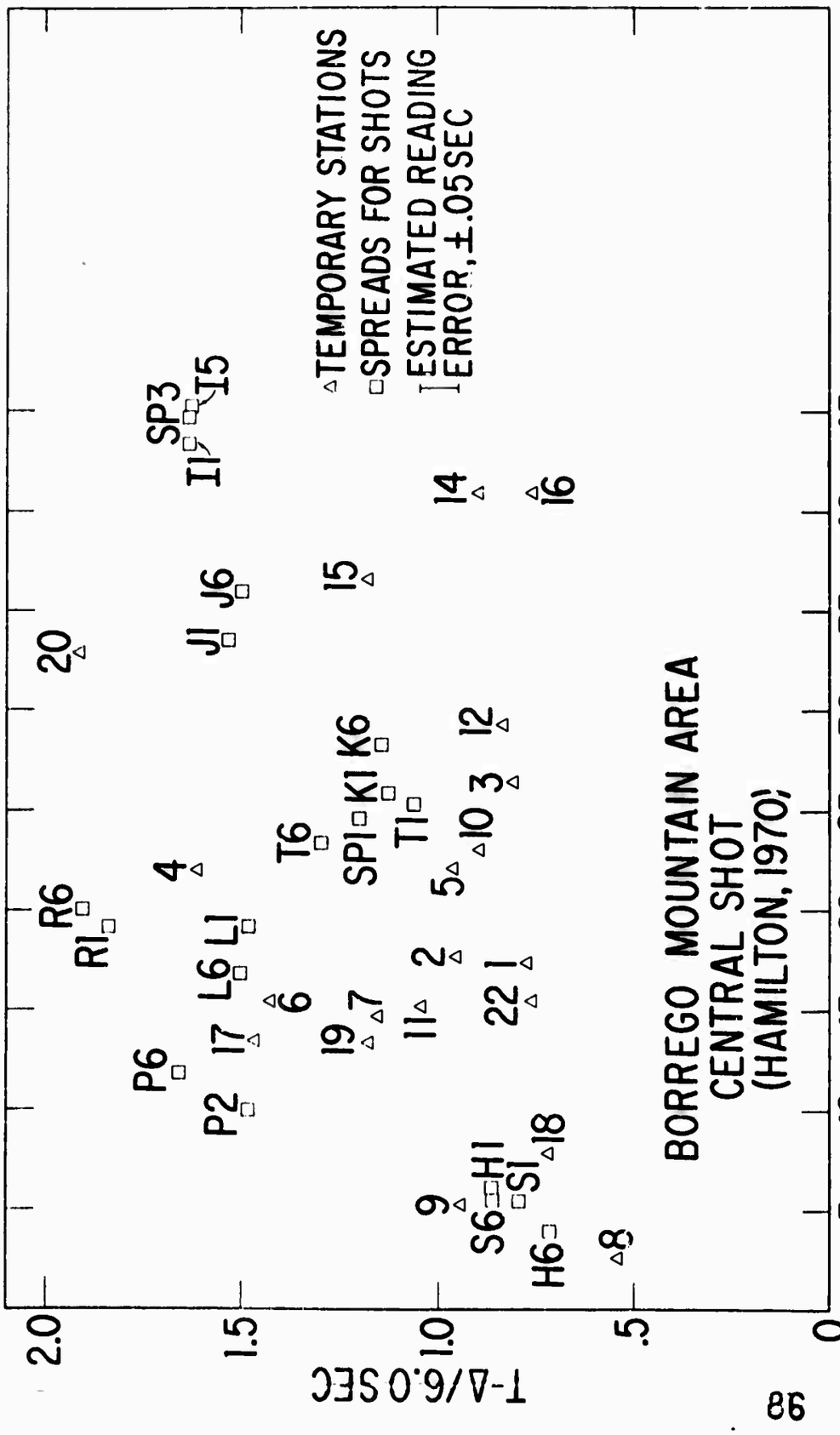
BORREGO MOUNTAIN AREA
CENTRAL SHOT
(HAMILTON, 1970)
TEMPORARY STATIONS
SPREADS FOR SHOTS
ESTIMATED READING
ERROR, ±.05 SEC
T-Δ/6.0 SEC
Δ, KM
2.0
1.5
1.0
.5
0
5
10
15
20
25
30
35
40
45
R6
R1
P6
P2
L6
L1
17
4
6
7
19
20
T6
SP1
K1
K6
T1
11
2
5
10
3
12
22
1
9
S6
H1
S1
18
H6
8
J1
J6
15
SP3
I1
I5
14
16

Fig. 4.6

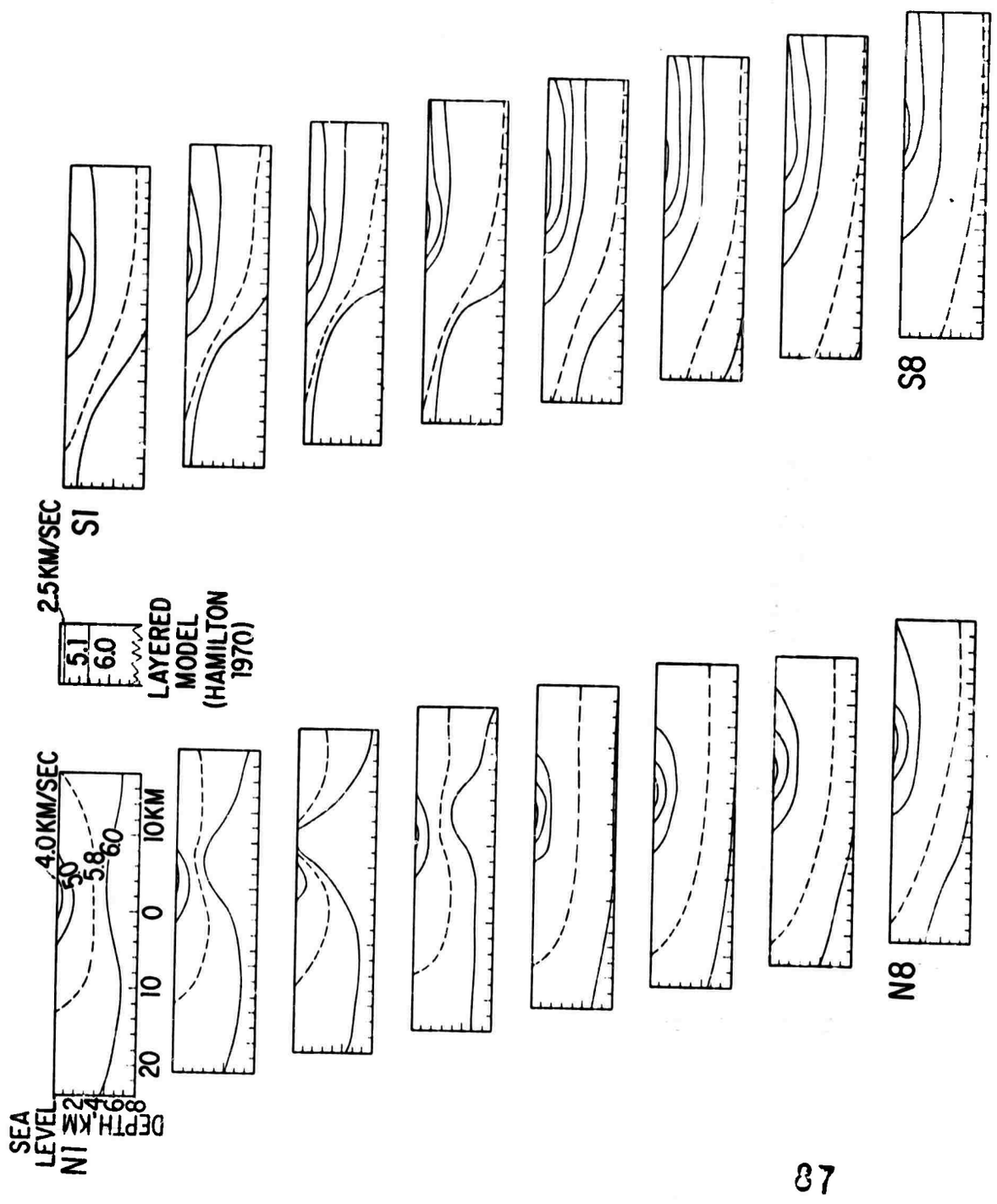
SEA LEVEL
N1
DEPTH, KM
2
4
6
8
20
10
0
10KM
4.0KM/SEC
5.0
5.8
6.0
2.5KM/SEC
5.1
6.0
LAYERED MODEL (HAMILTON 1970)
S1
S8
N8
87

Fig. 4.7

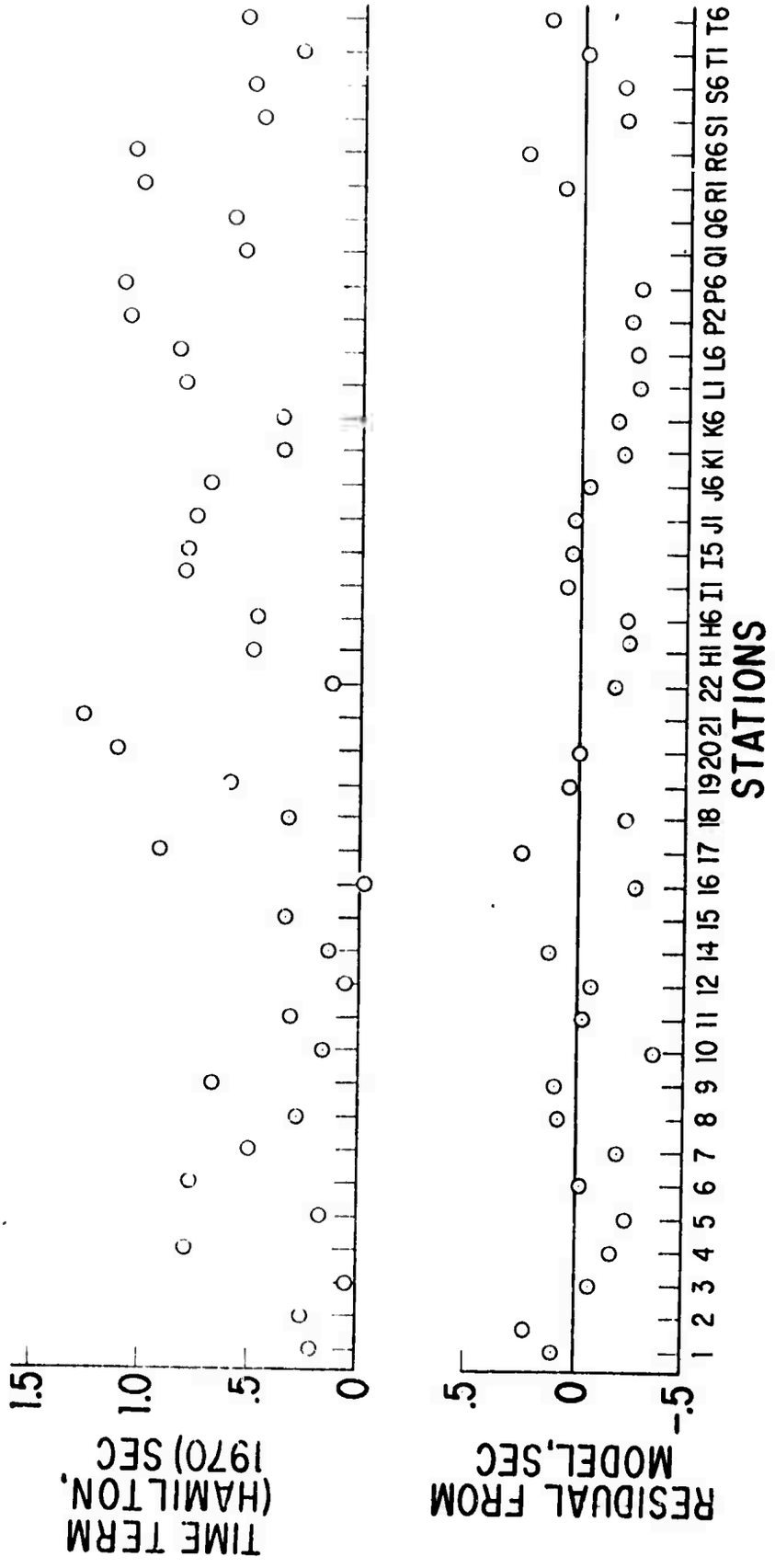
TIME TERM (HAMILTON, 1970) SEC
1.5
1.0
.5
0
RESIDUAL FROM MODEL, SEC
.5
0
-.5
1 2 3 4 5 6 7 8 9 10 11 12 14 15 16 17 18 19 20 21 22 H1 H6 I1 I5 J1 J6 K1 K6 L1 L6 P2 P6 Q1 Q6 R1 R6 S1 S6 T1 T6
STATIONS

Fig. 4.8

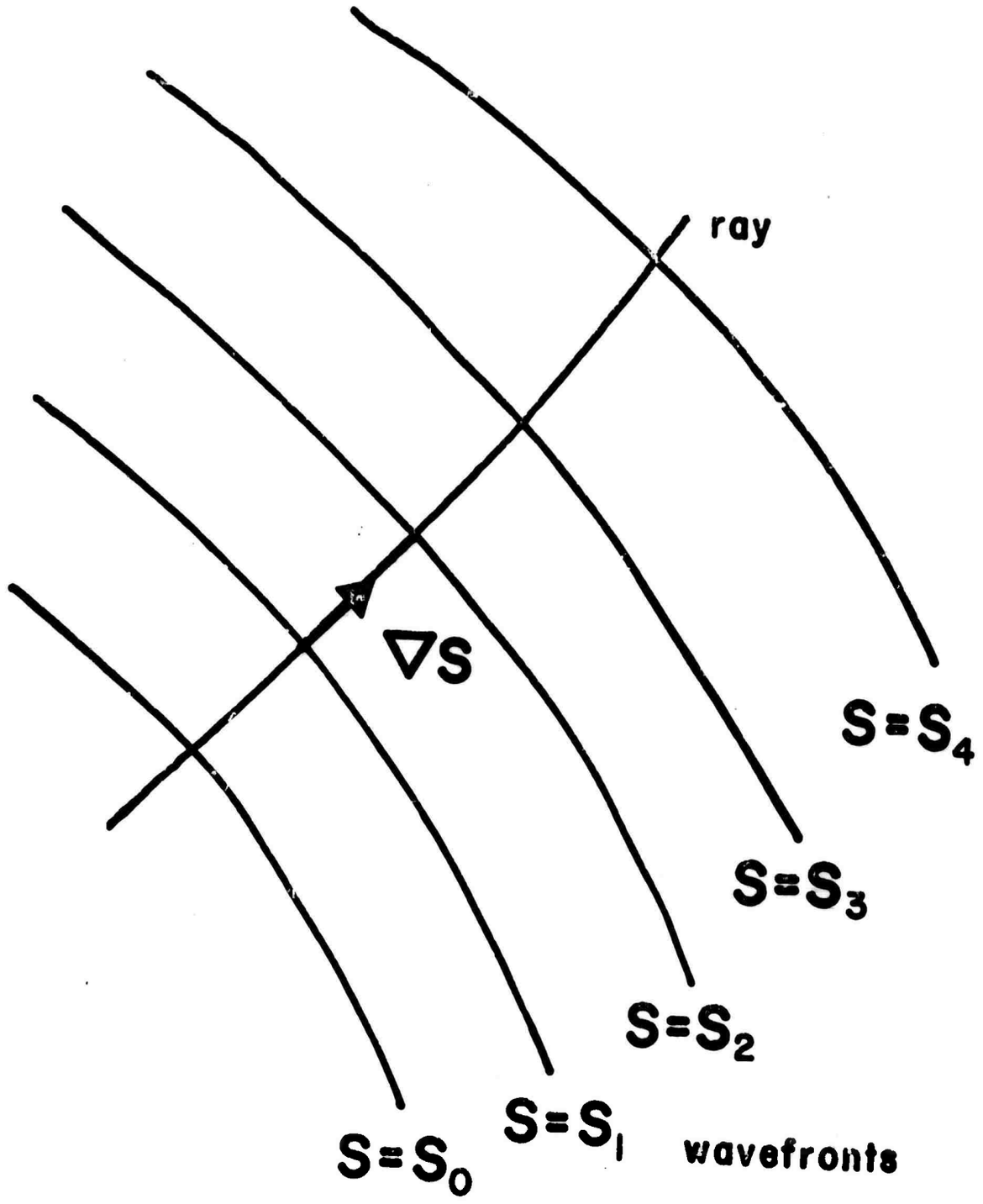

Fig. A.1

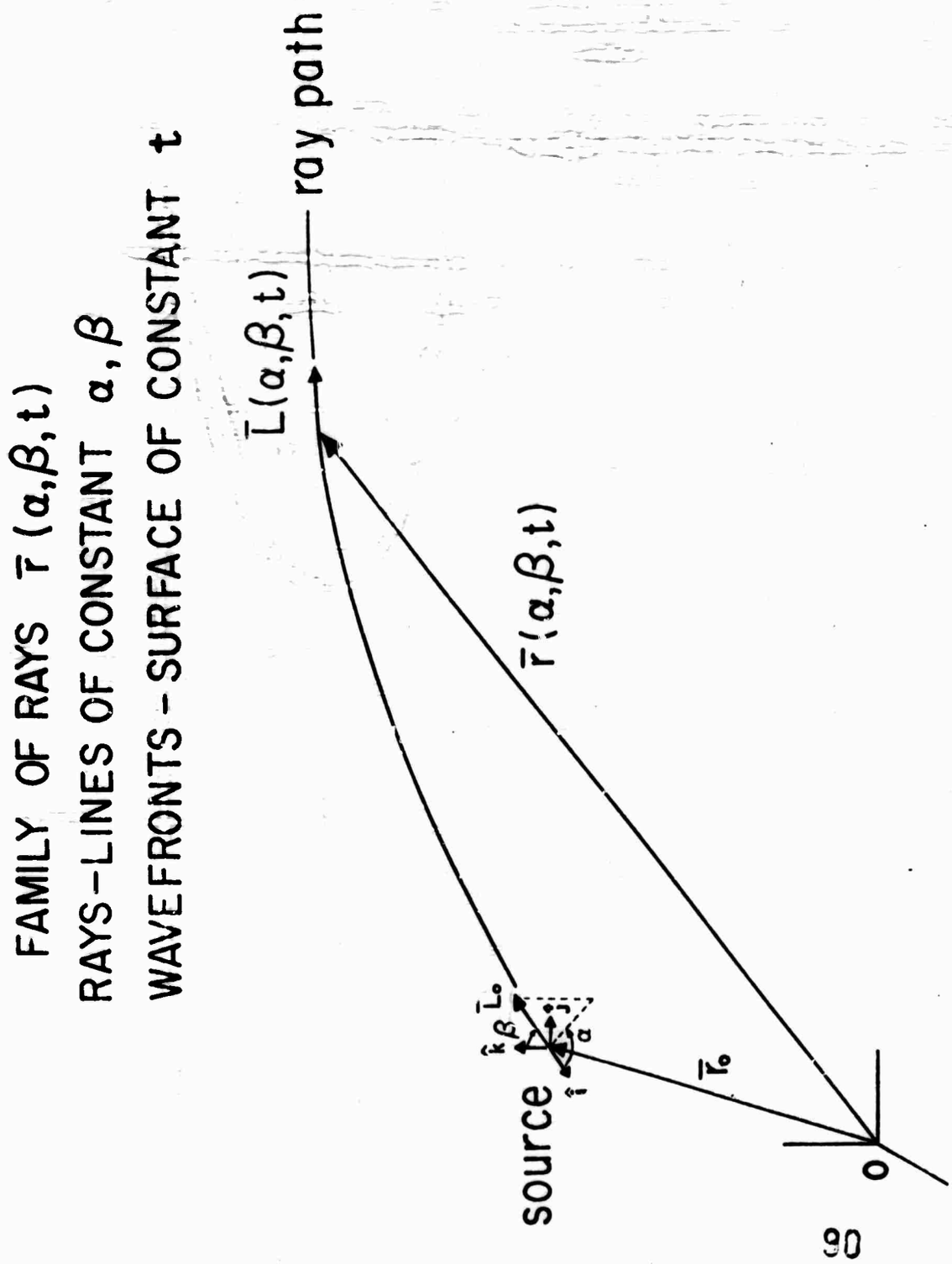
FAMILY OF RAYS $\bar{r}(\alpha,\beta,t)$
RAYS – LINES OF CONSTANT α,β
WAVEFRONTS – SURFACE OF CONSTANT t
$\bar{L}(\alpha,\beta,t)$
ray path
$\bar{r}(\alpha,\beta,t)$
$\bar{L}_o$
$\hat{k}$
β
$\hat{j}$
α
$\hat{i}$
source
$\bar{r}_o$
O
90

Fig. A.2

APPENDIX B

PKKP AND THE FINE STRUCTURE OF THE EARTH'S CORE

A DISSERTATION

SUBMITTED TO THE DEPARTMENT OF GEOPHYSICS

AND THE COMMITTEE ON THE GRADUATE DIVISION

OF STANFORD UNIVERSITY

IN PARTIAL FULFILLMENT OF THE REQUIREMENTS

FOR THE DEGREE OF

DOCTOR OF PHILOSOPHY

By

Teddy Godfrey Zengeni

March 1970

I certify that I have read this thesis and that in my opinion it is fully adequate, in scope and quality, as a dissertation for the degree of Doctor of Philosophy.

Robert L Kovach

(Principal Adviser)

I certify that I have read this thesis and that in my opinion it is fully adequate, in scope and quality, as a dissertation for the degree of Doctor of Philosophy.

I certify that I have read this thesis and that in my opinion it is fully adequate, in scope and quality, as a dissertation for the degree of Doctor of Philosophy.

92

Approved for the University Committee on the Graduate Division:

Lincoln E Moses

Dean of the Graduate Division

ABSTRACT

The slowness factor $dT/d\Delta$ for the core phase PKKP was measured at the Large Aperture Seismic Array (LASA), Montana, in the epicentral distance range $75° < \Delta < 125°$. Due to the high phase velocities involved, or equivalently, low slowness factor, corrections for simple geologic structures under the array were imperative. A method was derived to correct for the dipping M-discontinuity under LASA.

A velocity model for the earth's core was computed from the $dT/d\Delta$ observations, together with PKP travel times, using the Wiechert-Herglotz integration method. The PKKP core velocity model derived is essentially tripartite, but differs from other proposed models in important details.

The major part of the outer core exhibits no striking differences from the standard Jeffreys' model: fairly constant velocity gradients in the SKS and ABC (Bullen 'E') regions. However, at a radius of 1654 km there is a discontinuity in the velocity gradient and the next 250 km in depth is a distinct region of slightly higher velocity. The transition zone into the inner core is only 200 km in thickness and is characterized by a gentle negative velocity gradient. This zone has an average velocity of 10.45

km/sec. The inner core starts at radius 1217 km with an average velocity of about 11.20 km/sec and possesses a slight negative velocity gradient towards the center of the earth. A slight drop in compressional velocity in the mantle at the core-mantle boundary is also inferred.

It is conjectured that the transition zone (liquid or viscous) and the inner core (solid) are of the same chemical composition, but differ from that of the outer core.

ACKNOWLEDGMENTS

It is a pleasure to acknowledge my debt and gratitude to Professor Robert L. Kovach. He suggested the topic, provided guidance and encouragement during the research and in the final preparation of the dissertation. Thanks are due my colleague Robert L. Wesson for use of his ray-tracing computer programs, and Joan Gast for typing the manuscript. This work was completed during tenure of an AFGRAD Fellowship under the auspices of the African American Institute. The research was financially supported by the Advanced Research Project Agency and was monitored by the Air Force Office of Scientific Research under contract AF49(638)-1687.

TABLE OF CONTENTS

LIST OF ILLUSTRATIONS

LIST OF TABLES

I. INTRODUCTION

The existence of the core in the earth was postulated in the 1890's by Wiechert, and subsequently subdivided into a fluid outer core, and an inner core (most likely solid) by Lehmann in 1936. With only a few exceptions, most of the velocity models of the earth's core are derived from travel time data from the seismic core phases PKP and PKIKP in conjunction with scanty SKS observations. The classical velocity models are those of Jeffreys (1939) and Gutenberg (1958).

As more high quality data have accumulated these models have been continually modified. The list of proposed models for the core is sizeable. Bolt (1964) constructed a tripartite core model to explain the PKIKP (DF branch) forerunners that had previously been explained by diffraction at the caustic B. Adams and Randall (1963, 1964) have also proposed a tripartite core. Ergin (1967) postulated a more complex layered core model Engdal (1968) constructed a series of models modified from those of Jeffreys, Bolt, and Adams and Randall. All of these models were based on detailed observations of the core phase PKP. Other investigators, although not proposing new models, have studied PKP data to refine their travel times (Hai, 1961, 1963; Kovach and Glover, 1968: Subiza and Bath, 1964; and others). The models of Jeffreys, Gutenberg, Bolt, and

Adams and Randall are illustrated in Fig. 1.

The use of the free oscillations of the earth to determine the structure of the deep interior deserves brief mention. Although normal modes have been successfully accurate at determining, or setting limits to, the seismic parameters in the earth's mantle (Press,1968; Bullen and Haddon,1967, 1969) the method is not sufficiently sensitive to the deeper core structures (Anderson and Kovach, 1969) and hence cannot be used to determine the fine structure of the earth's core.

Most of the core models are essentially trial-and-error models which are adjusted to fit the observed travel time data. As a result they are not unique, as emphasized by the large number of Monte Carlo random models Press (1968) generated to satisfy given travel times. However, given sufficient data and as long as $dV/dr < V/r$ the direct use of $dT/d\Delta$ reduces considerably the number of possible models.

Travel time analyses for velocity determination even though carefully carried out are hampered by having lower resolution than direct $dT/d\Delta$ measurements using arrays. Extensive use of array data has resulted in the proposed refinement of the velocity distribution in the lower and upper mantle (Niazi and Anderson, 1965; Otsuka, 1966 a, b; McEvilly, 1966; Johnson, 1967, 1969; Chinnery and Toksöz, 1967; Fairborn, 1968; Kovach and Robinson, 1969).

Use of arrays for core phases has not been exploited and analyses of the slowness factor $dT/d\Delta$ have been limited. Prior to the installation of LASA, Hannon and Kovach (1966) used velocity filtering with a network of portable stations in Arizona to identify the various branches of the core phase PKP in the distance range 125°-160°.

Because of the very high apparent phase velocities (greater than 25 km/sec) or equivalently, low slowness factor ($dT/d\Delta$ less than 4.5 sec/deg) arrays with large apertures are required if observational errors are to be small relative to the small time delays. Husebye and Toksöz (1968) circumvented the difficulty by using the WWSSN and LRSM stations in North America as a continental size array to study the PKP core phase. Of course, if the array gets too large the coherence between stations decreases and the problem of correct identification of the various travel time branches again arises. The core model deduced by Husebye and Toksöz is outlined in the caption to Fig. 1.

The slowness factor for the core phase PKKP was determined using the Large Aperture Seismic Array (LASA), Montana, which has an aperture of 2° (or a diameter of about 200 km). A $dT/d\Delta$ vs Δ curve was used to determine the P wave velocity distribution in the core using the Wiechert-Herglotz technique.

The reason for the choice of the core phase PKKP to study the core velocity structure is two-fold. First, LASA

is strategically situated with respect to the high seismicity areas of the world, which lie within the epicental distance range for the observation of PKKP. Fig. 2. shows the location of the events used in this study. Second, the phase PKKP traverses a distance in the core twice as long as the phase PKP, and thus the observed branches are stretched out and less crowded, giving better resolution.

The core model derived in this thesis is essentially tripartite, similar to those of Bolt (1964) and Adams and Randall (1964), although differing in fine structure and the size of the transition zone between the outer and inner cores.

II. A BRIEF REVIEW OF THE THEORY OF dT/dΔ

The theory of the use of the slowness factor (slope of the travel time curve) in studying the velocity distribution in the earth is classical (Bullen, 1963). For the sake of continuity and the establishment of notation, a brief outline of the theory is presented.

In a spherically symmetric earth a ray is characterized by the parameter p, an invariant of the ray,

$$p \equiv \frac{r \sin i}{V(r)} \tag{1}$$

where r is the radius coordinate from the center of the earth, i is the angle of incidence between the ray and the radius, and V(r) is the seismic velocity at radius r.

The seismic ray parameter is in turn related to the slope of the travel time curve through the slowness factor dT/dΔ:

$$p \equiv \frac{r \sin i}{V(r)} = \frac{r_0 \sin i_0}{V(r_0)} \equiv dT/d\Delta \tag{2}$$

Fig. 3. illustrates the geometry considered.

If Δ is the epicentral distance from a surface focus to the observation point on the surface, then a functional relationship between the velocity and the radius can be

derived (Bullen, 1961) to give the famous Wiechert-Herglotz relation

$$\pi \ln \left\{\frac{a}{r_1}\right\} = \int_0^{\Delta_1} \operatorname{arc\,cosh} \left\{\frac{p(\Delta)}{\eta(r_1)}\right\} d\Delta \qquad (3)$$

where

$$\eta(r_1) = V(r_1)/r_1 \equiv p(\Delta_1) \qquad (4)$$

and a is the radius of the earth.

For the determination of the velocity depth function, $dT/d\Delta$ measurements are superior to travel time in many aspects. First, application of $dT/d\Delta$ dispenses with accurate knowledge of the origin time of the event. Certain significant corrections imperative when using travel time data are less crucial in $dT/d\Delta$ measurements. Elevation and ellipticity corrections can be ignored, and small errors in epicentral location are tolerable especially when using teleseismic observations. Even corrections for focal depth become less important since they do not affect the seismic ray parameter itself except that the ray must be projected back to the surface. In the case of core phases with steep angles of incidence (less than 15° from the vertical) focal depth corrections are negligible.

Planar structures in the earth's crust and uniform lateral gradients can be easily corrected for in array measurements of $dT/d\Delta$ (Zengeni, 1969). Also, identification of the various branches of a phase is less ambiguous using seismic array data.

III. DATA COLLECTION, SELECTION AND REDUCTION

1. LASA, MONTANA

The configuration of the LASA is shown in Fig. 4, and details of the seismometers used in this study are listed in Table 1. Because of the low slowness factor involved, only the center seismometers of the A0 subarray and the outer E and F rings were used. These seismometers are buried to a depth of 500 ft to reduce meteorological noise. Details concerning other aspects of the LASA are given by Forbes et. al. (1965).

2. MEASUREMENT OF TIME DELAYS

Readings of the relative arrival times were picked on copies of LASA short period film, obtained from the Teledyne Seismic Data Labs, Alexandria, Virginia. Only events of large magnitude (about 6 or larger) produced usable observations of the phase PKKP. Table 2 lists the earthquakes used.

Relative arrival times were picked to 0.05 sec by visual alignment of each channel with a reference seismogram. Since absolute time is immaterial, times were read on any suitable point on the wave packet comprising the phase, and not necessarily on the actual onset which might not be as clear.

SUBARRAY CENTER	COORDINATES CENTER ELEVATION		
	LATITUDE (N)	LONGITUDE (W)	(METERS)
A0	46° 41' 19"	106° 13' 20"	896.8
E1	47° 09' 46"	106° 03' 22"	837.9
E2	46° 30' 46"	105° 21' 53"	762.2
E3	46° 08' 58"	106° 20' 03"	913.7
E4	46° 45' 39"	106° 55' 00"	955.3
F1	47° 22' 15"	105° 11' 15"	892.5
F2	45° 54' 34"	105° 21' 53"	906.7
F3	45° 58' 22"	107° 04' 54"	989.7
F4	47° 24' 40"	106° 56' 37"	859.8

Table 1. Center seismometers of the A0 subarray and the E and F rings. Seismometers are placed at depth of 500 ft $\sim$ 153 meters.

TABLE 2.

DATE	ORIGIN TIME (h m s)	EPICENTER LAT.	EPICENTER LONG.	MAG	DEPTH (km)	AZIMUTH ω	AZIMUTH ω'	AZIMUTH ϕ	DISTANCE Δ	SLOWNESS (sec/deg) p'	SLOWNESS (sec/deg) δp'	SLOWNESS (sec/deg) p	
13Jan68	16 07 04.2	-24.2	-066.9	5.7	192R	-36.12	-42.84	06.72	79.01	2.06	.18	2.41	-
							-42.88	6.76		2.13	.11	2.47	-
							-42.93	6.81		2.30	.12	2.64	-
06Feb68	11 19 23.1	-28.5	-071.0	5.7	23	-30.90	-37.21	6.31	81.33	2.05	.06	2.42	-
							-45.54	14.64		2.29	.21	2.52	-
							-41.99	11.09		2.02	.11	2.33	-
13Aug67	20 06 50.6	35.3	135.3	6.0	357	133.36	135.09	- 1.73	81.44	3.02	.03	2.85	
28Feb68	12 08 01.5	32.9	137.7	5.8	349	130.36	133.01	- 2.65	82.10	2.92	.07	2.53	
							132.55	- 2.19		2.99	.03	2.59	
20Jly67	13 11 35.0	-28.1	-066.9	5.3	157	-34.37	-41.92	7.55	82.49	2.56	.12	2.88	-
26Sep67	16 11 23.9	-30.0	-071.5	5.8	55R	-29.89	-36.33	6.44	82.52	2.05	.09	2.42	-
17Jan67	01 07 54.3	-27.4	-063.3	5.5	590	-37.56	-41.61	4.01	83.33	2.57	.12	2.94	-
							-41.18	3.58		2.29	.13	2.68	-
31Jan68	02 03 29.3	-27.7	-063.2	4.9	580R	-37.55	-42.90	5.53	83.53	2.50	.09	2.85	-
03Sep68	08 19 52.2	41.8	032.3	5.7	5	209.84	196.47	13.37	84.49	2.40	.02	1.87	
14May68	14 05 06.0	29.9	129.4	5.9	168R	134.20	135.23	- 1.03	88.73	3.09	.04	2.97	+
							136.90	- 2.70		5.06	.09	4.71	+
							135.43	- 1.23		2.93	.02	2.51	+
26Sep68	08 41 22.0	-17.7	-178.5	5.1	578D	065.25	078.74	-13.49	91.11	2.63	.05	2.61	
							077.76	-12.51		2.78	.18	2.76	
12Nov68	00 44 12.8	27.5	128.4	5.-	48D	133.58	135.68	- 2.10	91.20	3.15	.06	2.75	+
18Dec68	20 03 43.9	-19.9	-177.6	5.5		063.18	076.09	-12.91	92.21	2.68	.13	2.68	
26Sep68	14 37 46.2	-20.9	-177.0	5.8	251D	062.10	074.14	-12.04	92.60	2.56	.06	2.58	
12Sep68	22 44 06.5	-21.6	-179.4	5.9	635D	063.34	075.34	-12.00	94.59	2.63	.07	2.64	
26Oct67	00 22 21.6	24.5	122.2	5.6	63	136.56	138.01	- 1.45	96.89	3.01	.10	2.60	+
04Nov67	05 07 18.0	24.3	122.2	5.0	76	136.56	137.48	- 0.92	96.89	3.28	.09	2.86	+
25Oct67	00 59 22.6	24.5	122.2	6.0	65	136.67	135.67	1.00	96.7	3.36	.04	3.50	
							138.16	- 1.49		3.20	.10	3.01	
							136.79	- 0.12		3.33	.06	3.31	
29Jan68	05 00 10.0	36.3	70.4	5.5	225	182.75	174.59	8.16	97.33	3.27	.07	2.99	+

TABLE 2 Continued

DATE	ORIGIN TIME (h m s)	EPICENTER LAT.	EPICENTER LONG.	MAG	DEPTH (km)	AZIMUTH ω	AZIMUTH ω'	AZIMUTH ϕ	DISTANCE Δ	SLOWNESS (sec/deg) p'	SLOWNESS (sec/deg) δp'	SLOWNESS (sec/deg) p	
08Jly67	00 58 54.7	-15.4	167.5	5.2		076.72	084.05	- 7.33	98.53	2.77	.10	2.71	
26Feb68	10 50 16.7	22.7	121.5	6.7	24	136.29	136.03	0.26	98.59	3.50	.12	3.05	
							136.80	- 0.51		3.32	.03	2.89	
02Jne68	08 18 36.2	-8.1	156.8	5.6	35	088.17	095.82	- 7.65	99.38	4.47	.05	4.23	
28Nov68	16 30 32.1	-6.8	156.2	4.3		090.80	096.44	- 5.64	100.11	4.48	.05	4.29	
23May68	18 43 01.0	-30.0	-177.7	5.6	70	056.20	061.64	- 5.44	100.30	4.34	.13	4.42	
							061.12	- 4.92		4.86	.05	4.94	
26Sep68	18 02 50.1	-30.5	-178.2	5.8	N	056.69	066.21	- 9.62	100.51	2.76	.05	3.08	
							069.63	-13.04		3.00	.08	3.01	
							067.96	-11.37		2.93	.06	2.87	
30May68	19 42 25.0	-31.0	-177.6	5.5	42	055.86	061.63	- 5.77	100.54	4.46	.09	4.55	
20May68	20 05 49.1	-30.7	-178.4	7.0	46	056.59	066.21	- 9.62	100.77	2.80	.06	2.87	
							070.92	-14.33		2.92	.07	3.00	
20Jau68	21 21 31.6	-29.9	-179.5	5.8	349R	057.85	070.39	-12.54	100.82	2.80	.07	2.86	
20May68	07 43 03.0	-30.9	-178.3	6.0		056.38	072.04	-15.62	100.87	3.01	.05	3.10	
							063.59	- 7.20		4.33	.10	4.43	
07Jan68	09 50 40.0	-05.1	153.0	5.6		094.34	098.50	- 4.16	101.08	4.47	.07	4.31	
							099.62	- 5.28		4.86	.08	4.64	
24Feb68	01 11 11.6	-32.5	-177.7	5.4	21	054.84	060.37	- 5.53	101.65	4.36	.08	4.45	
26Nov68	01 10 12.9	-05.3	152.0	5.5		094.90	100.25	- 5.35	101.90	4.56	.04	4.34	
							102.07	- 7.17		4.59	.08	4.29	
03Aug68	06 25 05.8	16.5	122.3	5.9	37	132.35	135.77	- 3.42	103.45	3.45	.06	3.10	+
							134.87	- 2.52		5.04	.06	4.68	+
02Aug68	13 30 23.3	27.5	060.9	5.7	62	191.84	184.30	7.54	105.25	3.41	.08	2.66	
03Jne68	09 17 46.2	-05.4	147.0	4.1	191	098.60	104.62	- 6.02	105.40	3.51	.05	4.40	
08Sep68	15 12 23.8	-03.7	143.0	6.0	29D	102.83	109.48	- 6.65	106.87	3.51	.07	3.22	
							107.88	- 5.05		4.70	.10	4.41	
							107.93	- 5.10		4.74	.07	4.45	
29Jly68	23 52 15.0	-00.2	133.4	6.1	12	113.17	119.03	- 5.86	110.22	3.75	.12	3.37	

TABLE 2 Continued

DATE	ORIGIN TIME (h m s)	EPICENTER LAT.	EPICENTER LONG.	MAG	DEPTH (km)	AZIMUTH ω	AZIMUTH ω'	AZIMUTH ϕ	DISTANCE Δ	SLOWNESS (sec/deg) p'	SLOWNESS (sec/deg) δp'	SLOWNESS (sec/deg) p
25Nov68	13 36 53.0	05.0	126.9	5.4	31	121.75	126.37	- 4.62	110.41	5.02	.05	4.49
							126.86	- 5.11		5.04	.08	4.45
06Jly68	19 28 55.3	-06.4	133.8	5.7	27	108.25	112.83	- 4.58	114.97	3.83	.07	3.58
							113.64	- 5.39		4.59	.09	4.23
06Feb68	04 37 11.9	-00.1	124.3	5.5	40	120.92	132.59	-11.65	115.85	4.87	.09	3.56
13Feb68	02 12 31.5	-05.5	131.1	5.8	67	111.20	114.48	- 3.28	116.00	3.78	.10	3.58
							113.78	- 2.58		4.72	.06	4.53
03Oct68	08 04 55.6	-03.8	128.5	5.6	97	114.48	118.99	- 4.41	116.39	4.05	.04	3.73
							119.44	- 4.86		4.72	.05	4.37
04Jan69	22 36 47.9	-06.8	129.8	5.7	107	111.33	116.41	- 5.08	117.86	4.04	.04	3.71
							114.39	- 3.06		4.70	.07	4.47
27Sep68	03 58 55.1	-06.8	129.1	6.1	127	111.93	115.46	- 3.53	118.31	4.07	.05	3.84
							114.75	- 2.82		4.68	.05	4.47
24May68	15 43 54.2	-06.8	118.9	6.0	609R	121.26	125.43	- 4.17	124.59	4.44	.05	4.03
27Jne68	22 14 01.3	-08.2	119.7	5.4	86	119.47	125.58	- 6.11	125.22	4.55	.03	3.96

TABLE 2. Events studied; origin time, epicenter, magnitude and depth are those published by the U.S.C.G.S. Latitude and longitude are negative in the southern and western hemispheres respectively. The computed azimuth ω, and the observed, ω', are measured in degrees from N; $\phi = \omega - \omega'$ is the azimuth anomally. p' and p are the observed and corrected slownesses respectively, and δp' is the RMS error in p'. The sign after p indicates which of $p = p' F_{\pm}$ is used (when applicable).

A least square procedure, described in Appendix A was applied to determine the parameters of the apparent wavefront traversing the array.

3. OBSERVATIONS

The observed azimuth of approach ω' was found to differ from the expected great circle azimuth ω by an amount unwarranted by the standard deviations of the measurements. The observed slowness factor $(\delta T/\delta \Delta)'$ exhibited (for the same epicentral distance) widely different values depending upon azimuth. Chinnery and Toksoz (1967) and Fairborn (1968) encountered the same problem while studying teleseismic mantle P waves. The former avoided the problem by considering only a narrow azimuth window, while the latter estimated local station corrections to eliminate the azimuth dependence. The azimuth anomaly $\phi = \omega - \omega'$ plotted against ω (Fig. 5) forms a pattern similar to that produced by a dipping interface e.g. the sloping M-discontinuity, or equivalently, anomalies produced by fairly gentle lateral velocity gradients in the crust or upper mantle. Because of the abundance of mantle P events detectable at the LASA, subdivision of the data into azimuth windows does not present a serious problem. However, observations of the core phase PKKP are more limited and such a method is not feasible.

4. CORRECTION FOR A SINGLE DIPPING INTERFACE

A method for correcting the observed PKKP values of $(\delta T/\delta\Delta)'$ for a tilted interface was developed (Zengeni, 1969). A detailed derivation of the relations can be found in Appendix B.

The interface is defined by the unit normal vector $\hat{n}$:

$$\hat{n} = (\sin D \cos \Omega,\ \sin D \sin \Omega,\ \cos D)$$

where D is the dip, and Ω is the direction of dip (i.e. azimuth of $\hat{n}$). The observed azimuth is ω', the epicentral great circle azimuth is ω, the velocity below the interface is V, and above is V'.

Two complementary correction formulas are used, each useful for a particular azimuth window.

$$\text{(i)} \qquad dT/d\Delta = (\delta T/\delta\Delta)' \frac{\sin(\Omega - \omega')}{\sin(\Omega - \omega)} \qquad (5)$$

$$\text{(ii)} \qquad dT/d\Delta = (\delta T/\delta\Delta)' F_{\pm}(\Omega, \omega, \omega', p', D, V, V') \qquad (6)$$

where $F_{\pm}$ are the roots of the quadratic equation

$$F\cos(\Omega-\omega) - \sqrt{P^2/p^2-F^2}\tan D = \cos(\Omega-\omega) - \sqrt{P'^2/p'^2-1}\tan D \qquad (7)$$

The two relations are mathematically equivalent, but when dealing with experimental data the two are appropriate

in different azimuth segments. Equation (5) is used in the windows

$$-150° \lesssim \Omega-\omega \lesssim -30° \text{ and } 30° \lesssim \Omega-\omega \lesssim 150°$$

and equation (6) is used in the remaining sections:

$$F_+ \text{ for } 0 \leq \Omega-\omega \lesssim 30° \text{ and } 150° \lesssim \Omega-\omega \leq 180°$$

$$F_- \text{ for } -30° \lesssim \Omega-\omega \leq 0 \text{ and } 180° \leq \Omega-\omega \lesssim 210°$$

Equation (5) is simple and depends on only one unknown, Ω. The rest of the parameters are either observed or computed. Ω can however be easily determined from a plot of the azimuth anomaly ϕ vs ω. [see Fig. 5, and also Niazi (1966), Otsuka (1966), McEvilly (1966) and Greenfield and Sheppard (1969)]. The envelope of the data points crosses the ω-axis at $\omega = \Omega$, $\Omega + 180°$.

Equation (6) depends on all the interface parameters. By a trial-and-error method in conjunction with $dT/d\Delta$ values already corrected by the first relation, D, V, V' can be easily estimated. The following values were used for the analysis of PKKP data observed at LASA:

$D = 5°$, $\Omega = N20°W$, $V' = 6.0$ km/sec, $V = 8.0$ km/sec

Fig. 6 shows the raw and corrected $dT/d\Delta$ values for PKKP.

As it turned out, the slowness separation δp between branches CI, IJ and the lower portion of BC is not much larger than the correction terms. Without the azimuth correction it would not be possible to separate the branches.

5. SOURCES OF ERROR

The theory of $dT/d\Delta$, as already pointed out, assumes perfect spherical symmetry and consequently azimuthal symmetry as well. For convenience deviations from such symmetry are treated together with all other sources of error. Because we assume plane wave fronts, near surface planar structures under the array should not (strictly) distort the plane wave front except merely to rotate it.

In reality, the LASA is gently curved and not planar, and wave fronts from teleseismic events are not truly planar but somewhat quadratic. These so called 'global' distortions are distinct from the 'local' distortions that arise from (i) near surface geological inhomogeneities under individual seismometers and (ii) the relative elevation of the seismometers above some datum level. All these local errors are imbedded in the time residuals $\delta T_i = T_i - T_i'$, where T_i and T_i' are the expected and observed relative arrival times at the i-th seismometer. δT_i also contains random experimental reading errors. Possible sources of global errors would be distortions due to deep inhomogeneities in the core and lower mantle.

IV. THE PKKP CORE MODEL

1. DERIVATION OF THE CORE MODEL

The construction of the core model from the dT/dΔ observations consisted of the following four steps:

(i) The mantle was stripped off using the Herrin (1968) P wave velocities.

(ii) Initially the Jeffreys SKS (Bullen 'E') region was assumed and later adjusted to link up continuously with the observed dT/dΔ data. The dT/dΔ curve for the stripped core is shown in Fig. 7. It should be pointed out here that since the caustic B is a consequence of the spherical geometry, the velocity structure of the mantle and the abrupt velocity drop at the core-mantle boundary (CMB), it is highly improbable that B should also represent a core phenomenon. Hence B is constrained to lie on a smooth curve ABC.

(iii) Using the Wiechert-Herglotz inversion method the velocity distribution in the core was computed down to point J, and continued to G by means of total reflection.

(iv) The remainder of the dT/dΔ curve and velocities were computed using the abundant PKP data available (Jeffreys, 1939; Bullen and Burke-Gaffney, 1958; Hai, 1961, 1963; Bolt, 1964, 1968; Adams and Randall, 1964; Hannon and Kovach, 1966; Shurbet, 1967; Kovach and Glover, 1968; Husebye and Toksöz, 1968; Engdal, 1968; Gogna, 1968).

2. DETAILS OF THE PKKP CORE MODEL

Except for fine details, the PKKP model is essentially tripartite, i.e. the outer and inner cores are separated by a transition zone. A summary of the numerical details of the derived core model is listed in Table 3. The velocity distribution is illustrated in Fig. 8. The subregions in the core are designated by the corresponding lettering of the travel time branched that scan (i.e. 'bottom' in) these sections.

The interfaces between the three regions of the core were constrained to have sharp velocity discontinuities for two reasons:

(i) Sharp velocity jumps produce the desired receding branches to link up with the succeeding refraction branches.

(ii) Very high velocity gradients give rise to unnecessary computational problems, especially when using the Mohorovicic velocity law (ar^b).

When a velocity discontinuity was reached, the shell above the interface was stripped off in order to compute the velocity distribution of the next region. These discontinuities are located at radii 1426 km and 1217 km marking the outer radius of the transition zone and the radius of the inner core respectively.

The Outer Core

The outer core comprises the SKS, ABC, CI, IJ subregions. Details of the SKS region are fairly arbitrary (without accurate SKS data) since there are not enough constraints (from

SUMMARY OF THE PKKP CORE VELOCITY MODEL

r/r_c	r km	v km/sec	
1.00	3476	8.10	
.96	3337	8.26	
.92	3198	8.44	
.88	3059	8.63	
.84	2920	8.85	
.80	2781	9.04	
.76	2642	9.23	
.72	2503	9.41	
.68	2364	9.57	
.64	2225	9.66	
.60	2086	9.75	
.56	1947	9.84	
.52	1808	9.93	
.48	1668	9.98	
.476	1654	10.025	I
.44	1529	10.08	
.410	1426	10.078	J
		10.47	G
.40	1390	10.47	
.36	1251	10.38	
.350	1217	10.36	H
		11.30	D
.32	1112	11.26	
.28	973	11.23	
.20	695	11.20	
.10	348	11.20	
0	0	11.20	F

Table 3. The letters are used to designate the discontinuities corresponding to the branches of the travel time curve. The radii are given to nearest whole km and the velocities are interpolated to at least two decimal places.

P wave observations above) apart from the demand that the AB branch should produce the correct travel times. Except for a slight compensating increase in velocity, the SKS region is similar to that of Jeffreys.

The region ABCI has a fairly steady velocity gradient which diminishes towards I. The velocities derived in this section are lower than most core models derived from PKP observations by about 0.05 km/sec; hence the velocity increase in the SKS region.

The subregion IJ has a humped velocity distribution with a very slight negative velocity gradient towards J.

The Transition Zone (GH Region)

The velocities in the transition region are intermediate between those in the outer and inner cores. The derived shell is narrower, only a little over 200 km, than the 400 km or so of Bolt, and Adams and Randall. This zone is characterized by a negative velocity gradient of about 0.5 km/sec/10^3 km.

The Inner Core (DF Region)

The velocity distribution in the inner core is fairly arbitrary. Analogous to the SKS region it is constrained mainly to satisfy the DF branch travel times of the core phase PKIKP. The model derived has a negative velocity gradient (with depth). The nature of the velocity distribution depends on the assumed velocity at the transition interface into the inner core, which in turn depends on the

location of the limiting point D. The position of D(PKP) was taken at 110° , fixing the velocity at the transition interface to 11.30 km/sec. If $\Delta_{PKP}(D)$ is increased well beyond 110°, the velocity at the interface decreases, and the velocity gradient in the inner core increases and could possibly become positive.

3. TRAVEL TIME AND SLOWNESS FACTOR

The travel time and dT/dΔ curves for the phases PKP and PKKP are shown in Figs. 9 and 10; receding branches are omitted for clarity. The letter designation of the branches is chosen to be as compatible as possible with that of existing core models, in particular those of Bolt (1964, 1968) and Adams and Randall (1964). The salient features of the curves are given in Table 4.

Phase PKP

The PKKP core model predicts a PKP travel time curve that comprises six refraction branches (AB, BC, CI, IJ, GH, DF) and two receding (reflection) branches (JG, HD). B, located at Δ = 146°, is the only observable high amplitude caustic. C and I are due to discontinuities in velocity gradient in the outer core at radii 1682 and 1654 km respectively. Thus the relatively high amplitudes observed in the neighborhood of Δ ∿ 145° - 146° (Shurbet, 1967; Shahidi, 1953) can be identified with the caustic at B. The large amplitudes around 143° can be explained in this model as the coherent superposition of the DF branch and the JG

Limiting Point	Seismic Ray Parameter sec/deg		Radius Scanned km	Wave Velocity km/sec	Phase PKP Δ deg	Phase PKP Travel Time min:sec	Phase PKKP Δ deg	Phase PKKP Travel Time min:sec
A	4.454	OUTER CORE	2426	9.50	186	22:35†	100	30:29†
B	4.25		2337	9.59			124.5	28:40.5
	3.50		1970	9.83	146	19:42		
C	2.940		1682	9.986	150.5	19:55	94.5	30:23
I	2.880		1654	10.025	147	19:45	101	30:04
J	2.470		1429	10.098	154.5	20:05	79.5	31:01
G	2.382	TRANSITION ZONE	1217	10.47	124	18:51	138	28:38
H	2.050			10.36	157	20:06	69	31:15
D	1.88	INNER CORE	0	11.30	110	18:33	160	28:15
F	0.0			11.20	180	20:11	0	31:51

†obtained by extrapolation.

Table 4. Slowness and travel time parameters for the core phases PKP and PKKP, (numbers are rounded off to the appropriate significant figures).

and GH branches; a conclusion independently reached by Shurbet (1967, p877).

In the distance range 145° ∿ 150° there is a clustering of different branches of the travel time curve, making it very difficult (if not impossible) to resolve them using PKP observations only. For example, around 148° there are as many as eight possible arrivals (two of which are reflections) separated by only fractions of a second. It is thus not improbable that in PKP observations the branches BC and IJ have not been identified separately. The PKKP data studied show no evidence for the extension of the IJ branch below the DF branch as postulated by Adams and Randall.

Branches GH and DF are similar to those of Bolt (1968) and most of the other tripartite models. However, the Bolt GH branch preceeds the GH branch derived here by as much as 10 sec around 125°. This discrepency is in the right direction to reduce the observed residuals to Bolt's GH branch (Kovach and Glover, 1968).

Phase PKKP

Theoretically, for each PKP branch there is a corresponding branch for the PKKP phase. However, there is one very significant except; the cusps B do not belong to the same ray parameter, and thus they do not scan the same depth (see Table 4). This point was raised earlier when the caustic B was ruled out as representing some outer core structure.

Travel time data for the core phase PKKP are not as

extensive as those for PKP. However, Gutenberg (1951, 1959) and Engdal (1968a, b) provide some data for comparison and discussion.

Branches AB and BC are well observed and clearly identified by their $dT/d\Delta$ values. Branch AB will be discussed later in the section dealing with the core-mantle boundary.

The most significant advantage of using PKKP observations is the clear separation of the branches BC and IJ. A cursory glance at Engdal's (1968b) data [reproduced in Fig. 11] might give the impression that the BC branch should be extended beyond 95° down to 79° (c.f. Gutenberg, 1951 p 385). However, the detailed study of array data shows a definite break in slope at 94°, as also noted by Engdal (1968a, p 52). This break in slope is actually caused by the formation of a new branch IJ (100° ~ 79°) linked to the BC branch by a short intermediate branch CI that extends for only 6° from 94° to 100°. (An array of aperture 6° or larger would not be able to resolve a branch of this small extent). Also to project BC to include IJ does not give a plausible PKP branch.

The GH branch extends from about 140° down to 69°, separated from the IJ branch on the travel time curve by less than 2 sec at 95° and only 7 sec at 80°. Attempting to identify IJ with GH as one and the same branch encounters a serious difficulty that requires explanation beyond geometrical ray theory. As a whole, the PKKP GH branch contains comparitively very low seismic energy. The presence of the

intermediate branch CI, IJ forces the GH branch to have a lower slowness factor than those of most core models.

The DF branch extends from 160° to 0°. One intuitively expects only meagre observations because of the large distances traversed in the core and the depletion of the energy during partial reflections at the many reflecting interfaces. This accounts for the fact that the DF branch was not observed for PKKP phase.

4. THE CORE-MANTLE BOUNDARY (CMB)

The velocity distribution at the base of the mantle and the CMB are still an issue of controversy. The branch AB of the core phases and, in particular, the location of the terminal point A are a useful tool in determining the parameters of the CMB. Intrinsic to the argument's validity is the following assumption: It is highly improbable that the limiting point A, a consequence of the abrupt velocity drop at the CMB, should also coincide with a velocity peculiarity in the outer core.

Since the section BC (Fig. 7) and the lower part of AB or the $dT/d\Delta$ curve for the stripped core are well established from the PKKP array observations, and are not critically influenced by the velocity distribution at the base of the mantle, it is reasonable to project the curve back into the SKS region continuously and smoothly to join the Jeffreys SKS curve. This portion of the curve (the insert, Fig. 7) provides superior control of the $p - \Delta$ relationship near A

than do the phases P, PcP, PKP or PKKP. Of the two core phases PKP is the less convenient to use because of the possible overlap of arrivals from either side of the globe if A is beyond 180°. Besides, PKKP advantageously doubles both the travel time and distance traversed in the core.

For all p

$$\Delta_K(p) = \frac{1}{2}\{\Delta_{PKKP}(p) - \Delta_{PcP}(p)\} \qquad (8)$$

and in particular at point A. For an n-multiply reflected core phase, equation (8) can be generalized to

$$\Delta_{PcP}(A) = \Delta_{PKn_P}(A) - n\,\Delta_K(A) \qquad (8a)$$

Unfortunately, the limiting values $\Delta(A)$ and $p(A)$ for both PcP and the core phases are debatable. In this study $\Delta_{PKKP}(A)$ is estimated to be 260°; c.f. 262° by Engdal (1968a, p 56). It is very unlikely that any short period wave diffraction mechanisms could account for the relatively good observations near 260° and beyond.

Equation (8) or (8a) is shown schematically in Fig. 12a by sketching iso-$\Delta_{PKKP}(A)$ curves on a p-$\Delta_{PcP}(A)$ plot. Reasonable bounds can be imposed on the variables, as indicated. From the data studied here together with data from Engdal (1968a, b), Johnson (1969), Fairborn (1968) and Herrin (1968), the following values were adopted:

$$p(A) \tilde{\sim} 4.45 \text{ sec/deg}$$

$$\Delta_{PcP}(A) \tilde{\sim} 109^\circ \text{(marking the edge of the P shadow)}$$

$$\Delta_{K}(A) \tilde{\sim} 77^\circ$$

Using the Herrin Tables, the $dT/d\Delta$ values for the Mantle P arrivals beyond 90° were adjusted and projected to the above limiting values. Fig. 12b shows the section under discussion. The velocities at the base of the mantle were recomputed, and are shown in Fig. 12c together with the Herrin (1968) P velocities.

The negative velocity gradient at the base of the mantle was proposed earlier by Gutenberg (1959, p 95) and other investigators, in particular those studying primarily core phases (e.g. Ergin, 1967; Husebye and Toksöz, 1968). The location of the edge of the shadow zone has varied as the number of investigators, for example 105° by Jeffreys (1939), 103.5° by Gutenberg and Richter (1934), 90° by Macelwane (1949), 96.5° by Sachs (1966), 100° by Johnson (1969), and on the average (Herrin 1968 Tables) 100°. Observations beyond this limit have been ascribed to diffraction around the CMB. Theoretical studies, notably by Sholte (1956), Alexander and Phinney (1966), Phinney and Alexander (1966), Phinney and Cathles (1969), and Richardson and Teng (1969) have been carried out to quantify the observations. When reduced to the stage of numerical evaluation by asymptotic or other methods, the diffraction theory

becomes (strictly) valid only for waves of longer periods than is observed in core phases (~1sec). As suggested earlier, the amount of energy of core phases in the 'shadow' is more than can be attributed to diffraction alone.

The negative velocity gradient proposed here leads to the following results:

(i) The edge of the shadow zone is farther than 100°, and in this thesis it is located at 109°.

(ii) The depletion of amplitude beyond 100° is due to the focussing of rays away from the mantle into the core.

(iii) As a consequence of (ii), observations preceeding A (as previously located) on branch AB of the core phases become true refractions, thus point A is relocated at 186° for PKP.

A change in velocity near the CMB also necessitates a reevaluation of the radius of the core. The radius r_c=3477 km was used as a guide although r_c = 3476 km was finally adopted as the radius of the core.

V. DISCUSSION OF THE CORE VELOCITY MODEL

A complete geophysical study of the Earth's interior consists of the determination of the existing physical conditions (temperature, pressure, etc.), the physical properties (density, incompressibility, rigidity, phase or state, etc.) and ultimately the composition and identification of the atomic and molecular constituents of the Earth's deep interior. In the case of seismic velocities, the model must also be consistent with a plausible distribution of density, incompressibility and rigidity.

In determining gross features of the earth, these considerations may not be critical. However, when inferring fine structure involving rapid or abrupt variations in seismic velocity, or ultimately changes in the fundamental variables (density, incompressibility and rigidity) it is essential that the model be checked against other experimental or theoretical evidence.

The velocity distribution derived here was obtained from $dT/d\Delta$ observations of the core phase PKKP, and PKP travel time data where PKKP data were insufficient or lacking. It is important to discuss some of the implications of the PKKP velocity model.

That the outer core (SKS, ABCIJ) is fluid is seismologically indisputable. The outer core velocity distribution derived here presents no difficulty because of the

absence of any drastic variations. The steady velocity gradients in these regions can be attributed to the influence of pressure and temperature. The velocity deviations in the region CIJ might be due to either a phase change or a slight chemical inhomogeneity in the deepermost parts of the outer core.

It has been postulated (Bullen, 1946, 1958) that the inner core material is in the solid state and therefore should transmit both dilatational and shear waves. The existence of the transition zone is widely accepted by most seismologists, and its complexity is also well recognized (Subiza and Bath, 1964). Gutenberg (1957, 1958) postulated a dispersive frequency-dependent region to explain the PKIKP or DF branch forerunner. Bolt (1964) used ordinary ray theory to explain these precursors by constructing a new refraction branch (GH) without recourse to diffraction or dispersion. Adams and Randall proposed a transition zone comprising two shells to explain their observations of the triplication of the PKP branch.

Although not observed in the PKKP core phase, PKP waves associated with the transition zone are peculiar and different from those whose ray paths scan the other regions. They are generally of shorter period (Gutenberg, 1958;Subiza and Bath, 1964). Husebye and Toksöz (1968, p8) describe the precursors as "in general long oscillatory trains similar to guided waves"; they further speculate them as such,

originating from the core-mantle boundary.

The presence of the transition zone, the negative velocity gradient deduced here, and the presence of the velocity structure IJ (Fig. 8) at the base of the outer core require explanation. It is conjectured that the transition zone is in the liquid or viscous state but is of the same chemical composition as the inner core. The inference that inner and outer cores are chemically different was postulated earlier by Bullen (1954).

The velocity discontinuity at the interface between the outer core and the transition zone follows as a consequence of the compositional change. The velocity jumps at the inner core interface is due mainly to the abrupt contribution of the rigidity to the wave velocity as a result of sudden solidity. The negative velocity gradient into the inner core could be accounted for in the following manner: both the density (ρ) and the incompressibility (k) increase with depth (varying with temperature and pressure) but k (in the absence of rigidity) changes more slowly over the extent of the transition zone such that k/ρ is a slowly decreasing function of depth.

It is not inconceivable that the liquid-liquid interface between the outer core and the transition zone permits the diffusion across it of the molten materials from either side, in particular, from the transition zone into the outer core giving rise to the structure IJ (Fig.8).

The slight decrease of the mantle P velocity at the CMB is physically not unrealistic; possible softening of the material would result in a corresponding drop in rigidity. The S wave velocities at the CMB would reflect better such a diminution in shear modulus (μ), thus providing a simple (though difficult to achieve) check on the postulated velocity distribution.

VI. SUMMARY AND CONCLUSIONS

From observations of the seismic core phase PKKP, as recorded at LASA, a new velocity distribution in the earth's core has been derived. The velocity model for the core is essentially tripartite, but differs in several significant points from other proposed models (Fig. 1 and 8):

(i) The velocity gradient in the SKS region is higher, and in the ABC region lower, than the standard Jeffreys model.

(ii) The well defined travel time branch (IJ) observed for the core phase PKKP leads to a new slightly humped velocity structure at the base of the outer core between radii of 1654 and 1426 km.

(iii) The transition zone is found to be narrower (about 200 km) than most existing tripartite core models and it is characterized by a slight negative velocity gradient.

(iv) The P wave velocities at the base of the mantle are deduced to possess a small negative gradient at the core-mantle boundary.

It is further postulated that the transition zone (liquid or viscous) and the inner core (solid) have the same chemical composition.

Besides the results summarized above, several other

important points can be made:

(i) dT/dΔ observations at LASA require azimuthal corrections to account for (possibly) the dipping Moho discontinuity, especially in the case of low wave slownesses.

(ii) Because of the convenient location, with respect to epicentral distance, of the relevant branches, observations of the core phase PKKP surpass PKP in deciphering the structure of the outer core. However, PKP observations provide better data for the study of the transition zone and the inner core.

(iii) The core phase PKKP can be used to discern the structure at the core-mantle boundary.

Further refinements in deciphering the fine structure of the earth's core, in particular details of the transition zone and the inner core must await detailed analyses of arrivals from the GH and DF branches of the PKP core phase, possibly using continental sized arrays.

BIBLIOGRAPHY

Adams, R. D., and M. J. Randall, Observed Triplication of PKP, Nature, 200, 744, 1963.

Adams, R. D., and M. J. Randall, The Fine Structure of the Earth's Core, Bull. Seism. Soc. Am., 54,1299-1313, 1964.

Alexander, S. A. and R. A. Phinney, A Study of the Core-Mantle Boundary using P Wave Diffracted by the Earth's Core, J. Geophys. Res., 71, 5943-5958, 1966.

Anderson, D. L. and R. L. Kovach, Universal Dispersion Tables III. Free Oscillations Variational Parameters, Bull. Seism. Soc. Am., 59, 1667-1693, 1969.

Bolt, B. A., The Velocity of Seismic Waves Near the Earth's Center, Bull. Seis. Soc. Am., 54, 191-208, 1964.

Bolt, B. A., Estimation of PKP Travel Times, Bull. Seism. Soc. Am., 58, 1305-1324, 1968.

Bullen, K. E., A Hypothesis on Compressibility at Pressures of the Order of a Million Atmospheres, Nature, 157, 405, 1946.

Bullen, K. E., Composition of the Earth's Outer Core, Nature, 174, 505-506, 1954.

Bullen, K. E., Solidity of the Inner Core, Contributions in honour of Beno Gutenberg, Pergamon Press, London, 113-120, 1958.

Bullen, K. E., Seismic Ray Theory, Geophys. J., 4, 93-105, 1961.

Bullen, K. E., Introduction to the Theory of Seismolcgy, 3rd Ed. Cambridge University Press, 1963.

Bullen, K. E. and T. N. Burke-Gaffney, Diffracted Seismic Waves near the PKP Caustic, Geophys. J., 1, 9-17, 1958.

Bullen K. E. and R. H. W. Haddon, Derivation of an Earth Model from Free Oscillation Data, Proc. Natl. Acad. Sci., 58, 846-852, 1967.

Bullen K. E. and R. H. W. Haddon, An Earth Model incorporating Free Earth Oscillation Data, Phys. Earth. Planet. Interiors, 2,35-49, 1969.

Chinnery, M. A. and N. Toksoz, P-Wave Velocities in the Mantle below 700 km, Bull. Seism. Soc. Am., 57, 199-226, 1967.

Engdal, E. R.,Core Phases and the Earth's Core, unpublished Ph.D. Thesis,Saint Louis University, 1968.

Engdal, E. R., Seismic Waves within the Earth's Outer Core: Multiple Reflections, Science, 161, 263-264, 1968.

Ergin, K., Seismic Evidence for a New Layered Structure of the Earth's Core, J. Geophys. Res., 72, 3669-3687, 1967.

Fairborn, J. W., Mantle P and S Wave Velocity Distributions from dT/dΔ Measurements, unpublished Ph.D. Thesis, MIT,1968

Forbes, C. B. et. al., The LASA Sensing System Design, Installation and Operation, Proc. I.E.E.E., 53, 1834-1841, 1965.

Gogna, M. L., Travel Times of PKP from Pacific Earthquakes, Geophys. J., 16, 489-514, 1968.

Greenfield, R. J. and R. M. Sheppard, The Moho Depth Variations under LASA and their Effect on dT/dΔ Measurements, Bull. Seism. Soc. Am., 59, 409-420, 1969.

Gutenberg, B., PKKP, P'P', and the Earth's Core, Trans. Am. Geophys. Union, 32, 373-390, 1951.

Gutenberg, B., Wave Velocities in the Earth's Core, Bull. Seism. Soc. Am., 48, 301-315, 1958.

Gutenberg, B., Physics of the Earth's Interior, Academic Press, New York, 240 pp., 1959.

Gutenberg, B., The Boundary of the Earth's Inner Core, Trans. Am. Geophys. Union, 38, 750-753, 1957.

Gutenberg, B. and Richter, On Seismic Waves, Gerlands Beitr. Geophysik, 43, 56-133, 1934.

Hai, N., Propagation des Ondes Longitudinales dans le Noyeau Terrestre d'apres les Seismes Profunds des Iles Fidji, Ann. de Geophys., 17, 60-66, 1961.

Hai, N., Propagation des Ondes Longitudinales dans le Noyeau Terrestre, Ann. Geophys., 19, 285-346, 1963.

Hannon, W. J. and R. L Kovach, Velocity Filtering of Seismic Core Phases, Bull. Seism. Soc.Am., 56, 441-454, 1966.

Herrin, E., Seismological Tables for P Phases, Bull. Seism. Soc. Am., 58, 1223-1225, 1968.

Husebye, E. S. and M. N. Toksoz, On the Structure of the Earth's Core, presented at the western A.G.U., San Francisco, 1968.

Jeffreys, H., The Times of the Core Waves (second paper) Mon. Not. Roy. Astro. Soc. Geophys. Supp., 4, 594-615, 1939.

Johnson, L., Array Measurements of P Velocities in the Upper Mantle, J. Geophys. Res., 72, 6309-6325, 1967.

Kovach, R. L. and P Glover, Travel Times of PKP in the Range $115° \leq \Delta \leq 140°$, Geophys. J.R. Astr. Soc., 15, 367-376. 1968.

Kovach, R. L. and R. Robinson, Upper Mantle Structure in the Basin and Range Province, Western North America from the Apparent Velocities of S Waves, Bull. Seism. Soc Am., 59, 1654-1665

McEvilly, T. V., Crustal Structure Estimation Within a Large Scale Array, Geophys. J., 11, 13-17, 1966.

Niazi, M.,Corrections to Apparent Azimuths and Travel-Time Gradients for a Dipping Mohorovicic Discontinuity, Bull. Seism. Soc. Am., 56, 491-509, 1966.

Niazi, M. and D. L. Anderson, Upper Mantle Structure of Western North America from Apparent Velocities of P Waves, J. Geophys. Res., 70, 4633-4640, 1965.

Otsuka, M., Azimuth and Slowness Anomalies of Seismic Waves Measured on Central California Seismographic Array. Part I Observations, Bull Seism. Soc. Am., 56, 223-239, 1966a.

Otsuka, M. Azimuth and Slowness Anomalies of Seismic Waves Measured on the Central California Seismographic Array, Part II, Interpretation, Bull Seism. Soc. Am., 56, 655-675, 1966b.

Phinney, R. A. and S. S. Alexander, P Wave Diffraction Theory and the Structure of the Core-Mantle Boundary, J.Geophys. Res., 71, 5959-5975, 1966.

Phinney, R. A. and L. M. Cathles, Diffraction of P by the Core: A Study of Long-Period Amplitudes Near the Edge of the Shadow, J. Geophys Res., 74, 1556-1574, 1969.

Press, R., Earth Models Obtained by Monte Carlo Inversion, J. Geophys. Res., 73, 5223-5234, 1968.

Richardson, P. G. and T. Teng, Diffracted P, SV, and SH Waves and Their Shadow Shifts, J. Geophys. Res., 74, 1537-1555, 1969.

Sachs, S., Diffracted Wave Studies of the Earth's Core, 1. Amplitude, Core Size, and Rigidity, J. Geophys. Res., 71, 1173-1193, 1966.

Shahidi, M., Variation of Amplitude of PKP across the .austic, Phys. Earth Planet. Interiors, 1, 97-102, 1968.

Sholte, J.G.J., On Seismic Waves in Spherical Earth, Konikl. Ned. Meteorl. Inst. Publ., 65, 1956.

Shurbet, D. H., The Earthquake P Phases which Penetrate the Earth's Core, Bull. Seism. Soc. Am., 57, 875-890,1967.

Subiza, G. P. and M. Bath, Core Phases and the Inner Core Boundary, Geophys. J., 8, 496-513, 1964.

Zengeni, T. G., A Note on an Azimuthal Correction for dT/dΔ for a Single Dipping Planar Interface, Bull. Seis. Soc. Am., in press.

APPENDIX A

LEAST SQUARES METHOD FOR DETERMINING THE SLOWNESS VECTOR

Refer to Fig. A1.

(a) Let $\vec{r}_i(r_i,\theta_i)/\vec{r}_i(x_i,y_i)$ be the polar/cartesian coordinates of the seismometer S_i, and the origin of the coordinate system is arbitrarily fixed near the center of the array, all coordinates measured in the tangent plane at the origin. In our case the center seismometer of the AO subarray was used as the origin.

(b) Assume that the plane wave front approximation is valid, and characterize the apparent wave front by

(i) T the arrival time (actual or relative) of the wave front at the origin

(ii) the slowness vector $\vec{L} \equiv (dT/d\Delta,\omega)$ where $dT/d\Delta=p$ is the slowness factor, and ω the azimuth of approach

(c) Let T_i be the computed time (i.e. expected under the assumed conditions of plane wave front approximation) and T_i' be the observed (measured) time at S_i.

The procedure is easily accomplished by minimizing σ, defined by

$$\sigma(p,\omega,T) = \sum_{i=1}^{n} (T_i - T_i')^2$$

Now, $T_i = T + \vec{L}\cdot\vec{R}_i$; $\vec{R}_i = \vec{r}_i/a$

or $T_i = T + pR_i \cos(\omega-\theta_i)$

where a is introduced to account for the units of $\vec{L}$ or p (sec/deg). T, p, ω are obtained in the standard way by setting the partial derivatives of σ equal to zero, where σ is explicitly given by

$$\sigma(p,\omega,T) = \sum_{i=1}^{n} \{T + pR_i \cos(\omega-\theta_i) - T_i'\}^2$$

Although the resulting equations are not linear in p,ω,T they are easily solved to yield p,T as functions of ω, and ω is obtained from a cubic in tan ω. The choice of the required root is obviated bythe fact that two of the three roots are always complex conjugates with finite imaginary parts; these solutions are discarded as unphysical. The uniqueness of the physical solution can easily be demonstrated by using the more commonly used cartesian coordinates $\vec{L} = (L_x,L_y)$ as variables instead of the polar $\vec{L} = (p,\omega)$. Hence

$$\sigma(L_x,L_y,T) = \Sigma_i(T + L_xX_i + L_yY_i - T_i')^2;\ X_i,Y_i = x_i/a, y_i/a$$

It is interesting to note the difference between the

method described above and other methods in common use, e.g. Otsuka (1966), in which $T = (\Sigma_i T_i')/n$ by choice of the origin at the 'center of gravity' of the array such that $\Sigma_i x_i = 0 = \Sigma_i y_i$. For an array where one or more seismometers may be out of order (or unreadable) at the time of arrival of an event, such method (e.g. Otsuka) demands the computation of a new origin each time. The method used in this thesis maintains the origin at the center seismometer of the AO subarray.

A computer program was written to find p, ω, T as well as $\delta T_i = T_i - T_i'$ from which the standard errors $\sigma_T, \sigma_p, \sigma_\omega$ are estimated. Note, the errors are determined without reference to any particular earth model. These errors reflect, first, the accuracy of the measurements (experimental errors), and second, local and global distortions of the assumed plane wave front. In the data analyzed errors in $\delta T/\delta\Delta$ are of the order of $\pm$ 0.10 sec/deg or less, and in $\omega \pm 1.5$ deg.

The method of least squares, i.e. minimization of the delay time residuals, is not the only one available for determining $(\delta T/\delta\omega)'$ and ω'. Another method is to use digital data together with beam steering.

Let $S_i(t)$ be the finite time series of the i th seismometer [series terminated to contain only the branch of the phase being studied]. The array is steered in a particular direction by delaying each channel by an amount related

to the slowness vector, and the traces summed to give the beam $S(\vec{L},t)$:

$$S(\vec{L},t) = \sum_{i=1}^{n} S_i(t - \tau_i)$$

$$\tau_i = \vec{L} \cdot \vec{R}_i = pR_i \cos(\omega - \theta_i).$$

The desired slowness vector is that which gives maximum energy ε

$$\varepsilon(\vec{L}) = \sum_{t} |S(\vec{L},t)|^2$$

such that $\vec{\nabla}_L \, \varepsilon(\vec{L}) = 0$

where $\vec{\nabla}_L \equiv \left(\frac{\partial}{\partial L_x}, \frac{\partial}{\partial L_y}\right)$ or $\left(\frac{\partial}{\partial p}, \frac{1}{p}\frac{\partial}{\partial \omega}\right)$

This method is similar to velocity filtering (Hannon and Kovach, 1966) in which the beam $S(\vec{L}, t)$ is used as the indicator of phase velocity.

APPENDIX B

AZIMUTHAL CORRECTION FOR $dT/d\Delta$ FOR A SINGLE DIPPING PLANE INTERFACE

When observing teleseimic events by means of an array (using the method of plane wave front), the objective is to measure the slowness vector $\vec{L}$, defined

$$\vec{L} \equiv (dT/d\Delta, \omega)$$

i.e., the vector of magnitude $dT/d\Delta$ (the slowness factor) and direction ω (the azimuth). We know in the case of a spherically symmetric earth $dT/d\Delta$ is equal to the seismic ray parameter p:

$$p \equiv \frac{r \sin i}{V}$$

However, in the presence of near surface planar strutures under the array, the observed slowness vector $\vec{L}'$ is different from that expected of the spherical symmetry. By use of the least square method on the time delays of the array seismometers, $\vec{L}'$ can be obtained:

$$\vec{L}' \equiv \{(\delta T/\delta\Delta)', \omega'\}$$

Note: $(\delta T/\delta\Delta)'$ is used to denote the observed slowness factor to avoid confusion with the $dT/d\Delta$ used in the case of perfect

spherical symmetry. ω' is the observed azimuth.

It is the purpose of this appendix to derive a convenient relation between $\vec{L}$ and $\vec{L}'$, and since ω can be computed from the epicentral azimuth, all we need is the relationship between $dT/d\Delta$ and $(\delta T/\delta \Delta)'$.

DERIVATION OF FORMULA

Fig. B1 shows the geometry considered. The dipping interface separating the two media of velocities V, V' is defined by the unit normal vector $\hat{n}$:

$$\hat{n} = (\sin D \cos \Omega, \sin D \sin \Omega, \cos D)$$

where D is the dip, and Ω is the azimuth of the normal. Cartesian axes are chosen to form a right-handed system with the z-axis vertical (up) and the x-axis pointing East. The incident and refracted plane wave beams are defined by their unit wave vectors $\hat{k}$ and $\hat{k}'$ respectively

$$\hat{k} = (\sin i \cos \omega, \sin i \sin \omega, \cos i)$$
$$\hat{k}' = (\sin i' \cos \omega', \sin i' \sin \omega', \cos i')$$

where the angles i, i'; ω, ω' are analogous to D and Ω.

Snell's law of refraction is conveniently written:

$$\hat{k}' = \frac{\hat{k} + \beta\hat{n}}{\sqrt{1 + 2\beta\hat{n}\cdot\hat{k} + \beta^2}} \tag{1}$$

where β is defined by the condition

$$\frac{\sin \alpha'}{V'} = \frac{\sin \alpha}{V} \tag{2}$$

α, α' are the angles the incident and refracted rays make with the normal:

$$\cos \alpha = \hat{n}\cdot\hat{k}, \quad \cos \alpha' = \hat{n}\cdot\hat{k}' \tag{3}$$

Equation (1) implies $\hat{k}$, $\hat{k}'$, $\hat{n}$ all lie in the same plane, and equation (2) is the usual condition of proportionality of sines and velocities in the two media.

Multiplying (1) by $\hat{n}$ and squaring gives

$$\cos^2 \alpha' = \frac{\cos^2 \alpha + 2\beta \cos \alpha + \beta^2}{1 + \beta^2 + 2\beta \cos \alpha} \tag{4}$$

Using (2) to eliminate α' gives

$$1 + \beta^2 + 2\beta \cos \alpha = (V/V')^2 \tag{5}$$

or that

$$\beta_{\pm} = -\cos\alpha \pm [\cos^2\alpha + (V/V')^2 - 1]^{1/2}$$

For the purposes of correcting $dT/d\Delta$ the distinction between β_+ and β_- is immaterial. However, β_+ is valid for $\hat{n}\cdot\hat{k}$, $\hat{n}\cdot\hat{k}' \geq 0$, and β_- otherwise. Also observe that β can be complex if $\cos^2\alpha + (V/V')^2 - 1 < 0$; this occurs when critical refraction is exceeded.

Using equation (5), equation (1) can be rewritten as

$$\frac{\hat{k}}{V} = \frac{\hat{k}'}{V'} - \beta\frac{\hat{n}}{V} \tag{6}$$

or in cartesian components

$$\frac{\sin i \cos\omega}{V} = \frac{\sin i' \cos\omega'}{V'} - \beta\frac{\sin D \cos\Omega}{V} \tag{7}$$

$$\frac{\sin i \sin\omega}{V} = \frac{\sin i' \sin\omega'}{V'} - \beta\frac{\sin D \sin\Omega}{V} \tag{8}$$

$$\frac{\cos i}{V} = \frac{\cos i'}{V'} - \beta\frac{\cos D}{V} \tag{9}$$

It should be pointed out that equations (7)-(9) are not independent; only two are, the third follows from the

normalization condition of equation (1). Thus, at most we can solve for only two variables. Normally one solves for either ω and i given ω' and i' or vice versa, for known V, V', Ω, and D. Hence we can use the three equations to extract two linearly independent equations appropriate for our use. Two different combinations of (7) and (8) give

$$\frac{\sin i}{V} \sin (\Omega - \omega) = \frac{\sin i'}{V'} \sin (\Omega - \omega') \qquad (10)$$

$$\frac{\sin i}{V} \cos (\Omega - \omega) = \frac{\sin i'}{V'} \cos (\Omega - \omega') - \beta \frac{\sin D}{V} \qquad (11)$$

Using (9) β can be eliminated from equation (11) to give

$$\frac{\sin i}{V} \cos(\Omega-\omega) = \frac{\sin i'}{V'} \cos(\Omega-\omega') + \left\{\frac{\cos i}{V} - \frac{\cos i'}{V'}\right\} \tan D \qquad (12)$$

We know

$$\frac{r \sin i}{V} = p = dT/d\Delta$$

and

$$\frac{r \sin i'}{V'} = (\delta T/\delta \Delta)' = p'$$

where p' will be used interchangeably with $(\delta T/\delta \Delta)'$ to facilitate writing. Also, define $P = r/V$, $P' = r/V'$ (r is the radius from center).

Now we can reduce equations (10) and (12) to

$$p \sin (\Omega - \omega) = p' \sin (\Omega - \omega') \tag{13}$$

$$p \cos (\Omega-\omega)-\sqrt{P^2 - p^2} \tan D = p' \cos (\Omega-\omega')-\sqrt{P'^2 - p'^2}\tan D \tag{14}$$

Equation (13) can also be written

$$dT/d\Delta = (\delta T/\delta \Delta)' \frac{\sin (\Omega - \omega')}{\sin (\Omega - \omega)} \tag{15}$$

Equation (15) depends only on the azimuth angles Ω, ω, ω'. It is remarkable that it does not depend on the dip D or the velocities V and V' explicitly. This is a great advantage for investigations of the earth's deep interior not directly concerned with the immediate geology under the array. Thus from the knowledge of Ω, $dT/d\Delta$ is easily corrected from the observed $(\delta T/\delta \Delta)'$ and ω', and the computed azimuth ω.

Equation (15) has one apparent set back. For real (numerical) data the formula is inappropriate for azimuth

ω in the neighborhood of Ω, i.e. for waves arriving perpendicular to the strike of the dipping interface. There is, however, no singularity at $\omega = \Omega$ because as $\omega \to \Omega$ so does ω'. Hence, by L'Hospital's rule, as $\omega \to \Omega$

$$dT/d\Delta = (\delta T/\delta \Delta)' \left. \frac{d\{\sin (\Omega - \omega')\}}{d\{\sin (\Omega - \omega)\}} \right|_{\omega,\ \omega' \to \Omega}$$

$$= (\delta T/\delta \Delta)' (d\omega'/d\omega) \Big|_{\omega,\ \omega' \to \Omega}$$

where $d\omega'/d\omega$ does not equal unity at $\omega = \omega' = \Omega$. Thus $(dT/d\Delta) \neq (\delta T/\delta \Delta)'$ at $\omega = \Omega$ as one might suspect at first glance of equation (15). The evaluation of $d\omega'/d\omega$ is awkward but can be circumvented by using equation (14) and letting ω, $\omega' \to \Omega$.

Another and simpler way of illustrating what happens as $\omega \to \Omega$, or $\Omega + 180$ is the following. Define the azimuth anomaly $\phi = \omega - \omega'$, and rewrite (15) or (13)

$$p = p' \{\cos \phi + \sin \phi \cot (\Omega - \omega)\} \qquad (16)$$

In the neighborhood of $\Omega - \omega = 0$ or $180°$, ϕ is very small and (16) becomes

$$p \simeq p' \{1 + \phi \cot (\Omega - \omega)\};\ \phi[\text{rad}] << 1 \qquad (17)$$

It can easily be seen that the correction term $\phi \cot (\Omega - \omega)$ gets very large for a small error $\delta\phi$ because $\cot (\Omega - \omega) \to \infty$ even though in the theoretical (analytical) case

$$\lim_{\phi \to 0,\ \omega \to \Omega} \{\sin \phi \cot (\Omega - \omega)\} \to \text{finite}.$$

Thus if $\phi \to \phi + \delta\phi$ (finite error), then

$$p \simeq p' \{1 + \phi \cot (\Omega - \omega)\} + p' \delta\phi \cot (\Omega - \omega) \qquad (18)$$

For finite error $\delta\phi$ it is clear the error in p is intolerable as $\Omega - \omega \to 0$ or 180°.

In these bad azimuth windows the use of equation (14) is recommended. Equation (14) is a quadratic in p. An estimate of the size of the window can be easily obtained from equation (18). We demand the following inequality

$$|\delta\phi \cot (\Omega - \omega)| << 1$$

In the data studied, $\delta\phi \sim 0.04$ rad or 2°. Hence $|\Omega - \omega| >> 0.04$ rad or 2°. Thus it is reasonable not to use (15) in the ranges $-30° \lesssim \Omega - \omega \lesssim 30$ or $150° \lesssim \Omega - \omega \lesssim 210°$, but instead use equation (14), which has solutions

$$p = p' F_{\pm}(\Omega, \omega, \omega', D, V, V') \qquad (19)$$

where $F_{\pm} = -B \pm \sqrt{B^2 - C}$

$$B = - \frac{\cos (\Omega - \omega)[\cos (\Omega - \omega') - \gamma \tan D]}{\cos^2 (\Omega - \omega) + \tan^2 D}$$

$$C = \frac{(V'/V)^2 (P'/p')^2 - [\cos (\Omega - \omega') - \gamma \tan D]^2}{\cos^2 (\Omega - \omega) + \tan^2 D}$$

$$\gamma = \{ (P'/p')^2 - 1 \}^{1/2}$$

F_+ holds for $0 < \Omega - \omega < 180°$, and F_- for $-180° < \Omega - \omega < 0$ although in their actual application in the reduction of array data they are more restricted to narrower windows. In these windows, errors in ϕ do not give excessively large errors in p or $dT/d\Delta$ unlike equation (15). Equation (19) requires knowledge of both the dip D and the velocity contrast V, V'. If unknown, estimates of D, V, V' can be obtained by trial and error noting the shift in $dT/d\Delta$ values relative to those values already corrected for using the first correction formula.

LIMITATIONS AND CONDITIONS OF USE

It should be emphasized that when using an array to determine $dT/d\Delta$, a fundamental assumption is made: that the medium above the depth of penetration, H, of the array (see Fig. B2) is homogeneous and uniform or as nearly close as the accuracy of the measurements demands. The relation

$$dT/d\Delta = p \equiv \frac{r \sin i}{V}$$

holds strictly only for V sufficiently uniform above a depth H, where

$$H = r\delta\Delta \sin i \cos i$$

$$= V^2 \frac{\delta\Delta}{r} p \, (P^2 - p^2)^{1/2}$$

where $\delta\Delta$ [radians] is the aperture of the array. This condition implies that measurements of $dT/d\Delta$ by plane wave approximation cannot resolve structures above a depth H. For the phase PKKP H $\sim$ 30 - 40 km and therefore the plane interface corrected for is probably the M discontinuity at depth 40 km or deeper. It is worth emphasizing that the method described in this appendix is essentially for correcting array $dT/d\Delta$ observations only, and not to discern exact near surface structures.

FIGURE CAPTIONS

Fig. 1 Existing core velocity models of the Earth (after Hannon and Kovach, 1966). The core model deduced by Husebye and Toksöz has a velocity gradient in the SKS region steeper than that of Jeffreys, a low velocity zone in the AB zone (r = 2000-2530 km), and a negative velocity gradient in the transition zone.

Fig. 2 Location of events with respect to LASA. Solid lines show azimuth directions to LASA.

Fig. 3 Geometry for the theory and array determination of $dT/d\Delta$. It is approximated that the array lies on the tangent plane rather than the curved surface.

Fig. 4 The Large Aperture Seismic Array (LASA), Montana. Only the subarrays used in this study are shown.

Fig. 5 Plot of azimuth anomaly versus epicentral azimuth. Ω = N20W is the estimated horizontal direction of normal to the dipping interface. Azimuth windows labelled $F\pm$ are the ranges over which the second correction formula $p = p'F\pm$ is used.

Fig. 6 $dT/d\Delta$ observations determined at LASA. The solid line is the best fit curve (by eye), the dashed line is that for the Bolt's model. Point labelled 'X' was ignored in the curve fitting because of its isolation and possible misidentification. Points 'Y' were also ignored because of the requirement that $dT/d\Delta$ should be a piece-wise monotonically decreasing function of Δ, and also because of their azimuth proximity to the direction of the normal to the dipping interface where the first correction formula is inapplicable. Where two distinct arrivals are measured in the vicinity of CI, the two points are joined by a thin line.

Fig. 7 $dT/d\Delta$ curve for the stripped core. The insert is a magnification of the curve in the vicinity of the limiting point A.

Fig. 8 The PKKP core velocity model together with the Jeffreys model and the Herrin P velocities at the base of the model for comparison.

Fig. 9 PKP slowness factor and travel time curves. Reflection branches are not shown on the travel time curves.

Fig. 10 PKKP slowness factor and travel time curves. Reflection branches have been omitted.

Fig. 11 Travel time observations of multiply reflected core phases (Engdal, 1969). The figure was kindly provided by Dr. E. Engdal. Only the phases PKKP and PKKKP are reproduced.

Fig. 12 (a) Schematic representation of the equation

$$\Delta_{PcP}(A) = \Delta_{PKKP}(A) - 2\Delta_{K}(A)$$

for various assumed Δ_{PKKP} and Δ_{K}.

(b) Reconstruction of the $dT/d\Delta$ curve for the mantle P waves at the base of the mantle.
(c) Resulting velocity model (thick curve) compared with the Herrin P wave velocities.

Fig. A1 Planar geometry considered for the least squares determination of the slowness vector.

Fig. B1 Geometry of the incident and refracted beams with respect to the dipping interface. Note, vectors are actually in 3-d and not necessarily in the plane of the paper.

Fig. B2 Definition of H, the depth of penetration of the array. Diagram is drawn in the plane of $\vec{L}$ and the radius from the Earth's center.

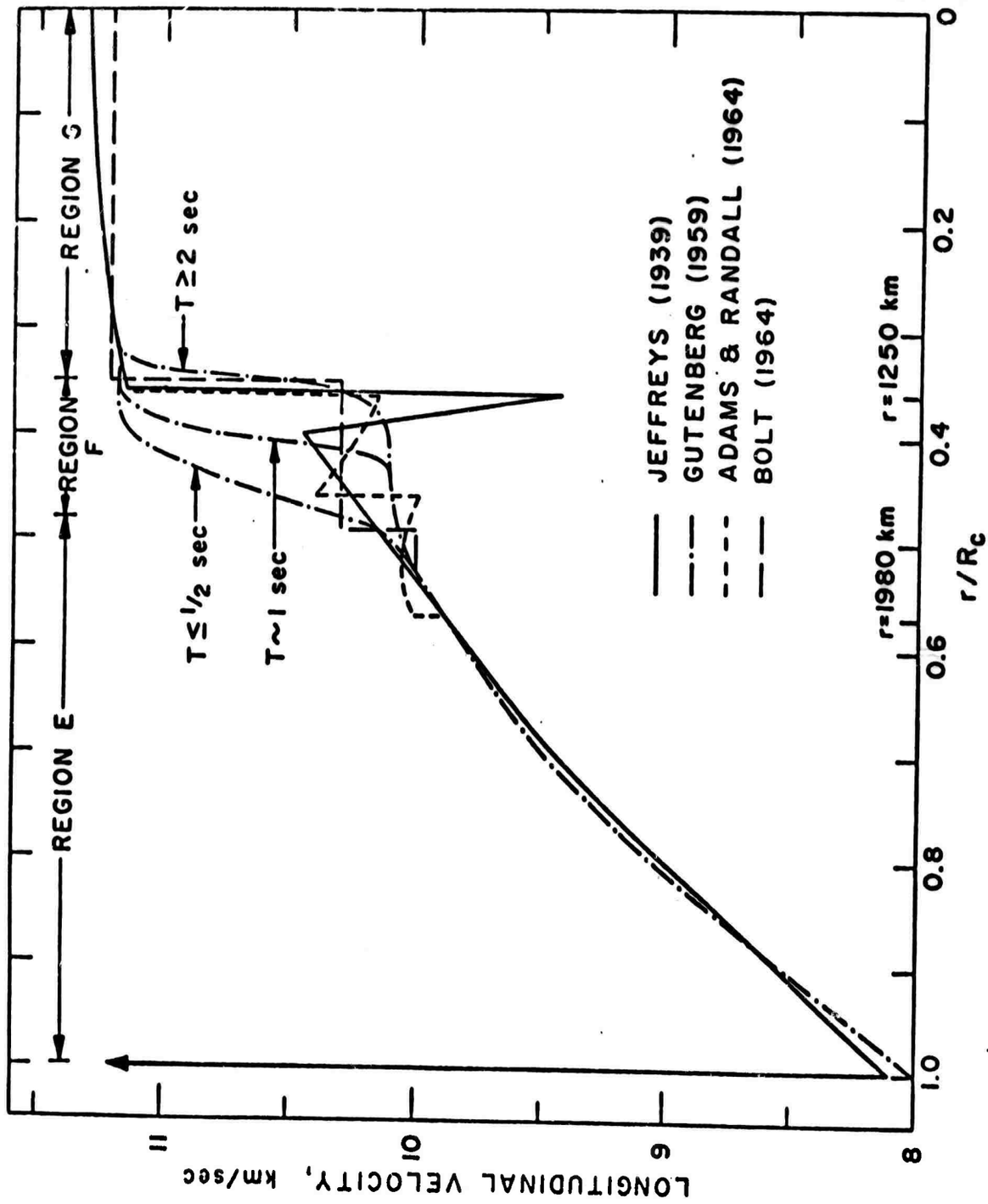
LONGITUDINAL VELOCITY, km/sec
11
10
9
8
0
0.2
0.4
0.6
0.8
1.0
r/Rc
r=1980 km
r=1250 km
JEFFREYS (1939)
GUTENBERG (1959)
ADAMS & RANDALL (1964)
BOLT (1964)
T≤1/2 sec
T~1 sec
T≥2 sec
REGION E
REGION F
REGION G

Fig. 1

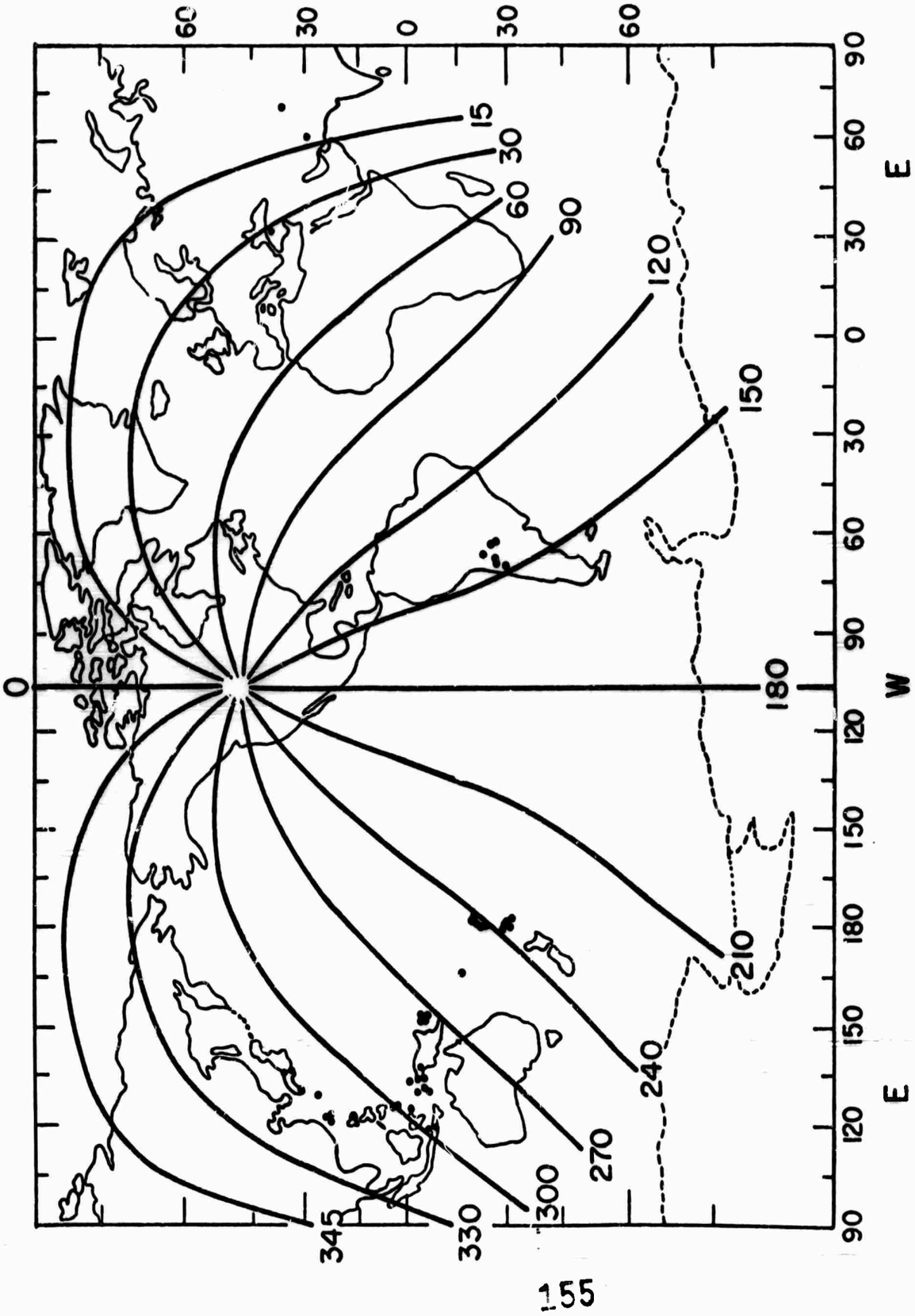
0
15
30
60
90
120
150
180
210
240
270
300
330
345
E
W
E
60
30
0
30
60
90
60
30
0
30
60
90
120
150
180
150
120
90

Fig. 2

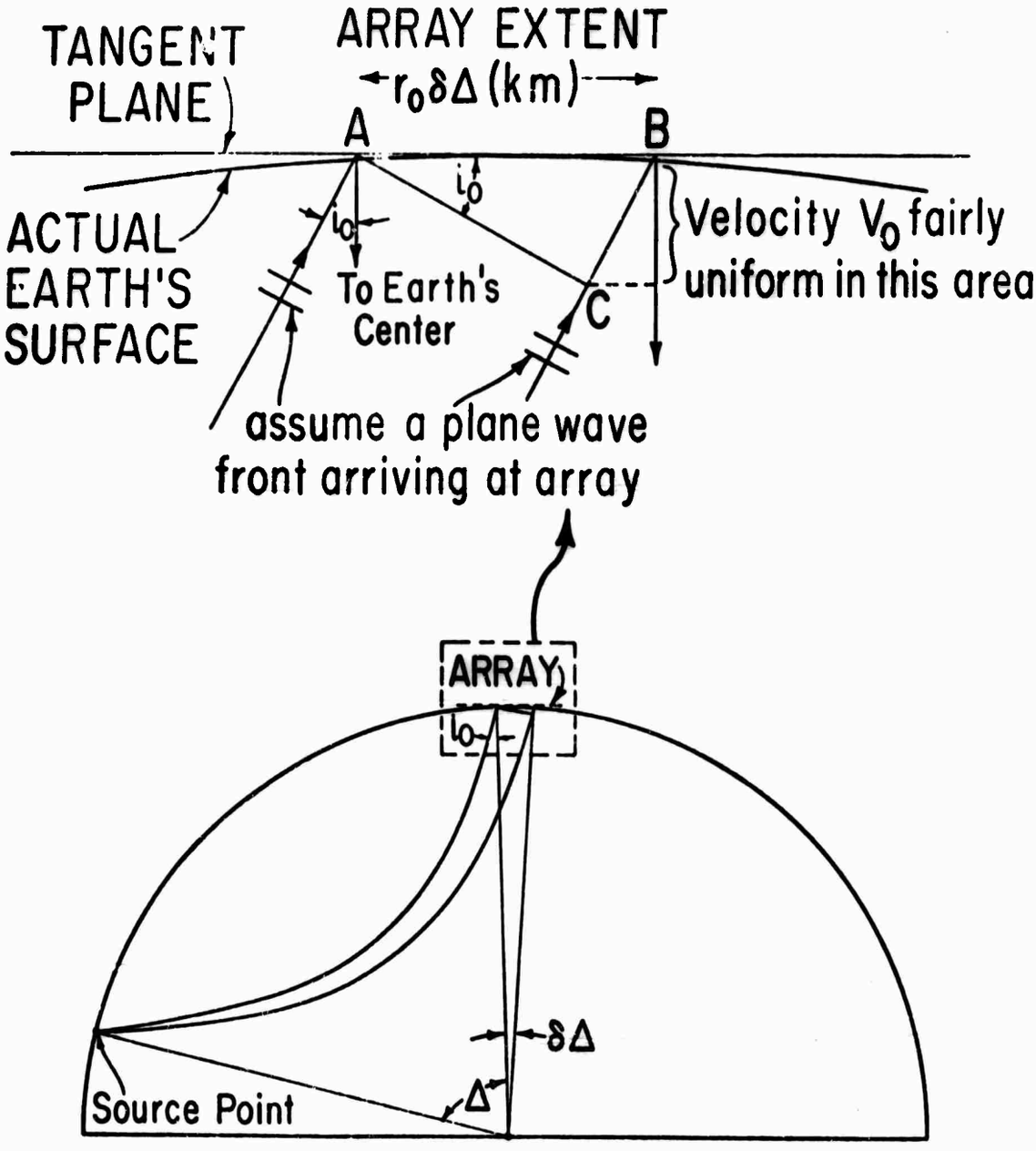
TANGENT PLANE
ARRAY EXTENT
$r_0\delta\Delta$ (km)
A
B
i_0
ACTUAL EARTH'S SURFACE
To Earth's Center
C
Velocity V_0 fairly uniform in this area
assume a plane wave front arriving at array
ARRAY
i_0
$\delta\Delta$
Δ
Source Point

Fig. 3

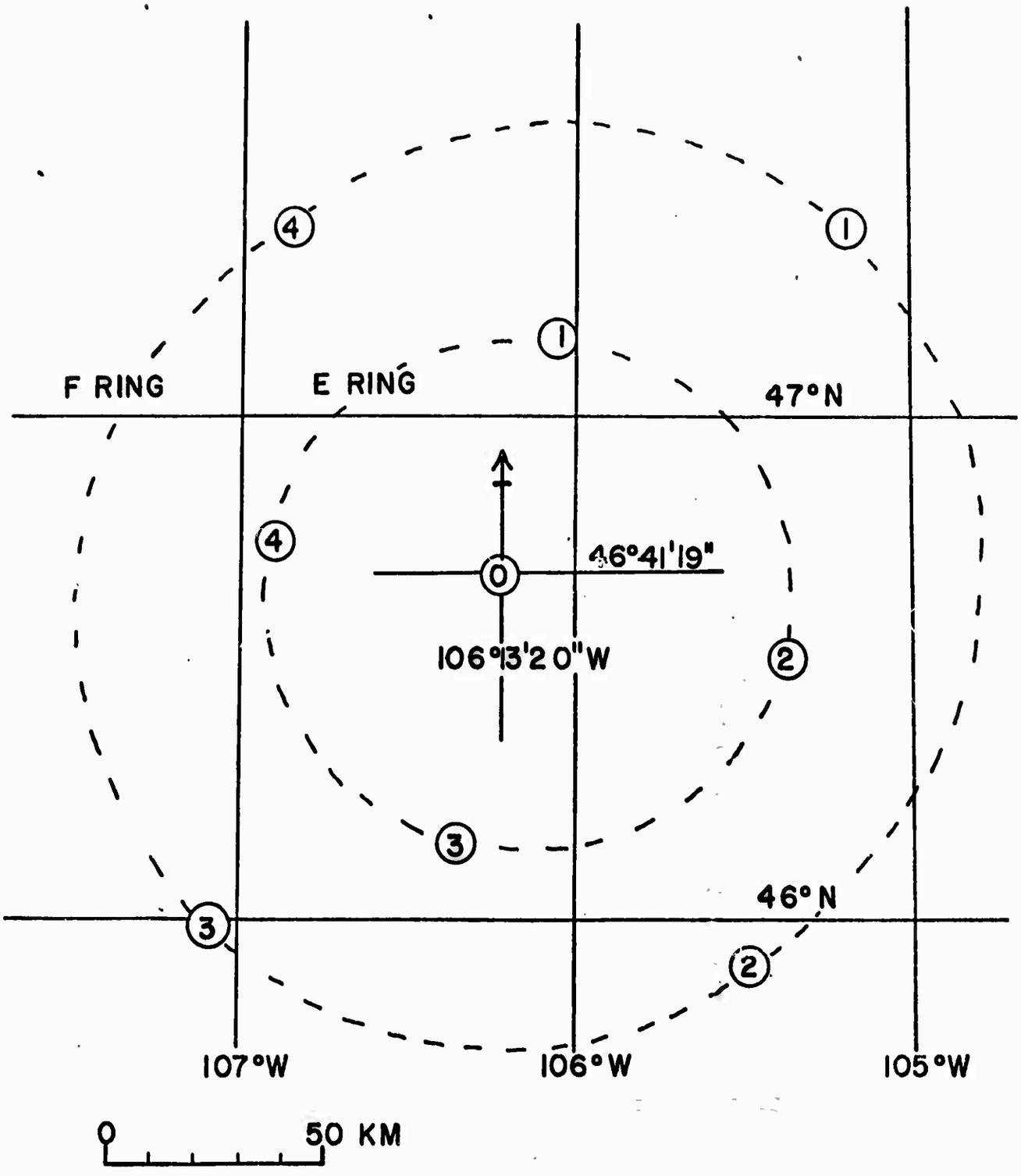

MONTANA LASA

Fig. 4

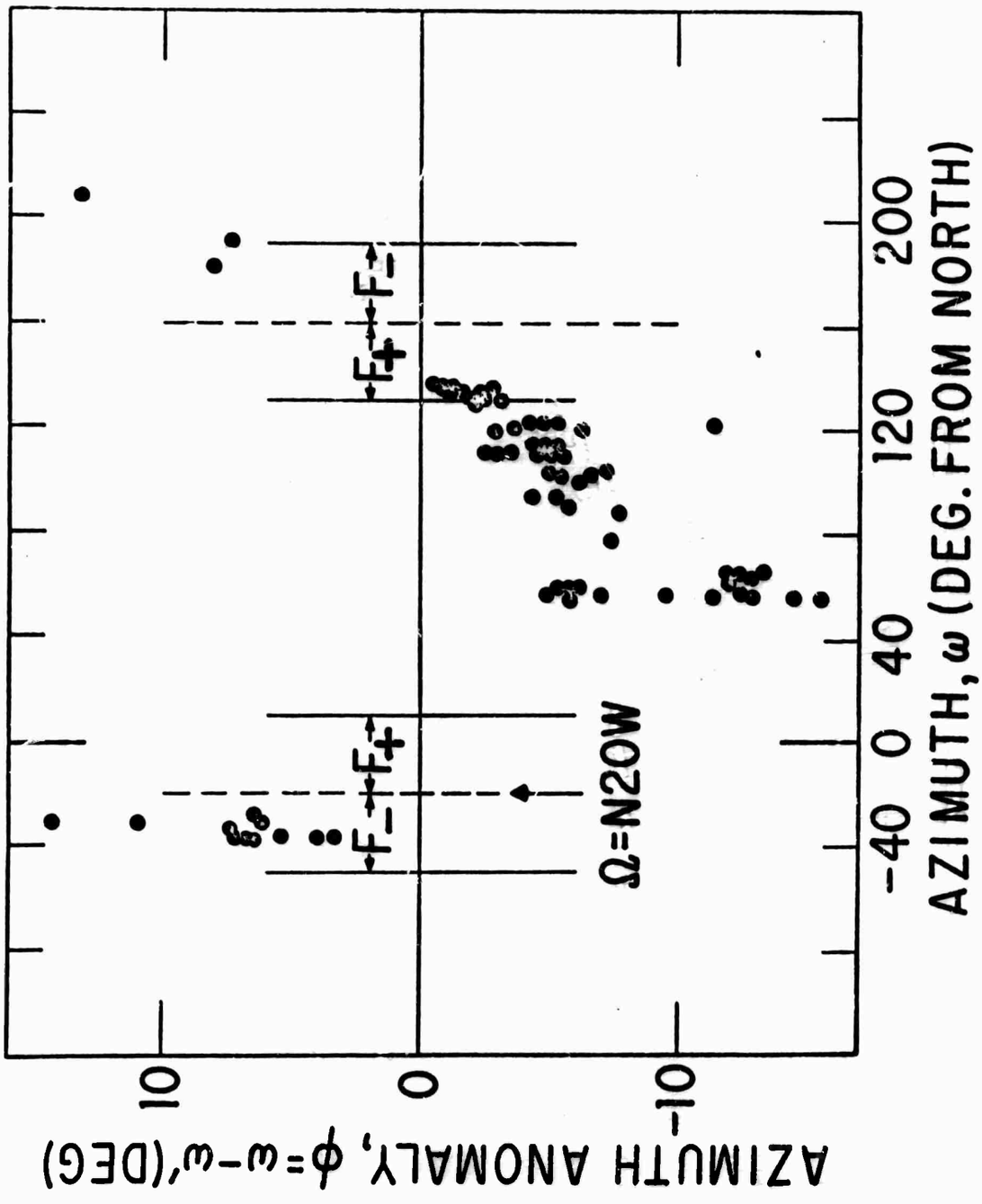
AZIMUTH ANOMALY, $\phi = \omega - \omega'$ (DEG)
10
0
-10
AZIMUTH, ω (DEG. FROM NORTH)
-40
0
40
120
200
Ω=N20W
F_-
F_+
F_-
F_+

Fig. 5

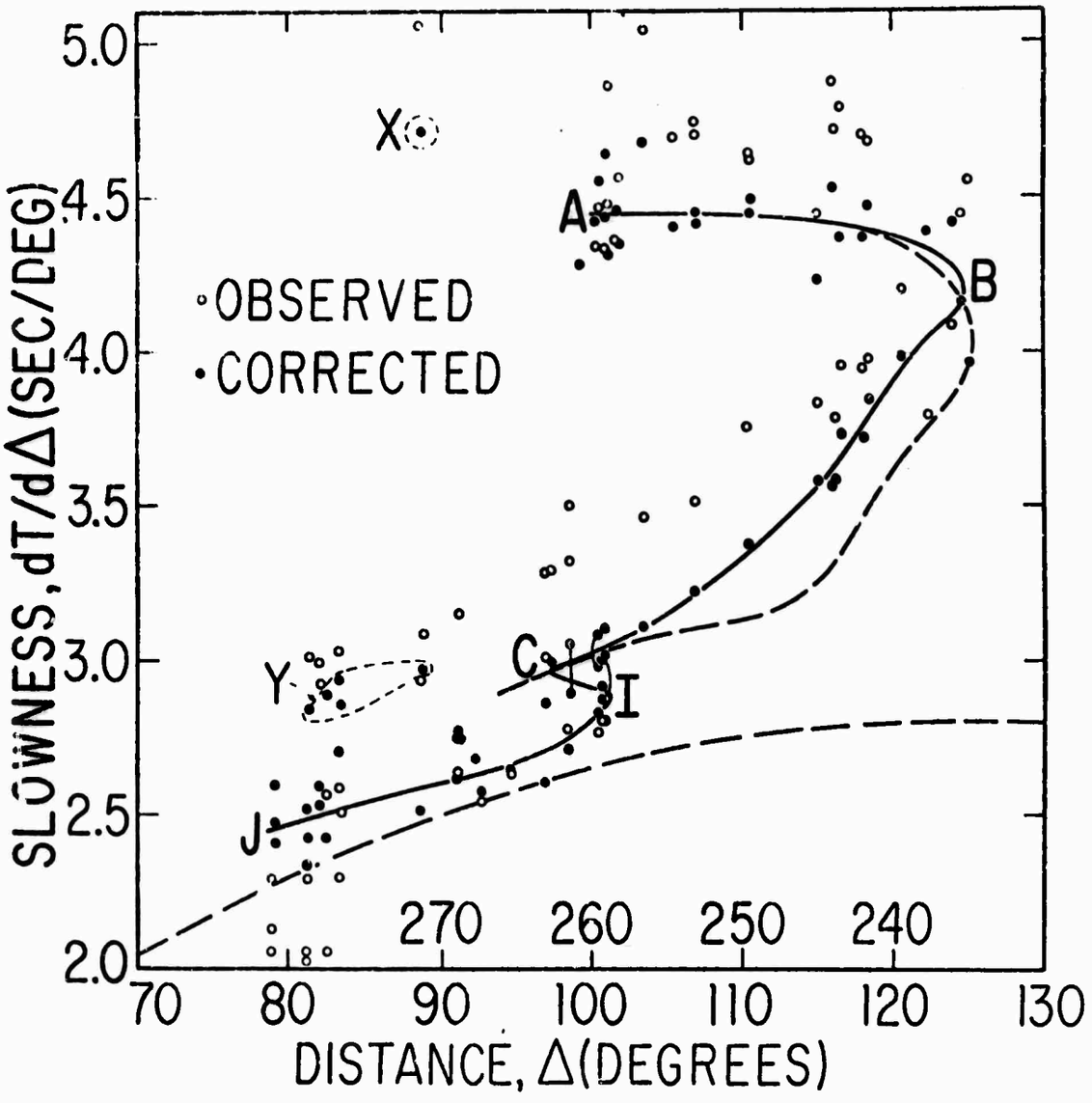
5.0
4.5
4.0
3.5
3.0
2.5
2.0
SLOWNESS, dT/dΔ (SEC/DEG)
X
A
B
C
I
Y
J
OBSERVED
CORRECTED
270
260
250
240
70
80
90
100
110
120
130
DISTANCE, Δ (DEGREES)

Fig. 6

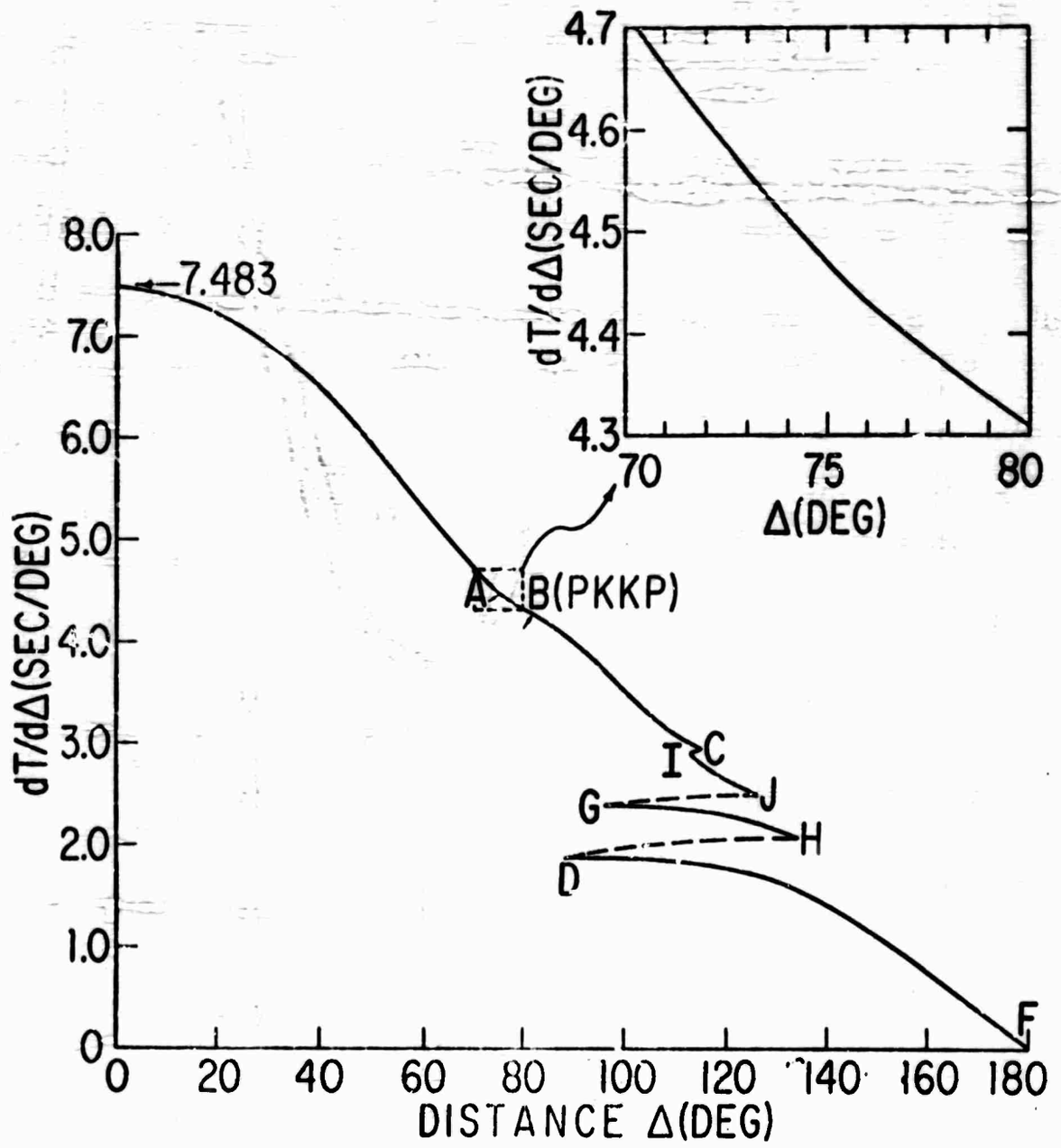
4.7
4.6
4.5
4.4
4.3
dT/dΔ(SEC/DEG)
70
75
80
Δ(DEG)
8.0
7.0
6.0
5.0
4.0
3.0
2.0
1.0
0
7.483
A
B(PKKP)
I
C
G
J
H
D
F
0
20
40
60
80
100
120
140
160
180
DISTANCE Δ(DEG)

Fig. 7

160

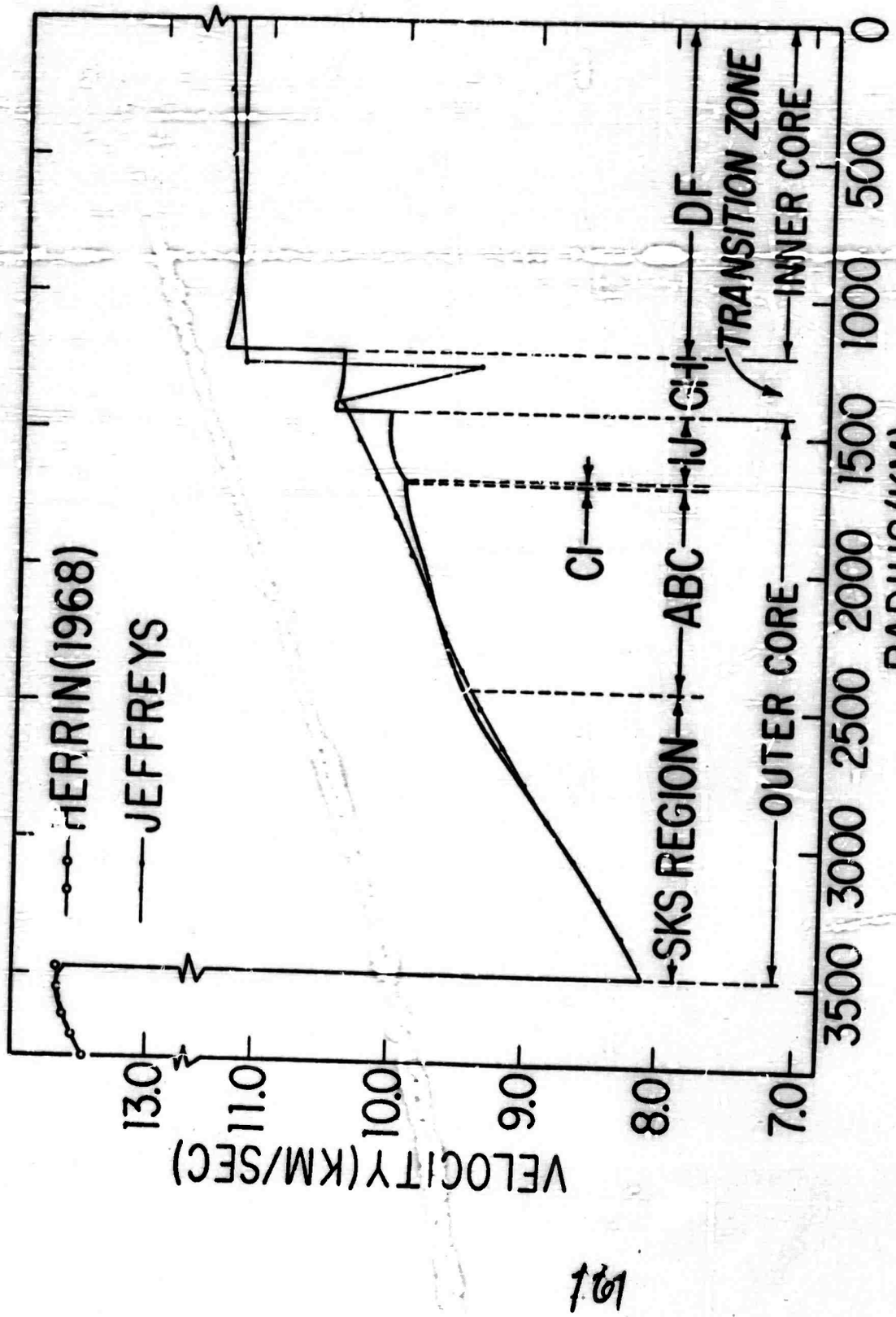
HERRIN(1968)
JEFFREYS
VELOCITY(KM/SEC)
13.0
11.0
10.0
9.0
8.0
7.0
3500
3000
2500
2000
1500
1000
500
0
RADIUS(KM)
OUTER CORE
SKS REGION
ABC
CI
J
DF
TRANSITION ZONE
INNER CORE

Fig. 8

161

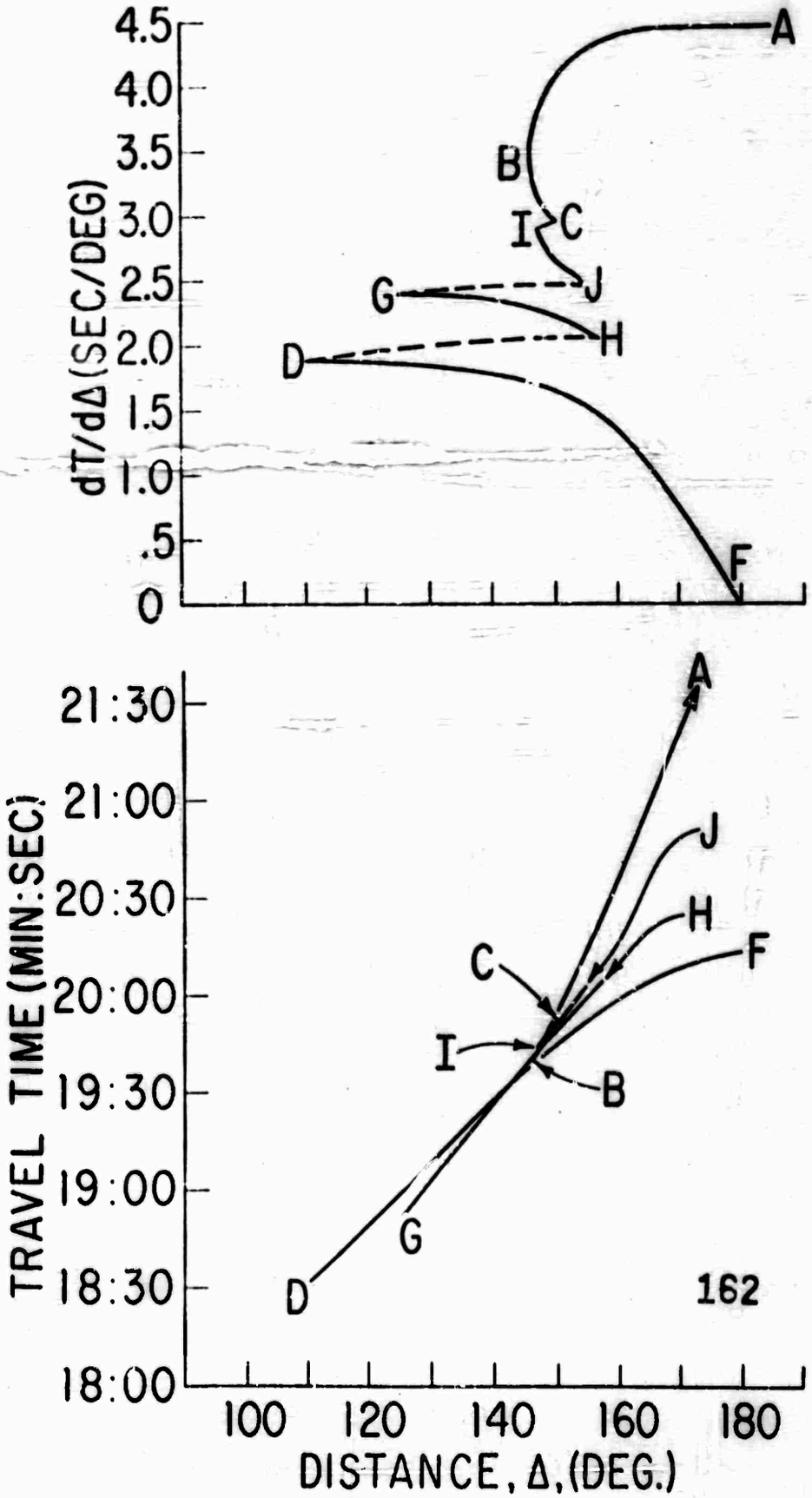
4.5
4.0
3.5
3.0
2.5
2.0
1.5
1.0
.5
0
dT/dΔ (SEC/DEG)
A
B
I
C
G
J
H
D
F
21:30
21:00
20:30
20:00
19:30
19:00
18:30
18:00
TRAVEL TIME (MIN:SEC)
A
J
H
F
C
I
B
G
D
162
100
120
140
160
180
DISTANCE, Δ, (DEG.)

Fig. 9

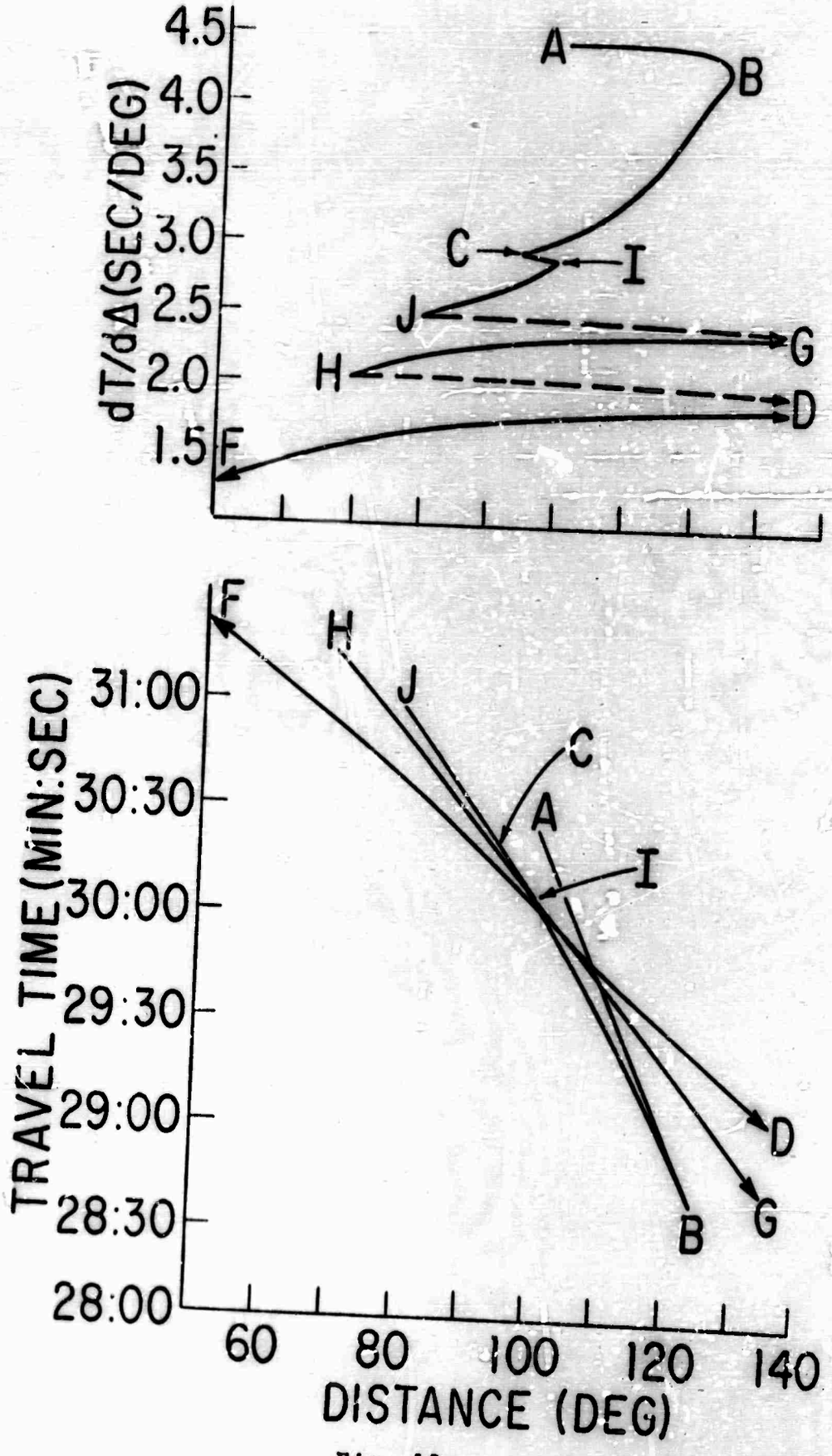
dT/dΔ(SEC/DEG)
4.5
4.0
3.5
3.0
2.5
2.0
1.5
A
B
C
I
J
G
H
D
F
TRAVEL TIME(MIN:SEC)
31:00
30:30
30:00
29:30
29:00
28:30
28:00
F
H
J
C
A
I
D
G
B
60
80
100
120
140
DISTANCE (DEG)

Fig. 10

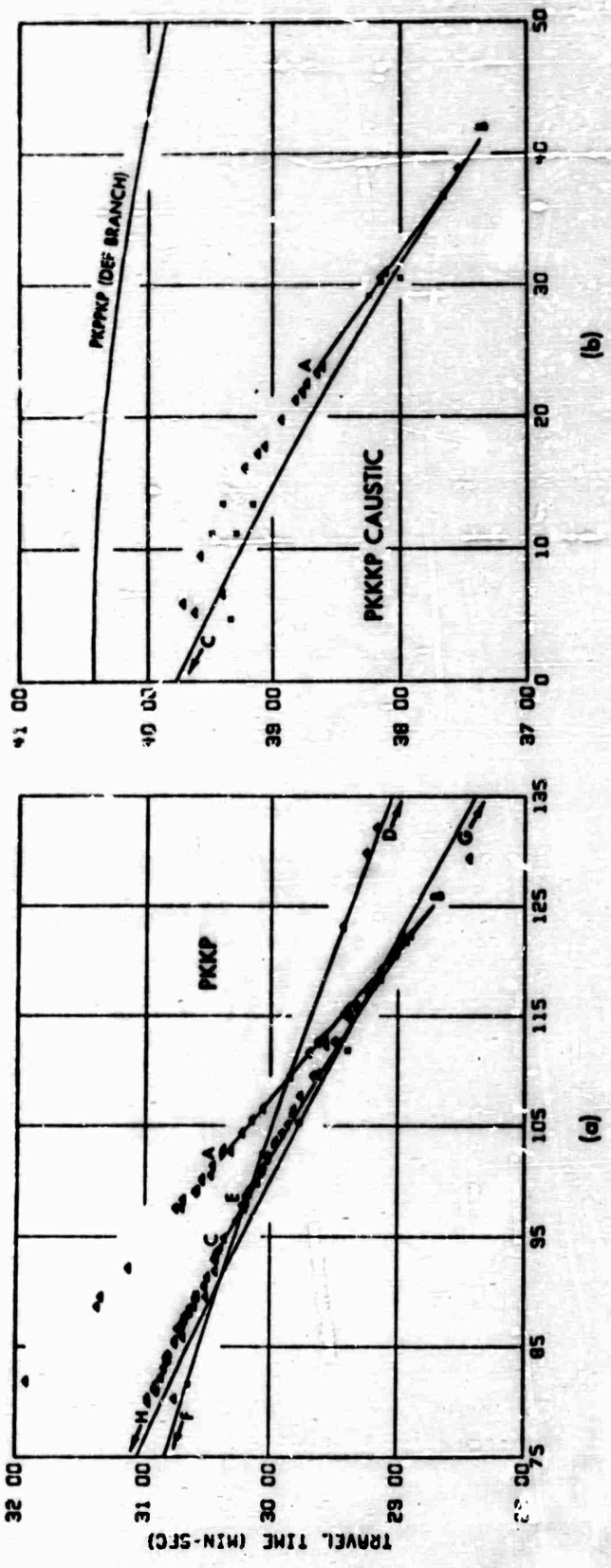

Fig. 11

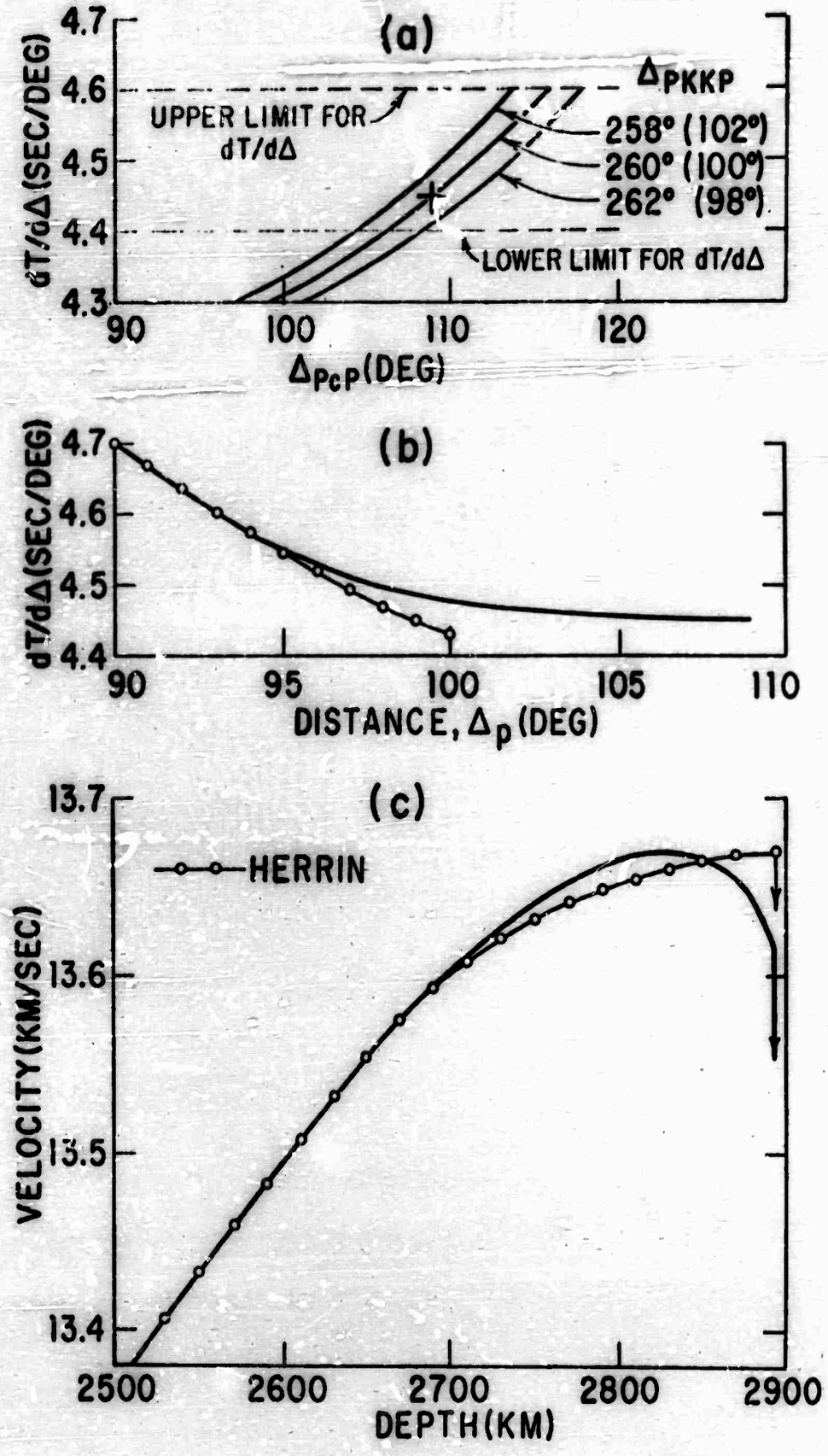
(a)
dT/dΔ (SEC/DEG)
4.7
4.6
4.5
4.4
4.3
UPPER LIMIT FOR dT/dΔ
ΔPKKP
258° (102°)
260° (100°)
262° (98°)
LOWER LIMIT FOR dT/dΔ
90
100
110
120
ΔPcP (DEG)
(b)
dT/dΔ (SEC/DEG)
4.7
4.6
4.5
4.4
90
95
100
105
110
DISTANCE, Δp (DEG)
(c)
HERRIN
VELOCITY (KM/SEC)
13.7
13.6
13.5
13.4
2500
2600
2700
2800
2900
DEPTH (KM)

Fig. 12

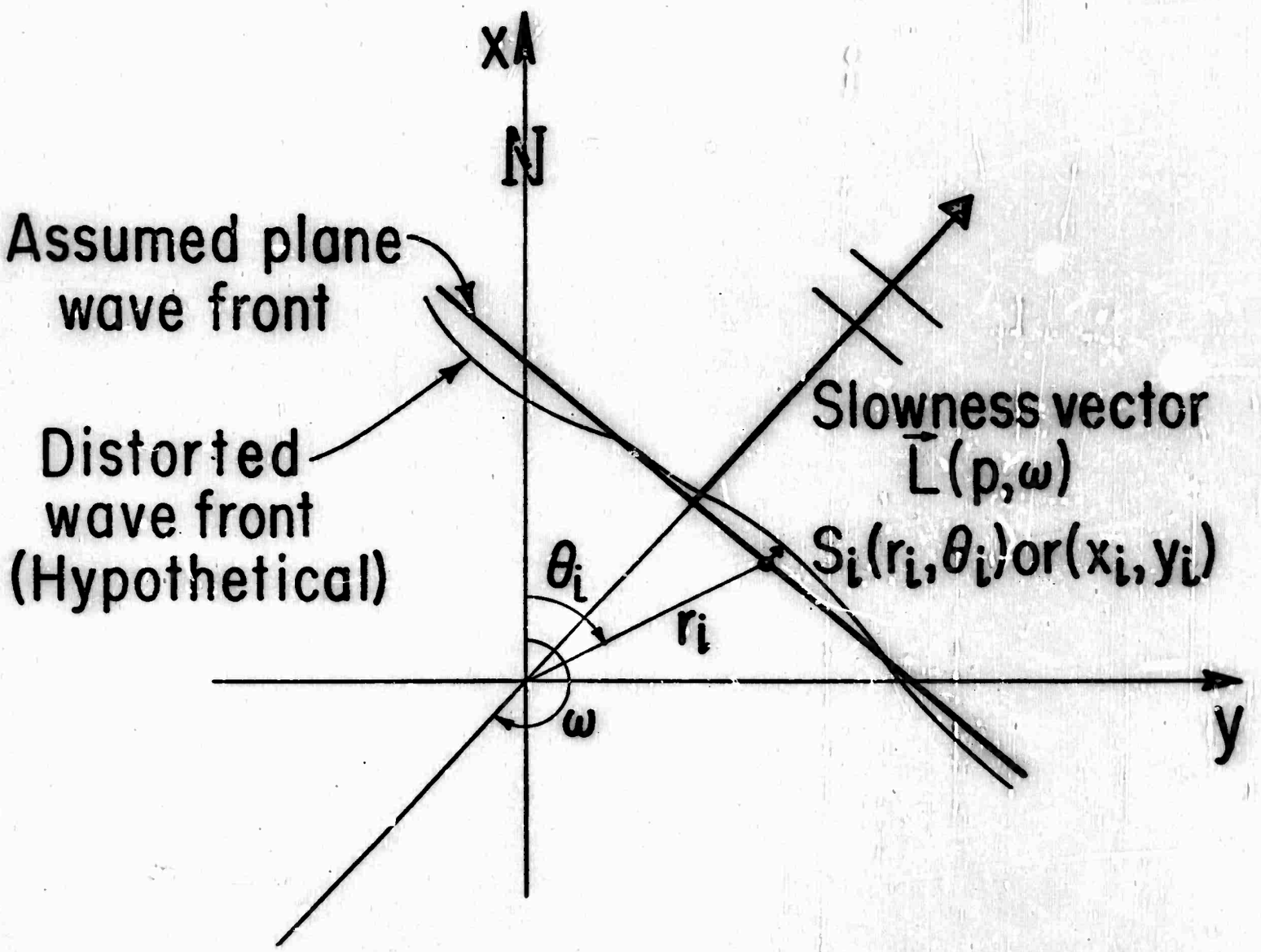
x
N
Assumed plane
wave front
Distorted
wave front
(Hypothetical)
Slowness vector
$\vec{L}(p,\omega)$
$S_i(r_i,\theta_i)$ or (x_i,y_i)
θ_i
r_i
ω
y

Fig. A1

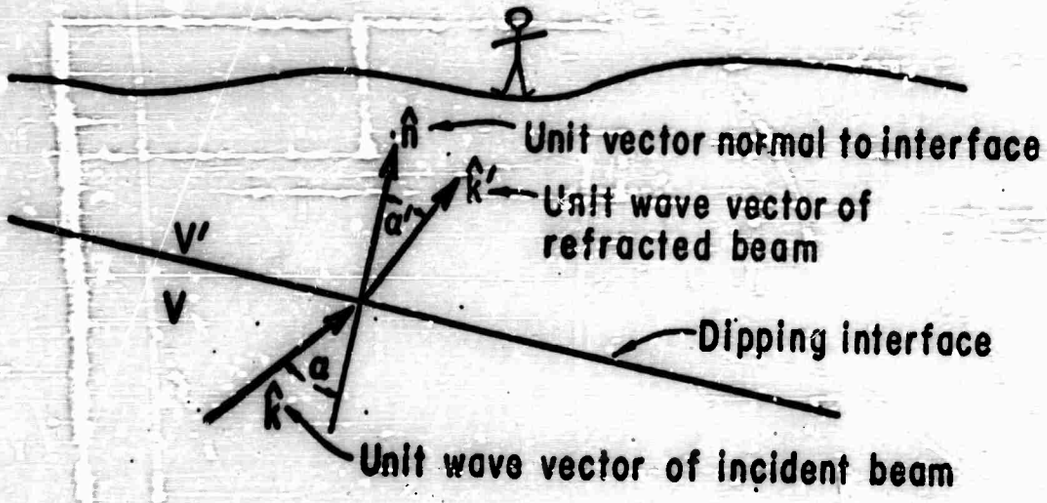
n̂
Unit vector normal to interface
k̂'
Unit wave vector of refracted beam
α'
V'
V
Dipping interface
α
k̂
Unit wave vector of incident beam

Fig. B1

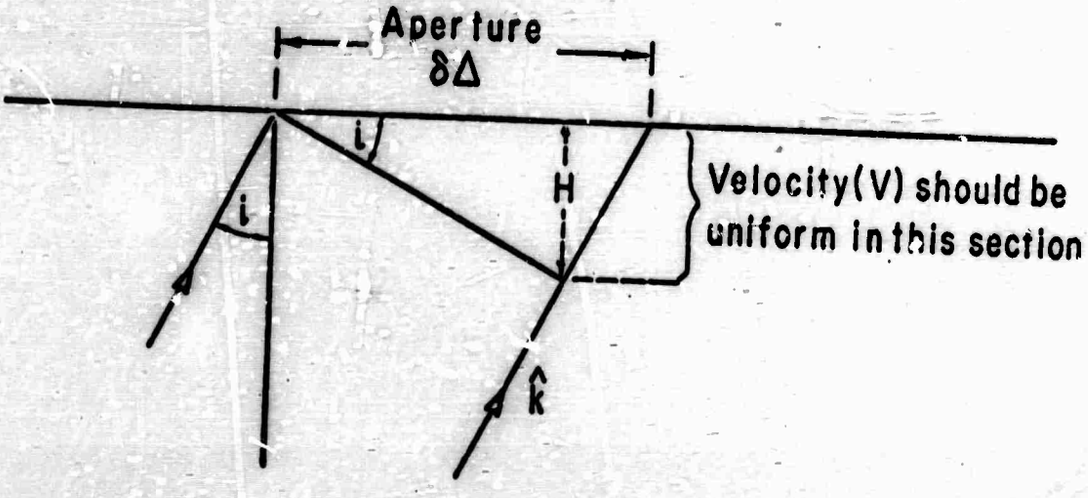
Aperture
δΔ
i
i
H
Velocity(V) should be uniform in this section
k̂

Fig. B2

Security Classification

DOCUMENT CONTROL DATA - R & D

(Security classification of title, body of abstract and indexing annotation must be entered when the overall report is classified)

1. ORIGINATING ACTIVITY (Corporate author)

Stanford University
Dept. of Geophysics
Stanford, California 94305

2a. REPORT SECURITY CLASSIFICATION: Unclassified

2b. GROUP:

3. REPORT TITLE

SEISMOLOGICAL ANALYSES OF VELA ARRAY DATA

4. DESCRIPTIVE NOTES (Type of report and inclusive dates)

Scientific.....Final

5. AUTHOR(S) (First name, middle initial, last name)

Robert L. Kovach

6. REPORT DATE	7a. TOTAL NO. OF PAGES	7b. NO. OF REFS
30 August 1970	168	24

8a. CONTRACT OR GRANT NO.	9a. ORIGINATOR'S REPORT NUMBER(S)
AF 49(638)-1687	
b. PROJECT NO. 62701D	
c. 8652	9b. OTHER REPORT NO(S) (Any other numbers that may be assigned this report) AFOSR 70-2934TR
d.	

10. DISTRIBUTION STATEMENT

This document has been approved for public release and sale; its distribution is unlimited

11. SUPPLEMENTARY NOTES	12. SPONSORING MILITARY ACTIVITY
TECH, OTHER	Air Force Office of Scientific Res. 1400 Wilson Blvd. (NPG) Arlington, Virginia 22209

13. ABSTRACT

This is a final report summarizing research accomplished under contract AF 49(638)-1687 for the time period 1 February 1966 - 31 July 1970. This research utilized seismic data recorded by VELA arrays, such as LASA and those formed by individual LRSM stations to 1) investigate the velocity structure of the mantle and core; 2) examine the attenuation characteristics of seismic waves; and 3) study the propagation of seismic waves across large arrays.

DD FORM 1 NOV 65 1473

Unclassified

Security Classification

14. KEY WORDS	LINK A		LINK B		LINK
	ROLE	WT	ROLE	WT	ROLE
Seismology, Arrays, Seismic waves					